DISCONTINUOUS ADVENTITIOUS LUNG SOUNDS: MEASUREMENT, CLASSIFICATION, AND MODELING

by

STEPHEN KENT HOLFORD

S.B., Massachusetts Institute of Technology (1969)
S.M., Massachusetts Institute of Technology (1976)
E.E., Massachusetts Institute of Technology (1976)

SUBMITTED IN PARTIAL FULFILLMENT
OF THE REQUIREMENTS FOR THE
DEGREE OF

DOCTOR OF SCIENCE

at the

MASSACHUSETTS INSTITUTE OF TECHNOLOGY

June 1981

Signature of Author Stephen K. Holford
Department of Electrical Engineering
and Computer Science
May 1, 1981

Certified by Kenneth N. Stevens
Kenneth N. Stevens
Thesis Supervisor

Accepted by _____
Arthur C. Smith
Chairman, Departmental Committee on Graduate Students

Table of Contents

LIST OF FIGURES

LIST OF TABLES

DISCONTINUOUS ADVENTITIOUS LUNG SOUNDS: MEASUREMENT, CLASSIFICATION, AND MODELING

by

STEPHEN KENT HOLFORD

Submitted to the Department of Electrical Engineering and Computer Science on May 1, 1981 in partial fulfillment of the requirements for the Degree of Doctor of Science

ABSTRACT

Discontinuous adventitious (abnormal) lung sounds (DALS) have been recognized by physicians for over 160 years, but their use in diagnosing and following the course of lung diseases has been limited by the lack of fundamental understanding of their nature and by the subjective methods used to describe them. DALS are commonly called rales, crackles, and crepitations. This report describes an objective method for defining the two most common kinds of DALS, fine and coarse, and shows how observations of their occurrence in patients correlate with a fundamental physical explanation of the DALS phenomenon.

Lung sound observations were made using microphones coupled to the chest wall. The signals were tape recorded and subsequently digitized and analyzed by computer. Acoustic and electrical calibration signals were used to standardize the microphone, recording, playback, and analysis equipment.

A classification method for fine and coarse DALS was developed using tape recorded sounds that had been described by an experienced chest physician as clear examples. These examples were used as a training set to develop a statistical pattern classifier that separates fine from coarse DALS using two measurements made on the time domain waveforms of the DALS. These two characteristic time features are the initial deflection width (IDW) and the two cycle duration (2CD). The method was tested and its utility verified using further examples from patients and from lung sound teaching tapes of other investigators.

The two-parameter classification scheme made it possible to categorize individual DALS complexes. Based on the observed wave shapes, it was hypothesized that coarse DALS originated further from the chest surface and in larger airways than fine DALS. It was expected that an individual coarse DALS complex would then be observed over a wider area of the chest wall since the vibrations would spread out more as they propagated further through the lung tissue. The surface distribution was investigated by studying DALS sig-

nals obtained from two microphones simultaneously applied at chest wall sites separated by 6 cm and 12 cm. DALS observed at each site were classified using the IDW/2CD method. An individual fine DALS observed at one site was measurable only 14% of the time at the other site 6 cm away. However, when a coarse DALS was observed at one site, it was seen at the other site 87% of the time. This observation that coarse DALS are more widely distributed on the chest wall suggests that they do occur in relatively larger airways.

These results were compared to the predictions of a fundamental model for the DALS phenomenon proposed by Fredberg. The DALS are modeled as a quadrupole source in an infinite, homogeneous, lossless, linearly elastic wave-bearing medium. The quadrupole excitation results from the stress relaxation occurring upon sudden opening during inspiration of an airway that had closed during the previous expiration. The model was used to predict the temporal, spectral, and spatial characteristics of the pressure response in the medium. The pressure waveforms and contours of equal energy were calculated at a chest wall plane for a range of model parameters believed to correspond to airways between 0.5 and 5mm in diameter. The estimated effects of the transduction process on the signal were accounted for by digitally filtering the model's pressure waveforms with a 200 Hz high pass filter and a 1 kHz low pass filter.

The model's DALS waveforms are similar in shape to DALS observed in patients. When classified by the IDW/2CD method, the model's DALS range in categorization from fine to coarse when the modeled airway diameter varies from small to large airways. Predictions based on the model of the area of the chest over which DALS could be measured at two transducers show the same connection between the waveform parameters and the extent of the surface distribution that is observed in patients.

The conclusion is that fine DALS occur in relatively smaller airways than coarse DALS, and that when observed on the chest, fine DALS occur over a smaller region. The quadrupole model is a plausible explanation for the DALS phenomenon. Better estimates for the lung's mechanical parameters and a more detailed understanding of transducer effects will be necessary for further evaluation of models. Successful verification of a DALS model could result in clinically useful techniques for noninvasive determination of local properties of the lung.

Thesis Supervisor: Dr. Kenneth N. Stevens

Title: Clarence J. LeBel Professor
of Electrical Engineering

Acknowledgements

My wife Meredith and my three children, Amy, Matt, and Casey, have made their own contributions to this work, and their support has been indispensable.

I am indebted to many other people and institutions for their generous help, both financial and intellectual, during the course of this project. Financial support was provided by the Institute of Occupational and Environmental Health, Montreal, P.Q.; the American Lung Association (Training Fellowship in Pulmonary Disease); and the National Heart Lung and Blood Institute (Grant HL23318). These funds were received through the kind cooperation of Dr. Raymond Murphy of Faulkner Hospital and Tufts University School of Medicine whose enthusiasm for studying lung sounds initially stimulated my own.

Valuable advice and critical comments were received from Prof. Kenneth Stevens, Thesis Supervisor, and the readers: Dr. Jeffrey Fredberg and Professors William Siebert and Forbes Dewey. Dr. Fredberg conceived the quadrupole model of Chapter 5. Professor Dewey helped interpret the surface distribution measurements of Chapter 4, which were partly performed by Ms. Enora Kunica as an S.B. thesis project.

Technical support was received from Ms. Elizabeth DelBono and Mr. Jonathan Berera. Mr. Berera constructed and maintained much of the transducer instrumentation. Ms. DelBono prepared lung sound tapes and made many of the illustrations for this document.

Biographical Note

Stephen K. Holford was born in Hutchinson, Kansas. He received the S.B. Degree in Electrical Engineering in 1969, the S.M. Degree in Electrical Engineering and Computer Science and the Electrical Engineer Degree in 1976 from the Massachusetts Institute of Technology.

From 1969-1973, he was a Research Engineer at the M.I.T. Instrumentation Laboratory (now Charles Stark Draper Laboratory) working on computer-driven graphic displays for space vehicles. In 1973 he entered graduate school at the Harvard University School of Public Health where he studied physiology. In 1974 he returned to the Department of E.E.C.S. at M.I.T. Since 1975, he has been associated with the Pulmonary Department of Faulkner Hospital, Boston, as a bioengineer. From 1977-79 he was recipient of a predoctoral Training Fellowship in Pulmonary Disease from the American Lung Association. He currently is a Research Associate in Medicine, Tufts University School of Medicine, Boston.

Chapter 1

Introduction and Background

1.1 Background

In diagnosing and following the course of disease, physicians spend much of their time using their senses to learn about conditions and events within the patient's body. The vibrations at the chest surface produced as air moves in and out of the lungs during respiration have been observed and studied since ancient times. They are referred to variously as lung sounds, pulmonary sounds, breath sounds, and chest sounds.

In one sense, lung sounds are not sounds at all. They are vibrations from within the gas or from the walls of airways that are transmitted to the chest wall. At the chest wall the amplitude of the vibrations may be much less than 10^{-6} meter, and this motion is superimposed on the far larger excursions of inspiration and expiration. Thus the fundamental problem of observation is to sense very small vibrations on a surface that is undergoing relatively large movements. Such small vibrations can usually neither be felt nor seen, but the remarkable sensitivity of the human auditory apparatus allowed the discovery in antiquity that

sounds could be heard during respiration by applying the ear directly to the chest wall (direct auscultation). It is important to note that the vibrations became "sounds" when transmitted through the auditory canal to the eardum and thence to the perceptual apparatus.

R.T.H. Laennec's invention in 1816 of the wooden stethoscope allowed a method of indirect or mediate auscultation that was technically better and more convenient [Laennec(1819)]. Physicians have since recognized the existence of various classes of normal and abnormal sounds related to respiration. The adventitious (abnormal) sounds are still classified using categories and names very similar to those Laennec first set forth. Laennec's investigations were carried out in the wards of a charity hospital in Paris, and today his work can still be considered the single most important contribution in this field. Ironically, during Laennec's lifetime his invention and his belief that it could be an effective tool in diagnosis of disease were not widely accepted by other physicians. It is said that at the time of his death in 1826 from tuberculosis, all the stethoscopes in existence were the product of his own hand.

Despite the efforts of many who followed Laennec, there are surprisingly few solidly documented instances where lung sounds provide important diagnostic or monitoring information to the clinician. There is still considerable difference of opinion about the clinical utility of lung sound observations. Continued work in the field has been

motivated by (1) the noninvasive nature of the auscultatory process, and (2) the belief that sufficient study of the lung and of the vibratory waveforms transduced at the chest surface would illuminate the physical mechanisms for sound generation.

Before devices were available to record and analyze pulmonary sounds objectively, studies relied on subjective observation by humans, sometimes coupled with pathologic examination at autopsy. These data were compared with other information about the patients and their diseases. The application of the resulting correlations was limited to physicians having the requisite auditory ability and extensive clinical training and experience. Prior to the development of x-ray imaging techniques, some physicians developed surprising ability to diagnose and follow the course of common lung diseases, especially pulmonary tuberculosis, using the stethoscope. But the x-ray gave superior, more objective, amd more widely understood diagnostic information. This was largely responsible for a decline in scientific study and clinical use of auscultation in pulmonary medicine. Today the average physician probably knows little more than Laennec did about lung sounds, and some know considerably less. In contrast, cardiologists rely heavily on auscultation of the heart sounds in diagnosis, and many worthwhile correlations between sounds and underlying cardiac pathology exist. An indication of the low regard of many for stethoscopic observations in pul-

monary medicine is this quote from the 1962 edition of a standard textbook:

> "The stethoscope is largely a decorative instrument insofar as its value in diagnosis of pulmonary disease is concerned. Nevertheless it occupies an important place in the art of medicine. Apprehensive patients with functional complaints are often relieved as soon as they feel the chest piece on their pectoral muscles." [Rubin and Rubin (1962)]

There are several problems encountered in auscultation of lung sounds that account for this skepticism. Most of these problems are not connected with the characteristics of the stethoscope itself. The variation among different kinds of stethoscopes, the impedance mismatches, and the uneven frequency response of the instruments have been studied [Ertel(1969)], but the primary problems in auscultation are related to the subjective observations that are made by the human observer about his auditory perceptions. Like other mortals, physicians vary in temperament; some are better able to focus on the subtle differences in sound pattern that occur among normals and in various diseases. The pulmonary sounds vary along many dimensions. So far as can be learned from the literature, no systematic study has been made of the features of the acoustic stimuli that are actually used by physicians in describing and categorizing the sounds.

Listening at a single site on the chest, a physician may make several observations - for example, types of sounds

present, their character, duration, and intensity. Because several sites are usually examined on a single patient, it often becomes difficult for the listener to remember all the significant observations he or she has made. When he does write his impressions in the record, they are subjective ones, and the physician may find it difficult to recall at a later time the exact details of his or her auditory perceptions from reading the description in the record.

On top of all these difficulties, the lung sounds themselves are subject to variability, the degree of which is not well known. Individual physicians must learn experientially the directions in which the sounds vary and by how much. They must also learn a set of names to describe the phenomena. In reference to the words used to describe lung sounds, Cabot and Dodge [1925] wrote:

> "It is evident that many of these terms are purely relative and only by experience and mutual agreement can any reasonable degree of uniformity in phraseology be attained."

Communication among observers has thus been hampered since the time of Laennec by confused terminology and differing classification schemes for the sounds. In this report a common standard classification system has been used as described in Appendix A.

Two factors have helped to foster a renewed interest in pulmonary auscultation. The first was the development of microphones, electronic amplifiers and wave filters, sound spectrographs, magnetic audio recorders, and computer-based

analysis and modeling. As these quantitative tools became available, each was used to study lung sounds [Cabot and Dodge (1925), McKusick et al (1955), Weiss et al (1972), Bethke and Seireg (1973), Grassi et al (1966), Murphy, Holford, and Knowler (1977)]. Second, the pattern of prevalence of lung diseases has changed greatly since the early 20th century. The most common chronic lung diseases (such as asthma, emphysema, and chronic bronchitis) are not so easily diagnosed by x-ray, particularly in their early stages, but abnormal lung sounds are often found in patients who are afflicted by them. This has been an impetus for the development of new diagnostic techniques and for the re-examination of old ones.

1.2 Literature Review

This section is a review of the literature pertaining to (a) clinical medical observation and description of discontinuous adventitious lung sounds (DALS), (b) analysis of lung sounds transduced by microphones, and (c) past attempts at discovering the physical mechanism(s) by which DALS are produced.

1.2.1 Clinical Knowledge of DALS

- Pulmonary "rales" were discussed by Laennec, who chose the French word rale, meaning rattle, which was associated with the death rattle heard in patients too weak to cough up secretions. However, Laennec used the term as a broad category

of abnormal lung sounds [Laennec(1819)]. He included both sounds now categorized as discontinuous noises (DALS) and those categorized as continuous adventitious lung sounds (CALS). The CALS include the familiar wheeze heard in asthma and the lower pitched noises heard in patients with bronchitis. Appendix A is a tutorial introduction to lung sounds that further describes their categorization and clinical associations. When using his nomenclature around patients, Laennec found "rale" unsuitable because of its mortal implications, so he began using its Latin equivalent "rhonchus" synonymously. After several stages of translation and redefinition, rale and rhonchus were no longer synonymous in a common clinical nomenclature for abnormal lung sounds [Fraser and Pare (1970)].

Still more confusing was the proliferation of adjectives used by various observers to describe DALS. In many instances, adjectives were applied, such as wet, dry, or bubbling, that implied mechanisms without knowledge of the real underlying events. These nomenclatural problems resulted from the essential subjectivity of the auditory observation process, and they have hampered research and clinical use of lung sound information through present times. It must be noted, however, that when consistently applied, some of the adjectives may correspond to significant differences in the fundamental phenomena occurring in the lung. Recognizing the complexity of the subjective descriptions, the American Thoracic Society has recently proposed a

standard nomenclature that uses only the descriptors "fine" and "coarse" for DALS (Appendix A), and these are the groups studied in this research.

1.2.2 **Characteristics of the Stethoscope** - Laennec's method of indirect or mediate auscultation allowed the sounds of the chest to be heard in a technically better and more convenient manner. Until the development of modern electronic instrumentation, the characteristics and quality of stethoscopes were judged soley by ear. Microphones allowed these characteristics to be measured and compared objectively among various stethoscope designs. It is interesting to note, however, that large stethoscope manufacturers still employ physician consultants to evaluate new designs subjectively.

Dawson [1964] discussed qualitatively the use of the stethoscope in auscultation. He considered the characteristics of various bell-type and diaphragm-type chest pieces, the effects of the length and elasticity of the conducting tubing, and the necessity for ear pieces which provide a tight seal in the ear canal.

Ertel et al [1969] offered a more sophisticated analysis of the stethoscope. They used a probe microphone and artificial ear cavities to evaluate the frequency response of various stethoscope types. Their data show variations of up to 15 dB in stethoscope response over the range of 100-500 Hz where most of the energy in lung sounds is found.

1.2.3 Auscultation with Electromechanical Transducers - In the 20th century, microphones and vacuum-tube amplifiers and wave filters became available for collecting and studying lung sounds. While these devices have now been available for decades, there is still no widely accepted set of standard equipment for transducing the vibrations of the chest wall into electrical signals. Several different types of microphones are in use, and methods of coupling them to the chest wall vary. Microphones using piezoelectric crystals for the sensor have been widely used in phonocardiography, and these have naturally been employed to observe lung sounds as well. Condenser or capacitor microphones, which are usually higher in quality, were used to study lung sounds soon after their development. The newer and less expensive electret microphones found in many small tape recorders and hearing aids have now also been used as heart and lung sound transducers. Such a device is incorporated in at least one commercial "electronic stethoscope."

Microphones have been coupled to the chest wall by means of small air chambers with and without intermediate diaphragms. Contact microphones consisting of sensors with a direct mechanical coupling to the chest wall are also available. Both methods impose a transmission network between the chest and the sensor that can make the response of the overall transducer, considered from the force exerted by the chest to voltage at the output, quite different from

the response of the microphone itself as measured in a sound chamber. Indeed, most microphones being used are good enough that the nature of the coupling to the chest wall is a more important determinant of overall transducer response than is the actual microphone characteristic. For example, a small electret cartridge of good quality might have quite flat frequency response from 75 Hertz to over 10 kHz, but when it is coupled to the chest via an air chamber, the overall transducer might have a frequency response that exhibits attenuation below 200 Hz and above 1 kHz. This fact has not been widely appreciated among lung sound investigators, and the literature must be read with this in mind. Transducer response is discussed in more detail in the next chapter, where the microphones used in this research are characterized.

1.2.4 **Lung Sound Recording and Analysis** - Listening to the vibrations in the lung is not the only way to observe them, and it may not be the best way (although it seems to be at present). The objective, of course, is to impart to the human observer as much of the information contained in the vibrations as possible in a form that is easily and quickly assimilated and interpreted. Once the vibrations have been transduced to an electrical signal, the signal may be processed by several techniques before being presented to the observer auditorily or visually. The auditory presentations can change the time scale of the sound, modify the am-

plitude or loudness of the stimulus, or alter the content of the signal in various frequency bands by filtering. More work is needed to determine whether these techniques are actually more helpful than just listening with a passive stethoscope.

Bass [1927] described a system for obtaining amplitude versus time plots of chest sounds using a condenser microphone and an oscillograph. He published the first known tracings of lung sounds on expanded time scales (4000 mm/sec) that allow inspection of the waveform patterns of the varieties of normal and abnormal sounds.

Metildi and Lyman described the use of a system consisting of a condenser microphone and vacuum tube amplifiers as well as an oscillograph for recording the sound patterns [Metildi and Lyman (1929), Hannon and Lyman (1929), Bishop, Lee, et al (1930)]. Metildi and Lyman's system also included a device for recording the circumference of the chest simultaneously with the sound so that inspiration and expiration could be distinguished. Their recordings were made in a specially constructed, soundproofed and electrically shielded room.

Toshima published one of the earliest amplitude versus time plots of lung sound showing the occurrence of DALS [Toshima(1954)]. The patients examined in his study had tuberculosis, and his plots are on compressed scales that do not allow the shape of the DALS waveforms to be studied.

Weiss et al [1972] described a system for recording

lung sounds that included a calibrated simultaneous flow measurement and a method for standardizing the recording and playback levels so that the tapes would be realistic for teaching purposes. They published intensity versus time plots of whole inspiration-expiration cycles from patients with a variety of diseases. It is difficult to distinguish reliably the types of adventitious sounds using plots on their compressed time scales.

Penkala and Litt [1970] and Penkala [1971] reported development of an improved respiration sound transducer. Their device consisted of a condenser microphone cartridge mounted in a rather elaborate housing that was said to provide acoustic isolation from artifactual room noises. Acoustical filtering was provided to attenuate heart sounds and reduce the effects of low-frequency patient motion artifacts. Their apparatus was housed in a soundproofed room and included a microphone positioning device that required the subject to be standing. This worked well for the normal subjects studied but would be very impractical and much too bulky for clinical use. The measured sound intensities of normal breath sounds in their microphone's 5.1 cm^3 air chamber were usually less than 35 dB SPL, and they reported finding respiration sounds with frequency components as high as the limit of their transducer's sensitivity at 7 kHz. They used analysis of variance techniques to examine the differences in frequency and intensity of the sounds recorded from several sites in ten normal young men.

Their primary conclusion was that the intensity of inspiration was always greater than that of expiration by 3-6 dB.

Wooten and Waring [1972] reported development of a respiratory sound recording and analysis system. A real-time spectral analyzer and two-channel integrating envelope detector were used with a calibrated microphone in studies of pediatric patients and normal children. They observed sounds from 30 to 60 dB SPL in their 3.3 cm^3 microphone chamber over the frequency range from 10 to 1000 Hz and below 40 dB SPL above 1000 Hz. The sound envelope plots allowed them to compare the relative intensity and the phase in the respiratory cycle of the sound from homologous portions of the lung. Homologous segments of both lungs were found to emit nearly the same sound pressure levels (about 55-60 dB with "moderately deep breath"). This peak level is attained early in inspiration with expiration being relatively silent (about 30-40 dB). They were able to identify DALS by characteristic changes in the sound envelope patterns, although the integration of the sound eliminates the possibility of relating the temporal pattern of the DALS to pathology. These DALS were observed to have sound pressures up to 88 dB SPL (0.5 N/m^2).

The techniques discussed so far involve presenting the data in the time domain as the amplitude of a signal plotted versus time or played versus time as a sound. Analogously, music can represented as the amplitude of a sound signal versus time, but we know that it can be represented more

compactly by specifying an instrument and a set of notes (frequencies) to be played for given times in a given order. The frequency domain thus contains the same information as the time domain, but it may happen that we can see features in frequency domain representations that are not obvious in the temporal plots. There are two basic ways of observing the frequency content of sounds. One, called real-time analysis, consists of playing the sound through a set of differently tuned frequency-selective filters and observing the output in each channel as the sound progresses. The second way is to store a segment of amplitude versus time data in a computer and then mathematically to transform the data into an amplitude versus frequency representation using digital (discrete) Fourier analysis.

Frequency analysis of lung sounds has a long history, and it has constantly benefited from improved technology. Cabot and Dodge [1925] used a system that included a Western Electric condenser microphone and electronic amplifiers and filters. They used low- and high-pass filters to determine the frequency ranges occupied by an assortment of heart and lung sounds. They concluded that DALS lie in the range between 100 and 1000 Hz, and they observed that coarse and fine DALS are associated with conspicuous low and high frequency components respectively.

About ten years after the development of the sound spectrograph, McKusick used it in a comprehensive study of heart and lung sounds [McKusick et al (1955), McKusick

(1958)]. He discussed percussion of the thorax and the natural frequency of the thorax, and he speculated about the origin of vesicular sounds. He showed spectrograms of vesicular, tracheal, and bronchovesicular sounds, and demonstrated the effects of consolidated lung tissue. He presented spectrograms of "moist" and "dry crackling" DALS and observed that the latter variety had a wider spectrum.

Murphy and Sorensen [1973] reported the analysis of lung sounds using digital signal processing techniques. They used a sampling rate of 4000 points per second and performed 512-point discrete Fourier transforms using a fast Fourier transform algorithm. Their time window was thus one-eighth second wide. A fortuitous result of this method was the observation that DALS and other adventitious sounds could rather easily be distinguished from one another in the time domain when they were plotted so that an eighth second of sound fit on an oscilloscope display 10 cm wide. This corresponds to a time scale of 800 mm/sec. Murphy and Sorensen showed the "time-expanded" plots of several common auscultatory phenomena, but their principal emphasis was on analyzing the fine DALS heard in pipecoverers at a shipyard where they were exposed to asbestos dust. The application of these expanded scale time plots in lung sound analysis was further discussed by Murphy [1975] and by Murphy, Holford, and Knowler [1977]. They demonstrated that the sound occurring during a whole breath could be conveniently plotted using a computer-based analysis system and that

selected portions could be expanded further to allow measurement of the details of individual waveforms. On the expanded plots, the several major categories of lung sounds have distinctly different waveforms. Bass [1927] made this same observation fifty years earlier using high speed oscillograph tracings, but his report lay unrecognized, and the potential value of plotting lung sounds on expanded time scales was not re-emphasized until the faster and more flexible computer-based methods were employed.

1.2.5 **Physical Mechanisms for DALS** - DALS are discrete vibrations thought to result from sudden release of energy stored in elastic or surface forces within the lung. Early explanations for DALS were based upon passage of air through fluid. While this may account for DALS occurring in the trachea or major bronchi when secretions are present, low flow rates make it hard to explain DALS in small airways as air bubbling through secretions. As one proceeds through the generations of branching in the lung, the total cross-sectional area increases as the calibre of airways gets smaller. Consequently, the velocity of the air flow is reduced drastically from the value measured at the mouth. Staub [1963] states that the flow is reduced by a factor of 10-100 at the eighteenth generation respiratory bronchioles (see [Altman and Ditmer (1971), p. 109ff] for discussion of generations and airway sizes). It is generally believed

that by the time the alveoli are reached, gas transport is accomplished largely by diffusion. At such low flow rates, a bubbling phenomenon is unlikely.

Forgacs [1967] suggested that the mechanism by which many DALS are generated is an explosive equalization of pressure when previously closed airways open suddenly. Forgacs based his theory on several observations about the nature of DALS (or crackles as he prefers to call them). By playing recordings of DALS at one-eighth normal speed he discovered that the individual DALS often occur in patterns that are the same in sequential breaths. He also noted that DALS are heard much more often during inspiration than during expiration. The repetitive patterns he heard seemed to be undisturbed by coughing. Forgacs claimed that these last two facts make it unlikely that secretions are involved since he expected DALS during both respiratory phases if the noises were created by air passing through secretions, and since the pattern of DALS would probably change as secretions were dislodged by coughing.

Forgacs observed that changes in patient posture often lead to changes in the pattern of DALS; indeed, sometimes the DALS disappear entirely after a change of position. In a later article on the relation of gravitational stress to lung disease, he reviewed the effects of the upright posture on the lung [Forgacs(1974)]. Since the lung rests on its own weight, there is a tendency for an airway near the bottom of the lung to have a smaller diameter than an airway

near the top that is at the same order in the branching tree. The pressure in the intrapleural space is negative with respect to atmospheric pressure, and this keeps the lung inflated. As expiration ends, the natural tendency of the tissue to shrink and the weight of overlying lung lead to closure of airways near the lung bases (bottoms) [Macklem (1971)]. In normal persons these airways reopen during inspiration without producing DALS that can be heard with a stethoscope.

Penkala [1971] quoted a private communication from Ertel reporting that when the relatively loud normal vesicular sound components are removed by high pass filtering at 1 kHz, DALS-like sounds may be heard in normal persons. These sounds were said to differ both qualitatively and quantitatively from DALS heard in disease. Using equipment developed by the author that included a four pole high pass filter at 800 Hz, a study of 79 normal student nurses revealed that 92% exhibited DALS upon breathing in from very low lung volumes [Workum et al (1981)]. In fact, in these normals, the DALS were observable with the stethoscope too, although less frequently. The low amplitude of the noises makes them difficult to hear in the presence of the normal vesicular breath sounds. It is speculated that these DALS occurring in normals are connected with the opening of airways that had closed at end expiration as described above.

In his original report, Forgacs [1967] noted that he

had observed the behavior of excised lungs during reinflation and of living lungs deflated during the course of surgical procedures and then reinflated. He found that the lung does not fill evenly and gradually. Instead, small regions of subpleural parenchyma are observed to fill quickly as if a resistance has suddenly been overcome. Listening over the surface of these lungs, Forgacs heard a crackling noise that he said was indistinguishable from the DALS heard on the chest surface in diseased persons. Since a group of adjoining alveoli fill at once, the obstruction must be in an airway common to them all.

Nath and Capel [1974a] studied the correlation between the time of occurrence of inspiratory DALS and the type of disease present. They found that DALS occurring early in inspiration are associated with severe airways obstruction, and these DALS are often observed to be transmitted to the mouth. It was theorized that they occur as large airways that had closed during expiration reopen near the beginning of inspiration. In contrast, DALS that are heard no earlier than the middle of inspiration are associated with a restrictive defect (i.e., the lungs are not able to be inflated to normal volumes). Nath and Capel emphasized the clinical observation that these DALS late in inspiration are almost never heard at the mouth. It was concluded that late-inspiratory DALS are caused by the reopening of the smaller airways.

In a later article [Nath and Capel (1974b)], they

presented a study of the relation of the time of occurrence of DALS having a repetitive pattern to the variables inspiratory time from zero flow, inspiratory flow rate, inspired volume, and esophageal pressure. Esophageal pressure was measured by a transducer connected by a catheter to a balloon located in the esophagus. They found that the time of occurrence of the DALS is most closely related to the esophageal pressure. This pressure is taken as a measure of the transpulmonary pressure (i.e., the difference between atmospheric pressure, which is inside the lung, and intrapleural pressure, which is outside the lung). Thus the time of opening of a collapsed airway was found to be associated with the occurrence of a critical value of elastic pull on its walls. Nath and Capel also found that inspired volume is almost as closely associated with the timing of the DALS as the transpulmonary pressure, but that the two flow measurements bear little relation to the timing of the DALS.

Thus, although Forgacs and Nath and Capel presented no quantitative physical models for the generation of DALS, their observations and reasoning supported the concept of an airway remaining closed for a portion of inspiration and then opening suddenly to produce a DALS. The lung downstream of the site of collapse may remain underexpanded until upstream air pressure and external tractive forces on the collapsed walls overcome the surface tension of the material on the airway wall. The airway may then open

suddenly, making possible a rapid equalization of pressure between the upstream and downstream airspaces, if such a pressure differential is present. A recent quantitative theory of DALS generation does not rely on air pressure equalization to explain the noise [Fredberg and Holford (1981)]. Instead DALS are modeled as the vibratory response to sudden relaxation of the stress field around the collapsed airway.

1.3 Objectives and Summary of Methods and Results

As noted earlier, Laennec and physicians following him have found it useful to divide DALS into subcategories based on subjective impressions of the sounds. This division was motivated by the belief that different sounding DALS reflected different physical events and conditions and, perhaps, different disease states. This seems eminently reasonable, but doubts have persisted about the usefulness of subcategorizing DALS subjectively [Hudson et al (1978)]. In view of the lack of solid objective evidence supporting the diagnostic usefulness of these subdivisions, a nomenclature committee of the American Thoracic Society (ATS) chose to divide DALS into the broadest possible categories, called fine and coarse (see Appendix A).

The goal of this research was to study individual fine and coarse DALS complexes to learn more about their properties and possible mechanisms. This made it necessary to

develop a way to classify an individual DALS waveform in a manner consistent with the subjective criteria used in overall characterization of DALS heard in a breath. A pattern classification method was developed using recorded examples of fine and coarse DALS as a training set (see Figure 1.1). A chest physician had classified each recording as containing DALS that were clearly fine or clearly coarse. Amplitude versus time plots of the sounds were studied, and two measurements made on individual DALS complexes in the plots were found that would separate the two categories objectively. The classification method was successfully tested on further recordings of DALS (see Chapter 3).

The waveforms and the known disease associations of fine and coarse DALS both suggested that coarse DALS might arise in larger airways than fine DALS. If this were true, it was reasoned that an individual coarse DALS complex should be observed over a wider area of the chest wall. To study the surface distribution of DALS, two microphones were applied sumultaneously to the chests of patients in whom DALS were heard using a stethoscope. As shown in Figure 1.2, the outputs of the microphones were plotted so that the association between DALS at the two sites could be studied. Each observed DALS was classified as fine or coarse using the previously developed two-parameter classification scheme. The presence or absence of a measurable DALS at the other site was noted. The results indicated that fine DALS

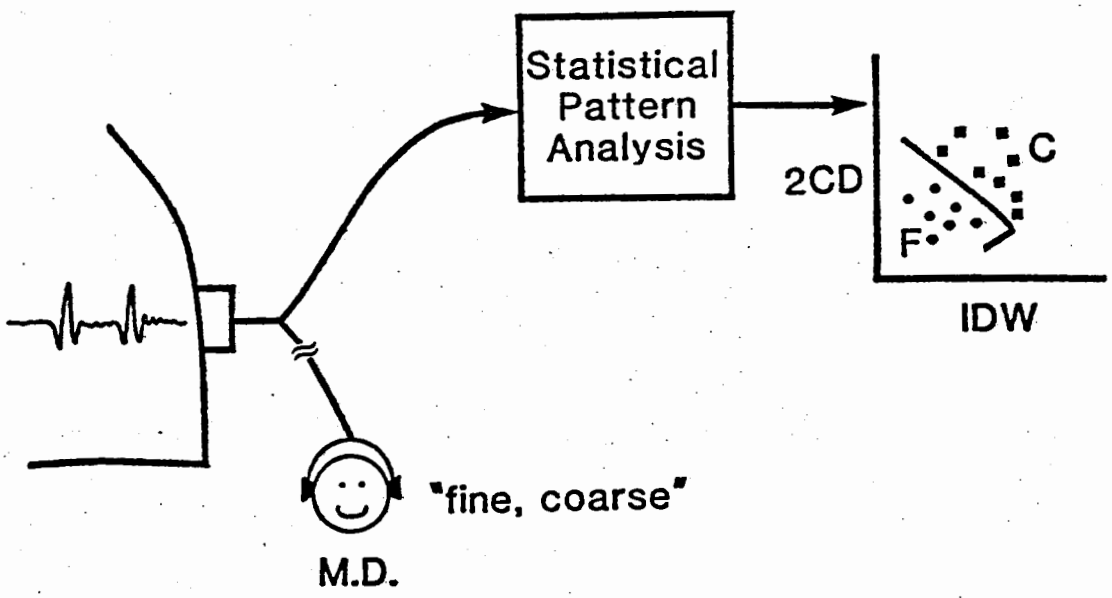

Figure 1.1 - Development of an objective classifier for fine and coarse DALS. A chest physician classified recorded DALS subjectively. The width of the initial deflection (IDW) and the duration of the first two cycles (2CD) were found to be good features for use in objectively reproducing the physician's categorization.

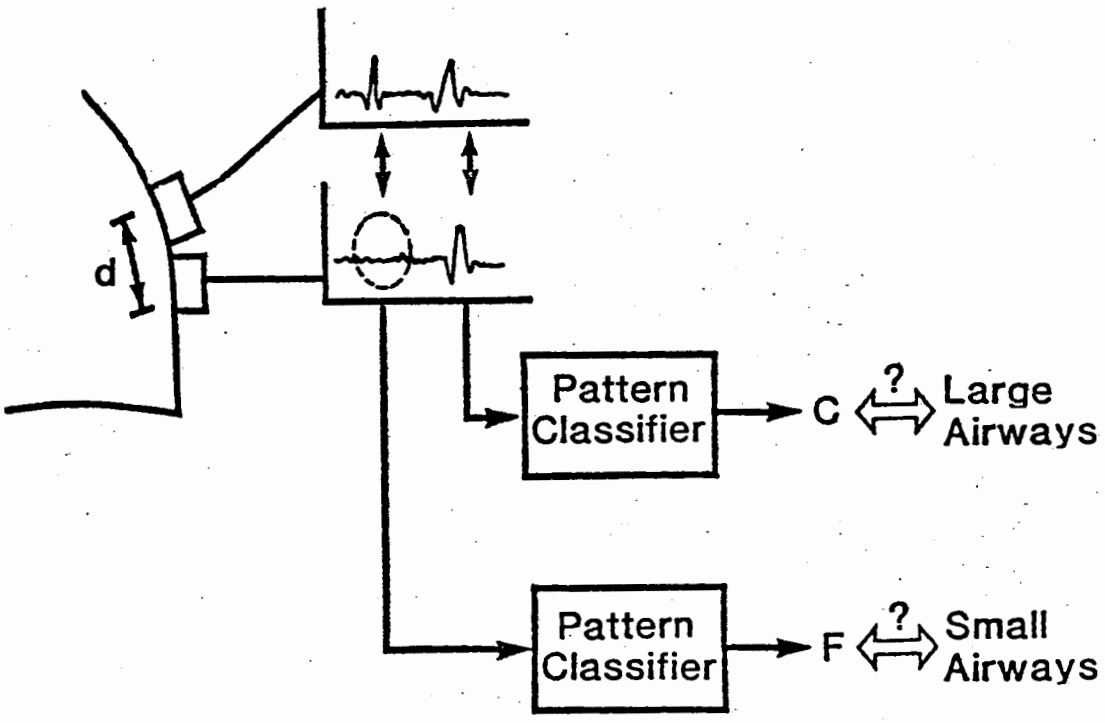

Figure 1.2 - Study of the chest surface distribution of fine and coarse DALS. DALS were observed at two microphones separated by d=6 or 12 cm. Each DALS complex observed at one of the microphones was objectively classified as fine or coarse by waveform measurements. When the two channels were compared, it was noted that a particular DALS usually appeared at both sensors only when it was coarse.

have a narrower distribution on the chest wall than coarse DALS (see Chapter 4).

The observed DALS shape and surface distributions were compared to the predictions of Fredberg's fundamental physical model for the crackle (DALS) phenomenon for a range of parameters believed to correspond to airway diameters varying from 0.5 to 5mm. The model predictions presented in Chapter 5 are consistent with the data of Chapters 3 and 4. Taken together, they support the hypothesis that fine DALS originate in smaller airways than coarse DALS (see Chapter 6).

Chapter 2

Equipment and Methods

2.0 Organization of this Chapter

This chapter consists of descriptions of the equipment and computer programs used in this research. The first section describes the method for transducing the chest wall vibrations and discusses the frequency response and sensitivity calibration of the microphone. Section 2.2 describes the preamplification and filtering applied to the microphone output before tape recording. That section also describes the constant amplitude standardization tone used to provide calibration of tape recordings. In section 2.3 the hardware components of the computer system are described, while the programs used to process the sampled signals are described in section 2.4

2.1 Transduction and Microphone Calibration

The chest wall vibration transducers were two varieties of air-coupled microphones. The first was a commercially produced chest microphone made by Cambridge Instruments (current model number 03040511). This device consists of a piezoelectric element mounted in an aluminum holder that provides the air coupling chamber and a second annular cham-

ber used for vacuum attachment to the chest. The second type of microphone used was a Cambridge Instruments aluminum holder with the piezoelectric element removed and a Sony ECM-30P electret cartridge glued in its place. This alteration was made because of the improved signal-to-noise ratio available with the electret microphone as compared to the high impedance crystal device. Figure 2.1 shows the dimensions of the air coupling chamber.

When we apply such microphones to the chest wall, we are most interested not in the frequency response of the microphone itself, but in the overall response of the transducer. That is, we wish to know the frequency response function that relates the voltage at the microphone's output to a mechanical parameter. For the air-coupled microphones, an appropriate mechanical variable is the force or pressure that would be exerted by the chest wall under the boundary

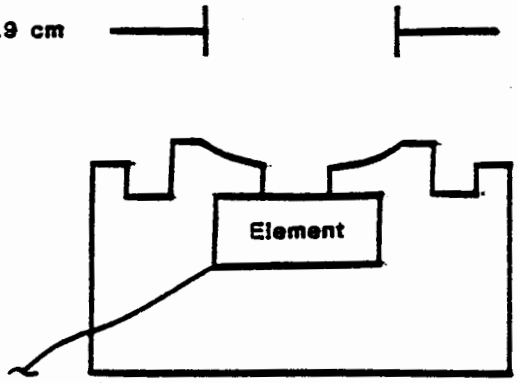

Figure 2.1 - Sectioned drawing of microphone case and air coupling chamber. The volume of the air enclosed between the skin surface and the sensing element is 0.8 cm^3. The surface contact area is 3.3 cm^2.

condition of zero surface velocity, that is, the blocked force or pressure.

If we had detailed knowledge of the mechanical impedances of the chest surface and of the transducer, we could correct for their interaction and derive the blocked force from the microphone's output voltage. There are a number of difficulties with this analytic approach. The air-coupled transducers have a complicated interface with the chest. There is a ring constraining the skin diaphragm that is in contact with the air chamber. Outside of that ring is another ring of skin that is sucked into the vacuum attachment chamber. Modeling this system is difficult since measurements of chest impedance under such constraints have not been reported. Glass and Fredberg [1980] measured the thoracic surface impedance using disk contacts. Their data show dependence on static load and contact area. In view of the complicated viscoelastic nature of soft tissue [Fung (1981)], the disk contact impedance measurements cannot be used to estimate the chest impedance for the the air-coupled microphone contact configuration.

The frequency response of the air-coupled microphone was investigated directly by comparing its output to that of a force gage when both were simultaneously applied to the chest of a normal subject. The force gage output of a Bruel and Kjaer (B-K) Model 8001 impedance head was conditioned by a B-K Model 2635 charge preamplifier for the experiment. The frequency response comparison was made by tape recording

the transducer outputs while the subject produced chest wall vibrations vocally. The tape recorded signals were simultaneously sampled and stored in disk memory. The matched aliasing filters are described in Section 2.3. The two sampled signals were then subjected to cross-spectral and coherency analysis.

The computed transfer function between the two transducers (Figure 2.2(a)) shows how the air-coupled microphone's output compares to the force gage measurement of blocked force. The magnitude squared coherency (MSC) function for the two signals, which ranges between zero and one, was greater than 0.5 between 200 and 1500 Hertz. Outside this range, the MSC dropped rapidly to zero. We should thus ignore as unreliable the parts of the curve below 200 Hz and above 1500 Hertz.

The fall in response above 1 kHz is presumed to be due to the interaction between the mass of the chest wall and the compliance of the air in the coupling chamber. Analysis of this effect is hampered by uncertainty about the effective mass of the chest and the doming of the skin diaphragm into the chamber. The roll-off in low frequency response is believed to be partly due to chest wall induced motion of the microphone case at low frequencies, which partially cancels the compression of the air in the chamber. The remainder of the low frequency roll-off is accounted for by the 2-pole drop in low frequency response of the electret microphone itself between 100 and 200 Hertz.

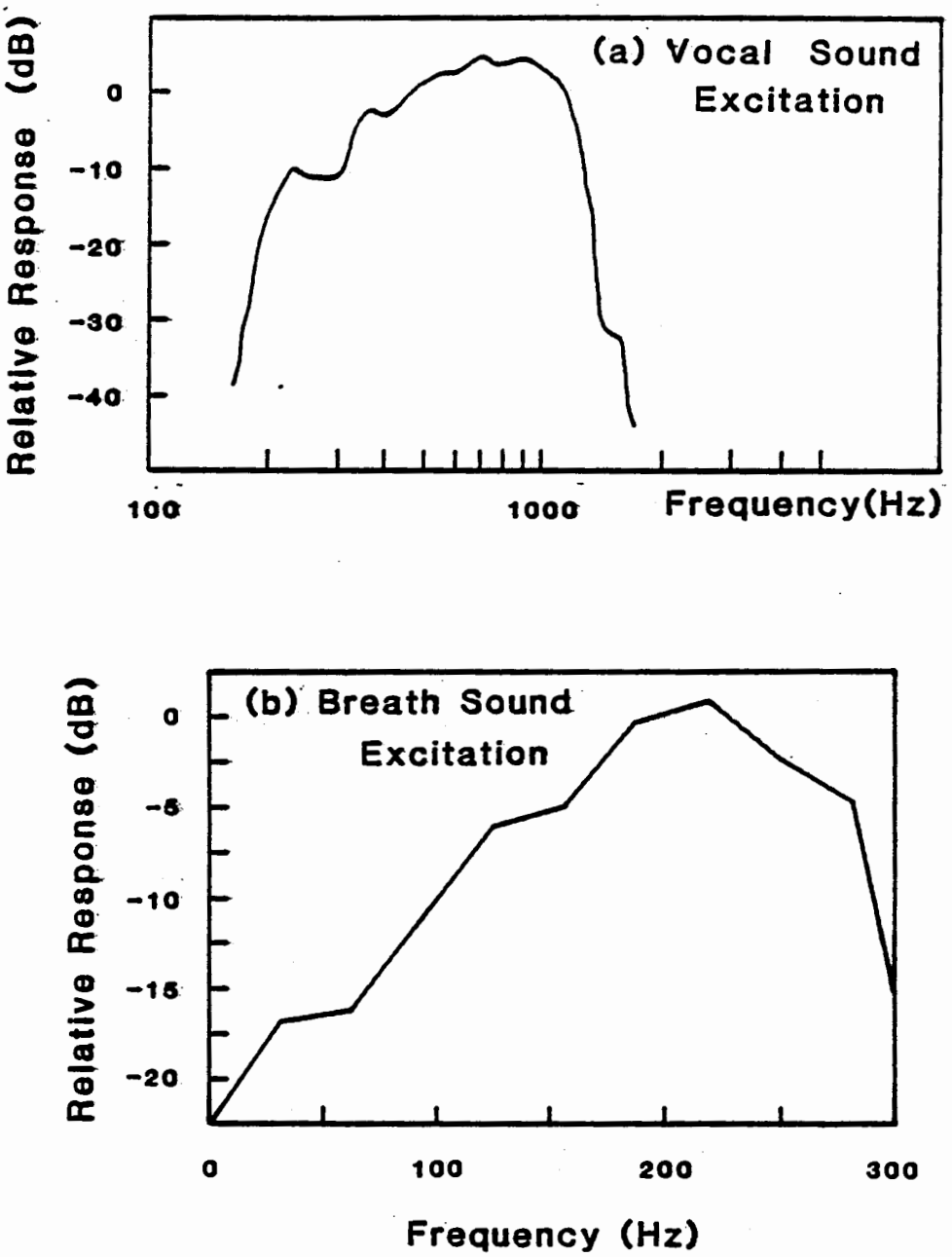

Figure 2.2 - (a) Relative response of the air-coupled microphone compared to the B&K force gage. Transducers were affixed to adjacent chest wall sites and excited by wideband vocalized sounds in a normal subject. (b) A better comparison at low frequencies was obtained using breath sounds as the excitation. Note the 20 dB/decade slope below 200 Hertz.

To further study the low frequency response of the air-coupled transducer, another comparison was made with the force gage using vesicular breath sounds as an excitation. Since the spectral content of normal vesicular sounds is small above 250 Hz, the resulting estimate of transfer function is limited to lower frequencies. The MSC of the transfer function estimate in Figure 2.2(b) was above 0.5 between 40 Hz and 220 Hertz. The dip in response above 220 Hz should be ignored. The significant result is the 20 dB/decade slope of the response below 200 Hertz. Since the force gage itself has a theoretical 20 dB/decade roll-off at low frequency [Fredberg and DeJong, unpublished], it seems reasonable to approximate the response of Figure 2.2(a) as the cascade of a four pole high pass filter at 200 Hz with a four pole low pass at 1000 Hertz.

The absolute sensitivity of the microphones was calibrated using a B-K model 4230 microphone calibrator. This device provides an air chamber in which a constant 1000 Hz pressure variation of 94 dB SPL (1 N/m^2 RMS) is maintained. This device was used along with a second constant tone generated in the preamp to amplitude standardize the transducers, preamps, filters, recording, playback, and analysis equipment as described in the next section.

2.2 Preamps, Filters, Standard Tone, and Recording

Figure 2.3 is a block diagram of the recording, playback, and digitizing systems. This diagram shows each ele-

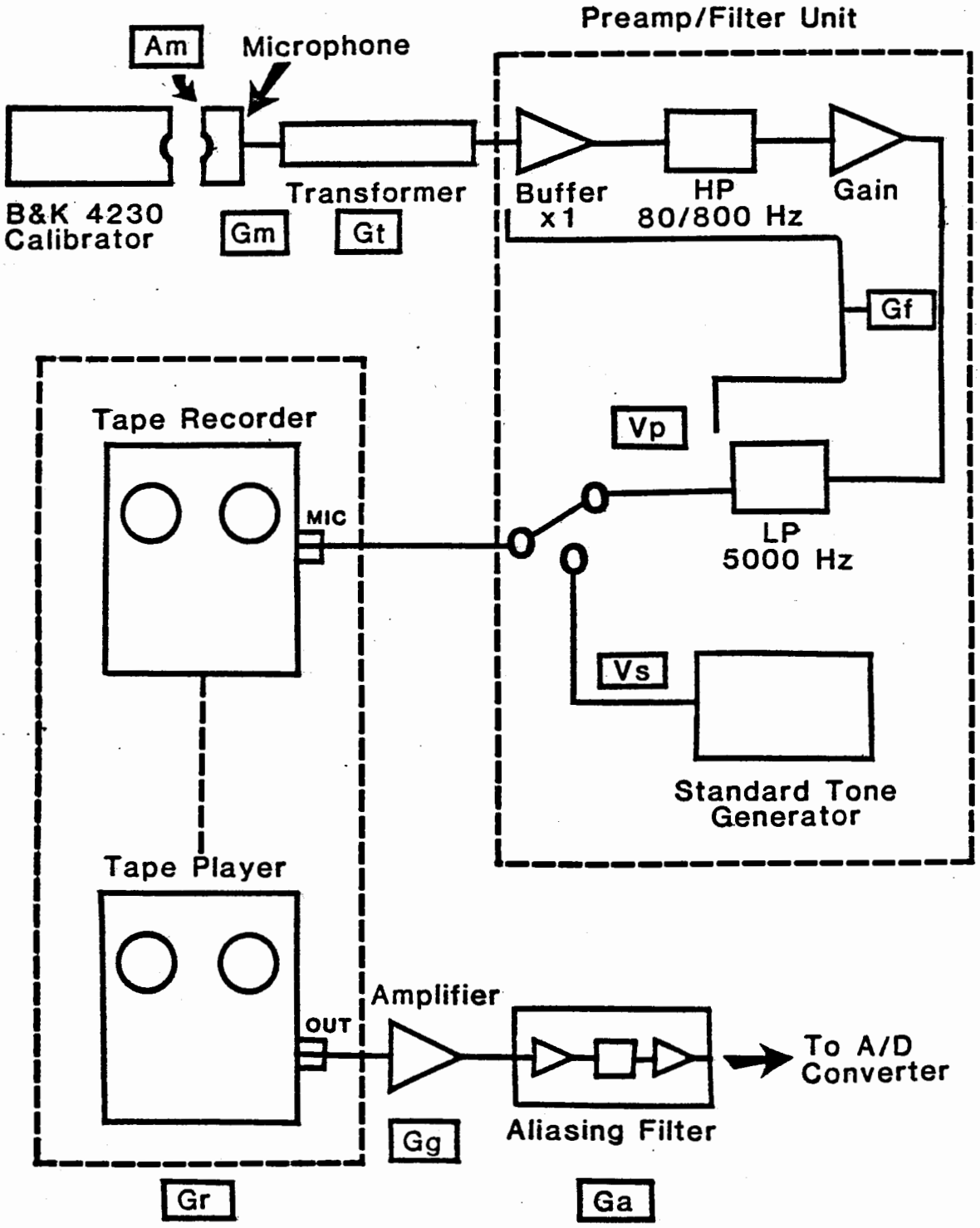

Figure 2.3 - Block diagram of the recording, playback, and digitizing systems. A_m is the acoustic calibrator input amplitude. The labels G_i represent the gain of the various elements. V_p and V_s are the preamp and standard tone output voltages respectively.

ment that processes the microphone signal on its way to being stored on the disk in sampled form. Each element has a transfer function, and each has been assigned a gain in the diagram. The characteristics of each block are discussed first, and then the amplitude calibration scheme is described. The previous section described the microphones and acoustic calibrator, so the following material begins with the matching transformer.

2.2.1 **Matching Transformer** - The Sony ECM-30P electret microphones have an output impedance of 250 ohms. To enhance the signal-to-noise ratio of the amplification system, transformers were used between the microphones and their preamps. These were standard AKG Model MCH-20TS transformers that step up the 250 ohm microphone output impedance to about 9 kohms and boost the output voltage by about 15 dB. There was appreciable variation from unit to unit in the turns ratio, and this required a compensating gain adjustment in the preamps. The frequency response of these transformers was found to be within 3 dB from 10 Hz to over 100 kHz.

2.2.2 **Preamplifier and Filters** - The poor mechanical signal-to-noise ratio at the chest makes it difficult to obtain good recordings of lung sounds. The chest wall vibrations of interest are estimated to range in amplitude from about 4×10^{-8} meter for DALS down to 10^{-9} m or less for

vesicular sounds. These vibrations are summed with the larger respiratory chest excursions, which are on the order of 10^{-2} m and occur at very low frequency. It is thus necessary to high pass filter the microphone's output before amplifying it to avoid preamp saturation.

The preamp/filter units used in this project are shown in block diagram form in Figure 2.3. Low noise, wide bandwidth integrated circuit amplifiers (Signetics NE5534AN) were used to realize the gain elements and filters. The first element is a unity gain buffer that prevents the source impedance of the input from affecting the high-pass filter characteristic. The first filter is a four pole Butterworth high-pass with the -3 dB point of the magnitude of its frequency response at 80 Hz. An alternate setting of 800 Hz was also available. After the high-pass filter is an optional gain element of +20 dB (i.e., times ten). The final filter, which is a four pole Butterworth low pass, had a -3 dB point at 5000 Hz. This filter was introduced to remove high frequency noise that is noticeable when listening to the signal.

In Figure 2.3 the overall gain of the preamp and filters is labeled G_f. This could be trimmed to compensate for variations among the microphones and matching transformers. Two matched transducer channels were required for the surface distribution study described in Chapter 4. They were obtained by exposing the two microphones to the same acoustic stimulus, and then trimming the preamp gains to

provide identical preamp outputs (labeled V_p in the figure).

2.2.3 **Standard Tone Generator** - It is inconvenient to place the acoustic calibrator on the microphone each time the recording level is adjusted. The level may need to be changed at different chest wall sites or for different breathing maneuvers. Therefore, an electrical standardization tone is generated, which is a 1000 Hz sine wave signal whose amplitude is regulated by comparison to a temperature stabilized voltage reference device. When a button on the preamp panel is depressed, the standard tone, V_s, is substituted for the preamp output. The voltage V_s is set so that the tone corresponds to a pressure disturbance in the microphone chamber of 1 μbar (0.1 N/m^2) RMS.

2.2.4 **Tape Recording** - Standard audio recorders were used for all recordings. These were operated at speeds of 3.75 or 7.5 in/sec using high output, low noise tape such as Scotch 206, Ampex 456, or Maxell UD-50. Since the lung sounds are limited to a band of 80-5000 Hz, the frequency response of nearly any recorder is adequate if it is flat in that band. However, the dynamic range of the signals can be 60 dB or more, and this requires high quality audio recorders and tape. Recorders used in this work were Tandberg models 3000 and 3300X, Teac models 2300 and 3340, and Dokorder model 1140.

The standardization tone accounts for the several gain

factors present in the recording/playback process. These are lumped into constant G_r in Figure 2.3. This element is followed by a general purpose amplifier, G_g, used to increase the level before the aliasing filter described below.

2.2.5 **Aliasing Filter** - The signal to be digitized must be low-pass filtered before sampling to avoid aliasing errors [Oppenheim and Schafer(1975)]. This was accomplished using a Precision Filters System 416. This unit provides multiple filter channels with remotely controlled corner frequencies. Each filter is preceded by a gain element (x1 to x50) and followed by a gain (x1 to x20). Splitting the gain allows the best combination of signal-to-noise ratio and overload protection. The filters in the System 416 have a low-pass characteristic that is optimized for time domain response. They are 6-pole, 6-zero active filters with an equiripple phase response that is linear within 2.5° out to 1.4 times the cutoff frequency. Phase matching between channels is guaranteed to be within 1° (typically 0.25°) from DC to the cutoff frequency. The amplitude characteristic has 0.2 dB pass band ripple and 70 dB stop band attenuation beyond 3.2 times the corner frequency. The aliasing filters are thus of very high quality and allow precise comparisons between two channels.

2.2.6 **Amplitude Calibration Scheme** - All the elements having been described, the calibration scheme can be detailed. The voltage at the analog-to-digital converter (ADC) input, V_c, per unit of acoustic input to the microphone, A_m, is given by:

$$\frac{V_c}{A_m} = (G_m G_t G_f)(G_r G_g G_a) = \alpha \times \beta = \gamma \qquad (2\text{-}1).$$

When the standard tone, V_s, is introduced,

$$\frac{V_c}{V_s} = (G_r G_g G_a) = \beta \qquad (2\text{-}2).$$

The procedure for producing calibrated recordings is to first record on tape the acoustic calibration signal followed by a standard tone at the same recording level. Subsequently, by recording the standard tone each time the recording level is readjusted, the calibration can be maintained. When the tape is analyzed, the amplitude of the acoustic calibrator signal is measured, yielding the constant γ. The amplitude of the following standard tone is measured, yielding β, from which α can be calculated by equation (2-1). Succeeding standard tones each give a new β, from which a new γ can be calculated, constant α remaining the same.

2.3 Computer System Description

The computer system used in this project is located in the research lab of the Pulmonary Department at Faulkner Hospital. Figure 2.4 shows the components of this system.

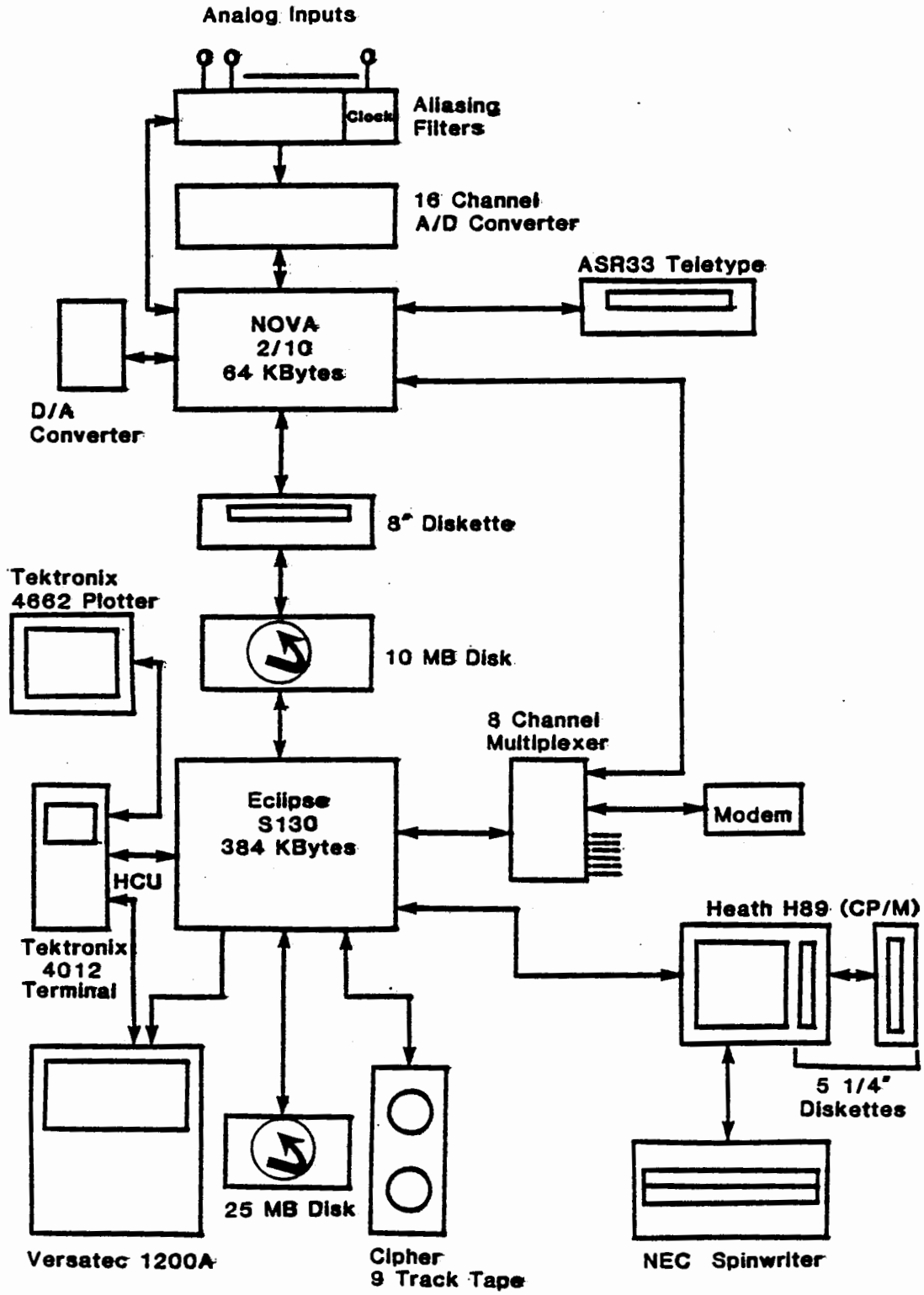

Figure 2.4 - Block diagram of computer system and peripheral devices.

Only a brief description is given here of the components that might affect results.

The analog signals to be analyzed arrive at the ADC from the aliasing filter, which was described in Section 2.2.5. The ADC has a multichannel multiplexer with differential inputs. The conversion yields a 12-bit digital number. The maximum sampling rate is about 30,000 points per second for one channel or 15,000 points per second for two channels. This rate is limited by disk memory access time rather than converter speed. The ADC is interfaced to a Data General Corp. (DGC) NOVA 2/10 minicomputer in a direct memory access mode.

The NOVA serves as a satellite processor to a larger system based on a DGC Eclipse S130 computer. The two processors communicate both by using a serial data link and by passing sampled data and other information in jointly accessible areas of a 10 megabyte moving head disk memory. This scheme frees the Eclipse from tending the ADC, which imposes severe response-time constraints. The Eclipse is then free to run a multi-user operating system. Both the NOVA and Eclipse are 16-bit word length processors. The NOVA has 64 kbytes of main memory, while the Eclipse has 384 kbytes. The Eclipse is also equipped with floating point arithmetic hardware.

Several other devices support the Eclipse. The graphical display devices used in this work include a Tektronix 4012 direct view storage tube terminal, a

Tektronix 4662 interactive digital plotter, and a Versatec 1200A electrostatic printer/plotter. A Heath/Zenith H89 system based on the Z-80 microprocessor was used to produce this document on an NEC Spinwriter.

2.4 Digital Signal Processing Programs

Programs were written in DGC FORTRAN IV, FORTRAN 5, and assembly language. Wherever possible, standard programs were used. Several elements of the I.E.E.E. digital signal processing package written in FORTRAN were modified as necessary and used. Each program was tested for accuracy by comparing results from test cases supplied with the package. Specific programs are described briefly here. For detailed descriptions and listings, the reader is referred to the I.E.E.E. Press book describing the whole set of programs [Digital Signal Processing Committee, eds.(1979)]. All program name references in section 2.4 refer to that book.

2.4.1 **Discrete Fourier Transforms** - DFT calculation was necessary for spectral estimation, coherency analysis, transfer function estimation, and convolution. Two different sets of fast Fourier transform (FFT) subroutines from the I.E.E.E. package were used.

When FFTs of two real waveforms were needed for coherency and transfer estimates, an FFT subroutine that accommodates a complex input sequence was used (FFT842). This allowed two real DFTs to be calculated simultaneously

so as to cut computation time in half. The convolution program used a real input, complex output FFT subroutine package (FAST).

2.4.2 **Coherence and Cross Spectral Estimation (CCSE)** - The CCSE package can be used to estimate various second-order statistics between two real sequences. The auto- and cross-power spectral densities are calculated by (1) segmenting the available data, (2) multiplying the segments by a smooth weighting function, (3) calculating DFTs as discussed in section 2.4.1, and (4) averaging the raw power spectral estimates from the N segments of p points each. The results are the spectral estimates $\hat{G}_{xx}(k)$, $\hat{G}_{yy}(k)$, and $\hat{G}_{xy}(k)$. The estimate of the transfer function between the two signals is then

$$\hat{T}_{xy}(k) = \frac{|\hat{G}_{xy}(k)|}{\hat{G}_{xx}(k)} .$$

The estimate of magnitude squared coherency is

$$\hat{C}_{xy}(k) = \frac{|\hat{G}_{xy}(k)|^2}{\hat{G}_{xx}(k)\ \hat{G}_{yy}(k)} .$$

2.4.3 **Fast Convolution** - The FASTFILT package was used in the DALS simulation to filter predicted waveforms. This package implements the overlap-add method [Stockham(1966),

Helms(1967)] and is designed to efficiently process data from disk files. The original I.E.E.E. programs process fixed point data. They were modified to work with floating point signals generated by the DALS simulation.

Chapter 3

Objective Classification of Fine and Coarse DALS

3.0 Organization of this Chapter

This chapter describes the development of the method for classifying fine and coarse DALS using measurements on amplitude versus time plots. Section 3.1 further describes the historical background and introduces the statistical pattern recognition methodology used to calculate the classification curve. Section 3.2 describes the method more rigorously and tells how the data sets used in deriving and testing the classifier were collected. Section 3.3 presents the results, including statistical tests of the separation between the clusters. Section 3.4 discusses limitations and generalization of the method.

3.1 Introduction

Laennec originally classified rales into two main categories, which he called "rale humide ou crepitation" and "rale muquex ou gargouillement". Translated, these are humid rales or crepitations, called fine today, and mucous or gurgling rales, called coarse today. Since he had no way of plotting, recording, or analyzing the sounds, Laennec documented their nature by comparing them to other naturally

occurring sounds. For example, his crepitations were said to sound like the noises made by salt in a very hot frying pan.

As noted in Chapter 1, descriptions of DALS have remained subjective until very recently. Cabot and Dodge [1925] demonstrated differences in frequency content between breaths containing DALS they called fine and coarse, but they did not propose a method for objective classification. In fact, any method based on analyzing the frequency content of whole breaths would be hampered by the occurrence of fine and coarse DALS in the same breath at one site in some patients. This problem could be solved by a technique that focuses on individual DALS. This has been made possible by modern high speed chart recorders or computer-based waveform analysis [Murphy, Holford, and Knowler (1977)].

Given the ability to isolate individual DALS complexes, a method was needed for reproducing the fine/coarse classification made by stethoscope, but using measurements obtained from plots of individual DALS. The techniques of statistical pattern recognition have been used with success in similar problems, especially when it was desired to reproduce natural categorizations. A classical example is Fisher's classification of three different species of irises by measurements made on their parts [Fisher (1936)].

The basic method is to select a set of prototypical examples of each class, which is often called the training set. If possible, a set of measurements is found that will

allow the training set data to be correctly classified. The method is then tested using different examples (the test set). Usually measurements, or features, are selected one at a time based on their helpfulness in separating the classes. Given a particular set of features, an entity to be classified is measured and assigned a set of feature values. Thus each entity to be classified can be represented by a point in a "feature space." If a significant set of features has been chosen, the points for entities in a particular class are grouped together in the feature space, and are thus called a cluster.

One method of classifying test set points is to plot their locations in the feature space and to measure the distance to each training set cluster. The test point is then classified as belonging to the "nearest" of these clusters, nearness being measured by some distance metric that must be defined. This minimum distance method was used in the fine/coarse classifier to be described.

It is often not good enough simply to measure the linear distance between a test point and the clusters. Classification performance may be improved by applying different weights to distances along the various feature axes, the weights being derived from statistical analysis of a cluster's variability in each direction. Such a method was used in the fine/coarse classifier. Section 3.2 describes these mathematical methods and describes the selection of DALS to train and test the classifier.

3.2 Methods and Materials

When DALS are present in lung sound tracings, they can nearly always be identified as individual discrete events. That is, they are usually few enough that the time spacing between them is long compared to their individual duration of 10-20 msec. DALS for the training and test sets were obtained from the tape recorded lung sounds of patients with a variety of lung diseases. Typical complexes were chosen from breaths that had been sampled and viewed on a CRT screen. Such complexes were of relatively large amplitude so that their characteristics could be measured unambiguously. While relatively few examples were used as training set points, the resulting classifier performed quite well on test cases.

3.2.1 **DALS Measurements** - Several features were evaluated for their suitability in classification. The two that provided the most significant classification and were easiest to measure have been named the initial deflection width (IDW) and the two cycle duration (2CD). Figure 3.1 illustrates the measurement of these parameters. Other possible features evaluated were (1) the peak of a smoothed spectral estimate, (2) the frequency at which the spectrum dropped to 20dB below its peak value, and (3) the ratio of the amplitudes of the initial deflection and the maximum

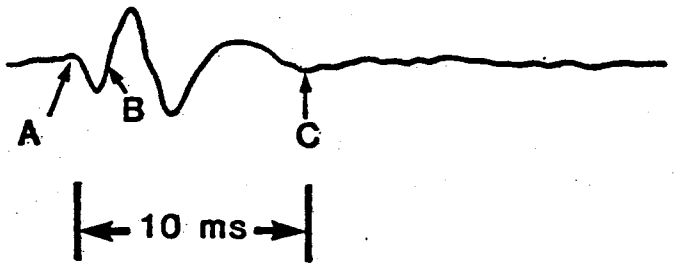

IDW - Time from A to B
1.2 ms for this DALS

2CD - Time from A to C
8.2 ms for this DALS

Figure 3.1 - Measurement of waveform features IDW and 2CD.

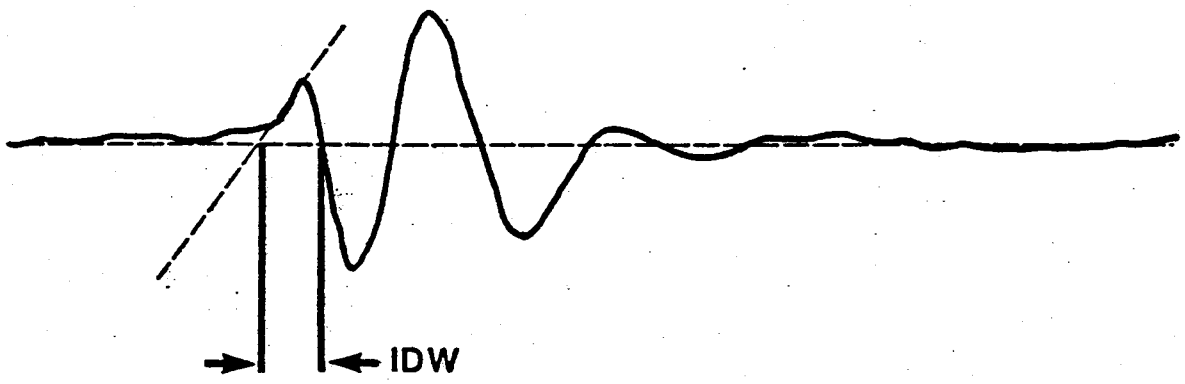

Figure 3.2 - Measurement of IDW in the presence of wandering baseline. The reference point for IDW measurement is obtained by extending a tangent from the most rapid part of the initial deflection to its intersection with the zero line.

deflection of the complex. Scatter plots were made taking these features in pairs, and correlation calculations were made for each pair. The pair (IDW,2CD) was chosen because of its performance and the relative simplicity of the feature measurement process. The two features do not require a spectral estimate, and they can be measured from simple amplitude versus time plots.

The IDW is the time between zero crossings of the first deflection of the DALS complex. In a few cases this is difficult to measure. Since the DALS are generally superimposed upon background vesicular lung sounds, there is sometimes a wandering baseline to confuse the zero crossing identification. When the baseline was obviously wandering, the zero crossings were taken as baseline crossings instead. A second difficulty sometimes encountered is the rounded knees on the beginning of the first upstroke or downstroke of the complex. This effect makes it difficult to know where the zero crossing actually is. The procedure adopted was to extend a tangent from the most rapid part of the first deflection to the baseline and identify the intersection as the zero crossing. This method is shown in Figure 3.2.

The 2CD is measured from the first IDW point to the point where the DALS waveform has completed two complete cycles of variation. This was chosen as a measure of complex duration since nearly all observed DALS have at least two complete cycles, but in many cases the background

variations make it difficult to identify the end of the complex.

3.2.2 Training Set - A research technician selected examples from a data base of clinical recordings that included DALS from ambulatory and hospital patients as well as from industrial workers. A chest physician experienced in lung sound categorization reviewed the recordings and classified the DALS from each patient as fine or coarse. Only clear examples were chosen for inclusion in the training set. DALS were selected from these tapes and measured as described in the preceding section. At the time of processing and measurement, the physician's classification was unknown. This method was adopted in an attempt to minimize bias in the selection and measurement processes. Plots of the resulting set of six fine and six coarse DALS are given in Figures 3.3(A)-3.3(F) and 3.4(A)-(F).

3.2.3 Test Set - DALS recorded and classified by other investigators were used as an initial test set. The examples were taken from teaching tapes that were available from Humetrics Corporation and from the American College of Chest Physicians. Four coarse and two fine DALS were obtained from these tapes. These are shown in Figures 3.5(A)-3.5(F). Further test examples were selected from clinical recordings after the independent examples had been processed.

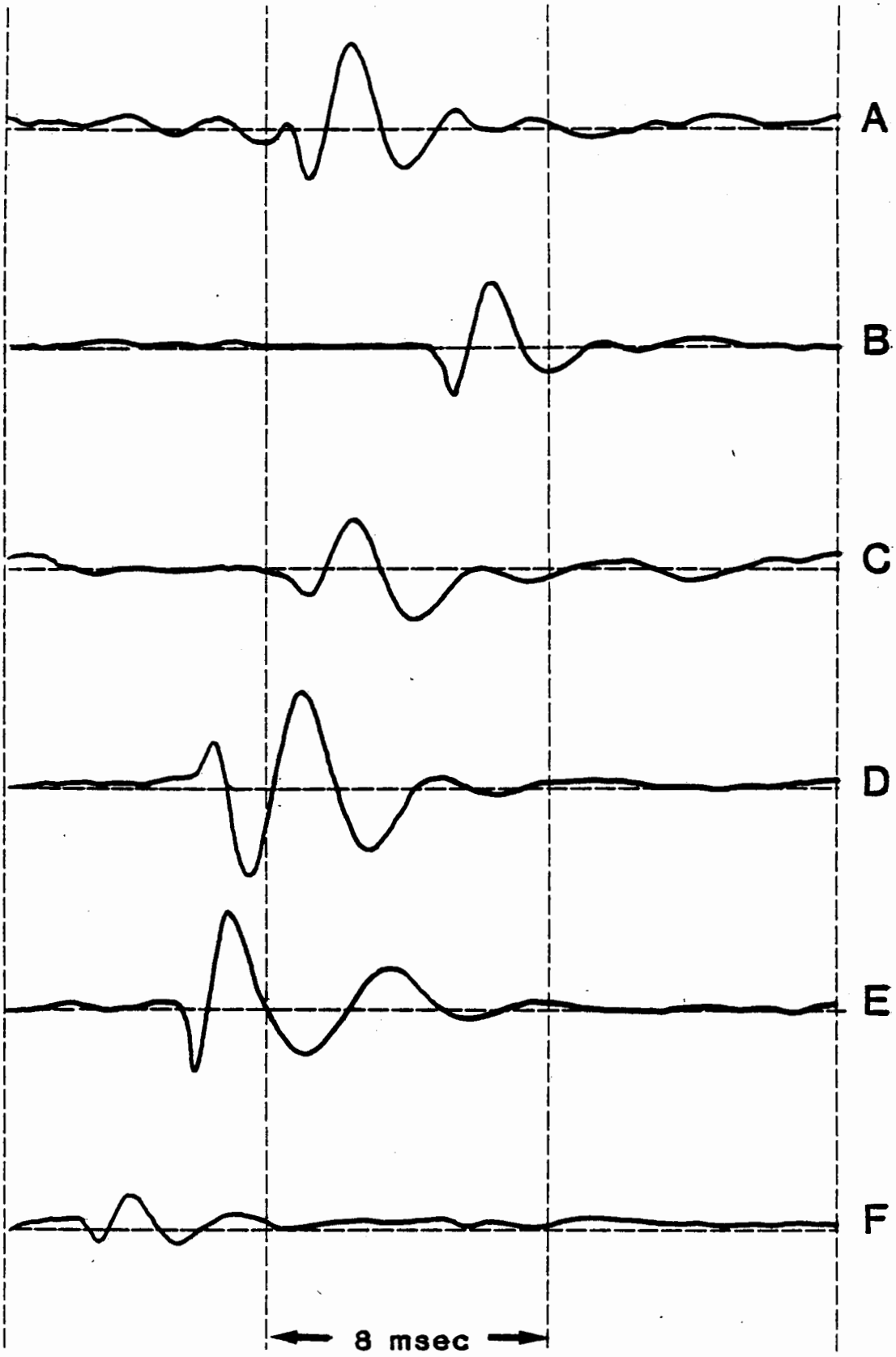

Figure 3.3 - Training set of fine DALS.

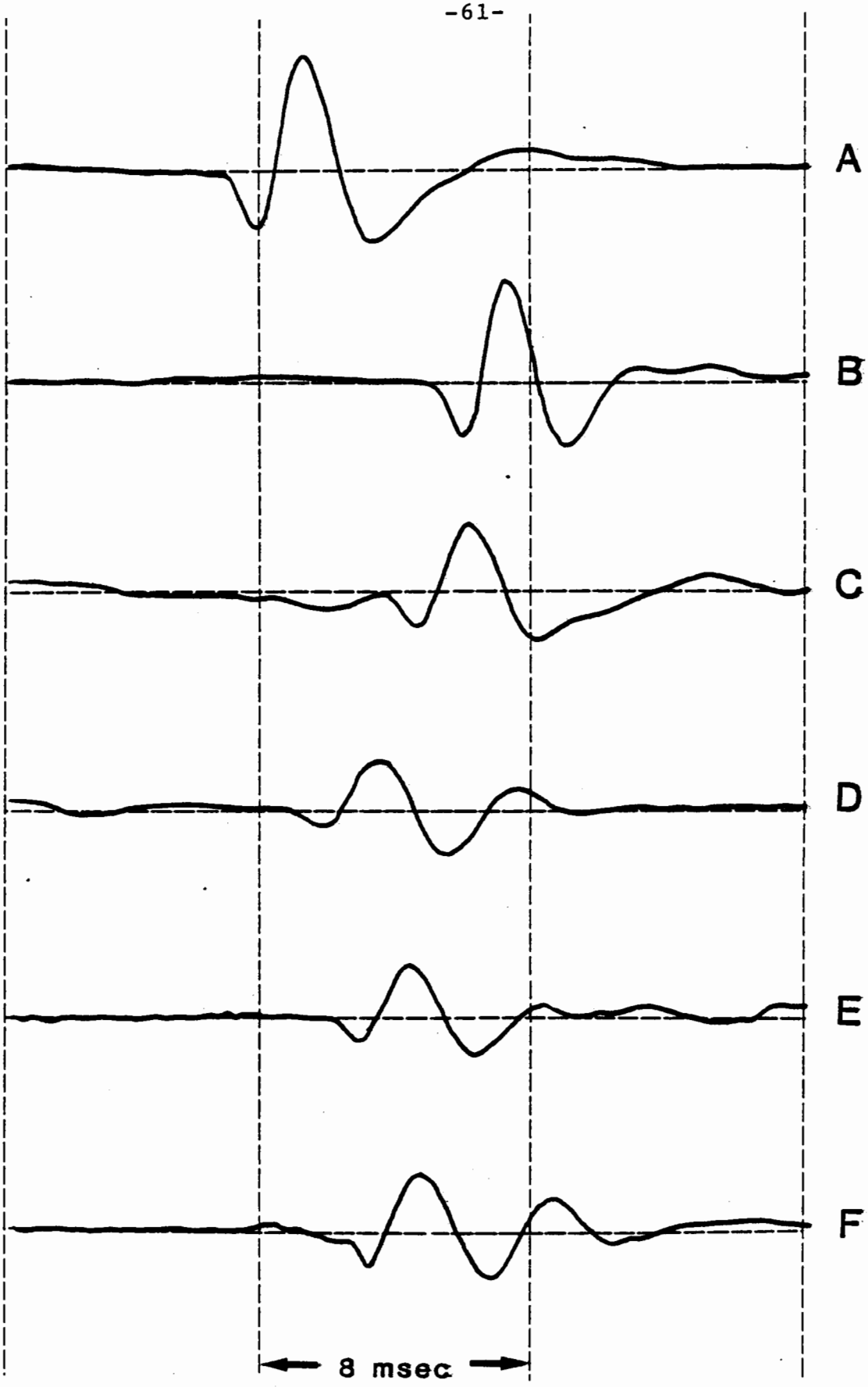

Figure 3.4 - Training set of coarse DALS.

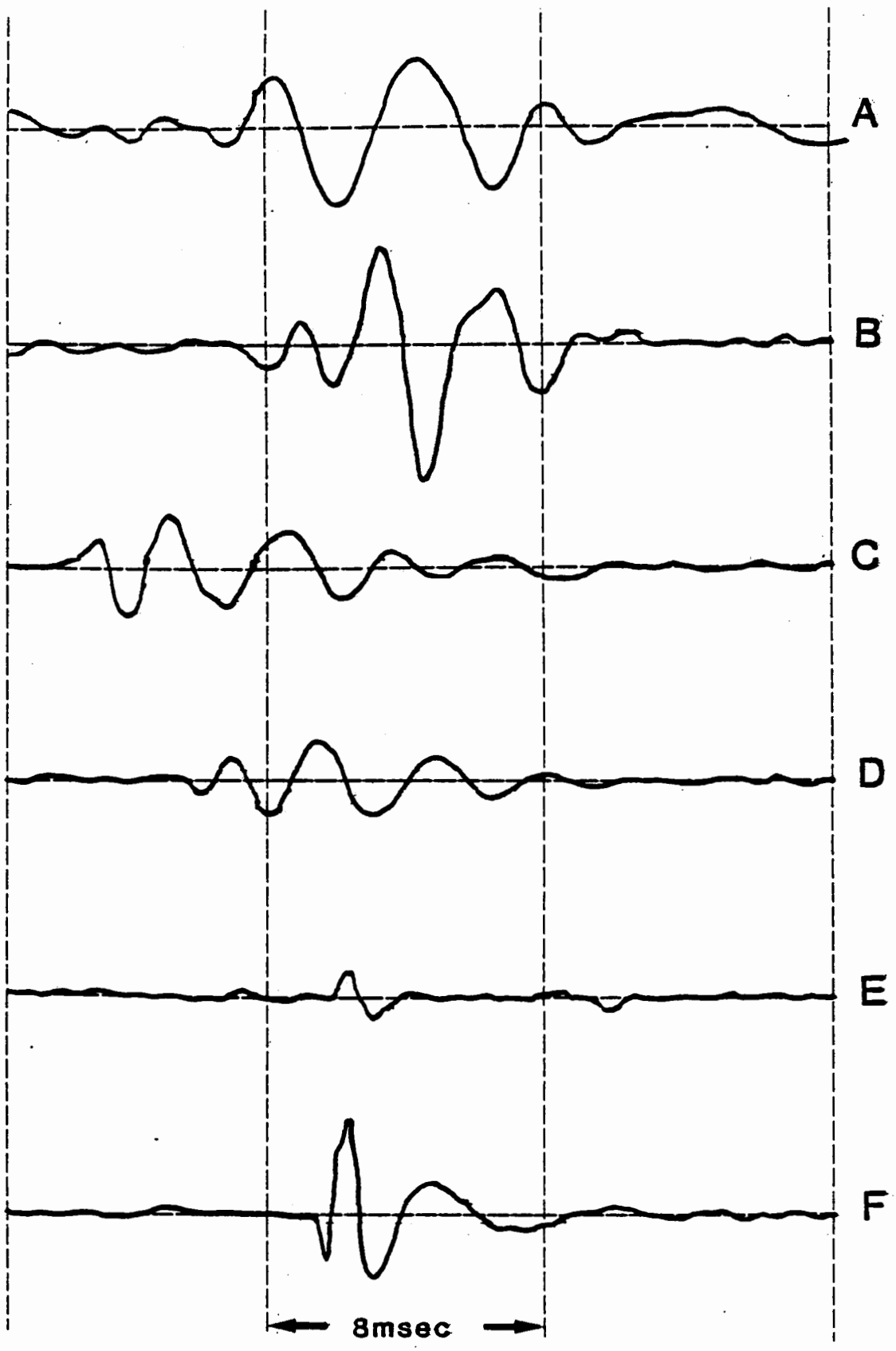

Figure 3.5 - Test set of fine and coarse DALS from teaching tapes. Examples A, C, D, and E are coarse. Examples B and F are fine.

3.2.4 **Minimum Distance Classification** - As mentioned in the introduction to this chapter, the basic idea of minimum distance classification is to assign a new data point to a category by measuring the distance from the data point to each existing cluster. To do this, one must define how the distance is to be measured, and this section gives that definition along with an example that illustrates the properties of the chosen distance metric.

A simple way to measure the distance to a cluster would be to use a ruler. If the feature space had more than three dimensions, this would have to be accomplished mathematically. In the case where the features are statistically independent and have the same variance, this Euclidean distance metric is adequate. When these conditions are not met, the Euclidean measure can be improved upon.

Figure 3.6 illustrates the problem. Suppose we wish to classify individuals as male or female by measuring their height. If we know the distribution of heights for the two classes in the population of interest, we could classify the subject as female when the measured height is arithmetically closer to the mean of the female distribution than to the mean of the male distribution. The figure shows how this might work. Suppose the males have a higher mean height and a larger variance in height. An unknown subject of height 67 inches would be classified as female by a Euclidean metric since the distance to the mean of the female cluster is only 2 inches. But we can easily see that classifying

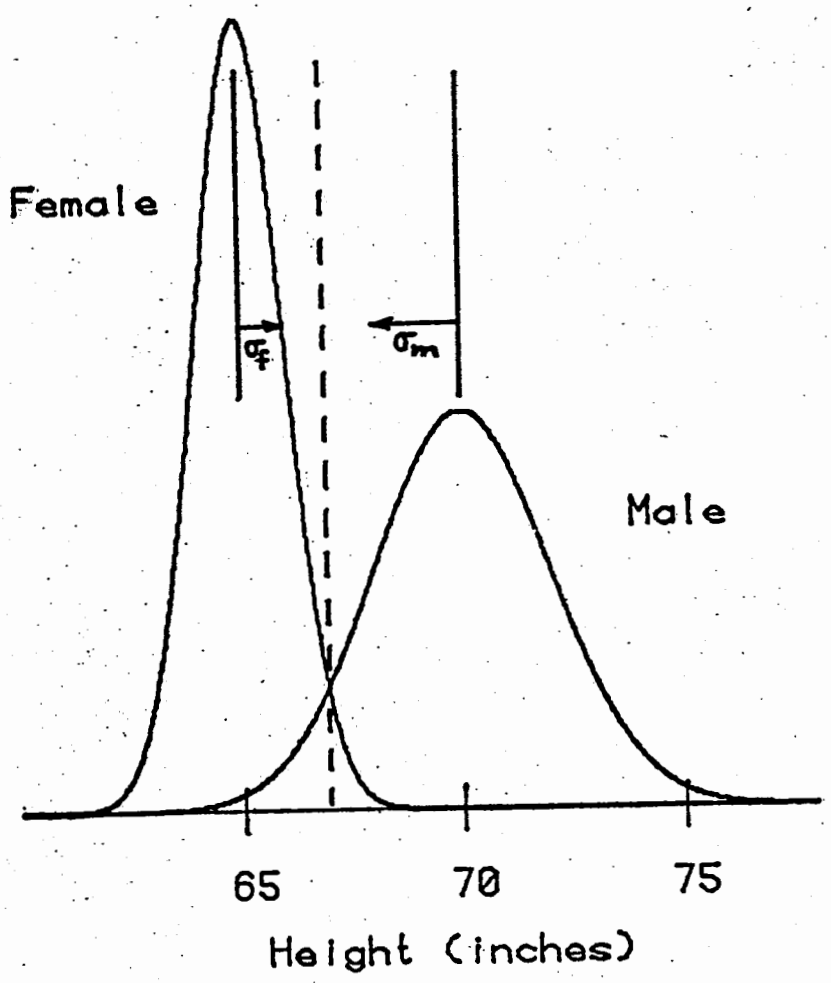

Figure 3.6 - One-dimensional illustration of methods for distance measurement. Suppose we wish to categorize an unknown subject as male or female based on their height. We know the population distributions of height and their standard deviations σ_f and σ_m. We might classify an individual who is 67 inches tall as female because 67 is closer to the peak of the female distribution at 65. However, we obtain a lower probability of error by classifying the unknown as male because the distribution of male heights has a larger standard deviation.

the subject as male would yield a lower probability of error since more area of the tail of the male distribution is cut off by the line representing the height of the unknown. Our answer would be better if we were to measure the distance to a cluster in units of the standard deviation of that cluster. The unknown is about 1.5 standard deviations from the male cluster and 2 standard deviations from the female cluster. Thus we need to measure distances using a ruler whose scale is adjusted for each cluster.

This example illustrates the one dimensional case of the method to be detailed below. Although matrix algebra is used to represent the rules for multidimensional cases, the fundamental idea remains of measuring distances from a cluster based on the known or estimated variability of the cluster. In the multidimensional case the mean of the cluster becomes a mean vector, and the variance becomes a covariance matrix.

Suppose there are k classes to which an unknown point might be assigned. The minimum distance method is to measure the distance, D^2, to each cluster and to assign the point to class i when

$$D_i^2 = \min \{D_1^2, \ldots, D_k^2\} \qquad (3\text{-}1).$$

Each unknown point is represented by a set of feature measurements that we can denote as a vector $\underline{X}$. The mean vector for each cluster is then $\bar{\underline{X}}_i$, and the covariance matrices are S_i. The distance measure is

$$D_i^2 = (\underline{X} - \bar{\underline{X}}_i)^t \, S_i^{-1} \, (\underline{X} - \bar{\underline{X}}_i) \qquad (3\text{-}2).$$

D_i is called the Mahalanobis distance [Mahalanobis (1936), Duda and Hart (1973)]. In the case of the multivariate normal distribution, the contours of constant probability density are hyperellipsoids of constant Mahalanobis distance to the mean point of the distribution.

Specializing the discussion to two dimensions with the classes being fine and coarse DALS, the decision rule expressed by equation (3-1) becomes:

$$\text{DISCR} = (\underline{X}-\underline{\bar{X}}_F)^t S_F^{-1}(\underline{X}-\underline{\bar{X}}_F) - (\underline{X}-\underline{\bar{X}}_C)^t S_C^{-1}(\underline{X}-\underline{\bar{X}}_C) \begin{matrix} C \\ > \\ < \\ F \end{matrix} 0 \qquad (3\text{-}3).$$

That is, when DISCR is greater than zero, the point is further from the fine cluster, and we classify it as coarse and vice-versa. For more details on the method, the reader is referred to books on pattern recognition [Duda and Hart (1973)].

3.3 Results

3.3.1 **Derivation of Discriminant Curve** - The feature measurements on the training set waveforms numbered F1 through F6 [Figs. 3.3(A)-(F)] and C1-C6 [Figs. 3.4(A)-(F)] are listed in Table 3.1. The table also shows the sample mean vectors and sample covariance matrices for the two classes. As a first step, the nature and separation of the clusters were tested statistically.

Class Fine	IDW	2CD
F1	1.0	5.1
F2	0.9	5.3
F3	1.2	6.2
F4	0.9	6.4
F5	0.7	7.5
F6	0.8	5.6

$$\overline{X}_F = \begin{pmatrix} .917 \\ 6.02 \end{pmatrix}$$

$$S_F = \begin{pmatrix} .03 & -.06 \\ -.06 & .78 \end{pmatrix}$$

Class Coarse		
C1	1.4	13.0
C2	1.2	9.0
C3	1.2	11.6
C4	1.5	8.0
C5	1.2	7.2
C6	1.0	7.1

$$\overline{X}_C = \begin{pmatrix} 1.25 \\ 9.32 \end{pmatrix}$$

$$S_C = \begin{pmatrix} .03 & .16 \\ .16 & 6.0 \end{pmatrix}$$

Table 3.1 - Feature measurements for the training set DALS. $\overline{X}_C$ and $\overline{X}_F$ are the mean vectors. S_F and S_C are the covariance matrices.

The hypotheses that the fine and coarse clusters did not have differing mean values of IDW and 2CD were examined using Student's t-test [DeGroot (1975)]. The equal mean hypothesis can be rejected at the 99% confidence level for the IDW values and at the 98% confidence level for the 2CD values when it is assumed that the data are normally distributed with unknown and unequal variances. The F-test was used to test the hypotheses that the variances of the fine and coarse groups were the same along the two axes. This hypothesis could be rejected for the 2CD values at the 95% confidence level. The equal variance hypothesis could not be rejected for the IDW data (p=.25). Going back to the t-test for differing means of IDW, assuming equal variances improves the confidence in rejecting the equal mean hypothesis to 99.9%.

Figures 3.7 and 3.8 show the fine and coarse training set measurements plotted in the IDW-2CD plane. The crosses represent the mean point for each cluster. Superimposed on each set of points are three ellipses that represent contours of equal Mahalanobis distance as defined by equation 3.2 for D^2=5,7, and 9 in each case. The equations for the ellipses were calculated based on equation (3-2) and the values in Table 3.1. These give:

$$D_F^2 = 39.4(IDW)^2 - 108(IDW) + 5.88(IDW)(2CD) - 23.4(2CD) + 1.50(2CD)^2 + 120 \quad (3-4),$$

$$D_C^2 = 37.2(IDW)^2 - 74.8(IDW) - 1.95(IDW)(2CD) - 1.15(2CD) + 0.192(2CD)^2 + 52.1 \quad (3-5).$$

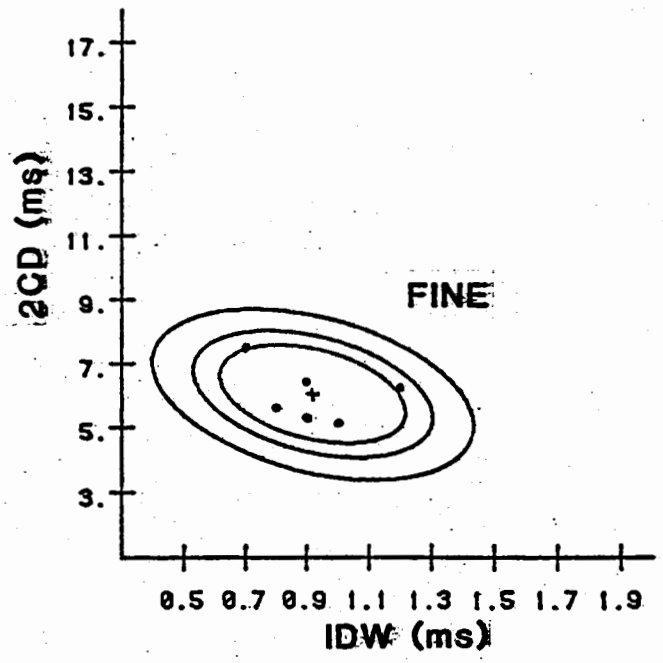

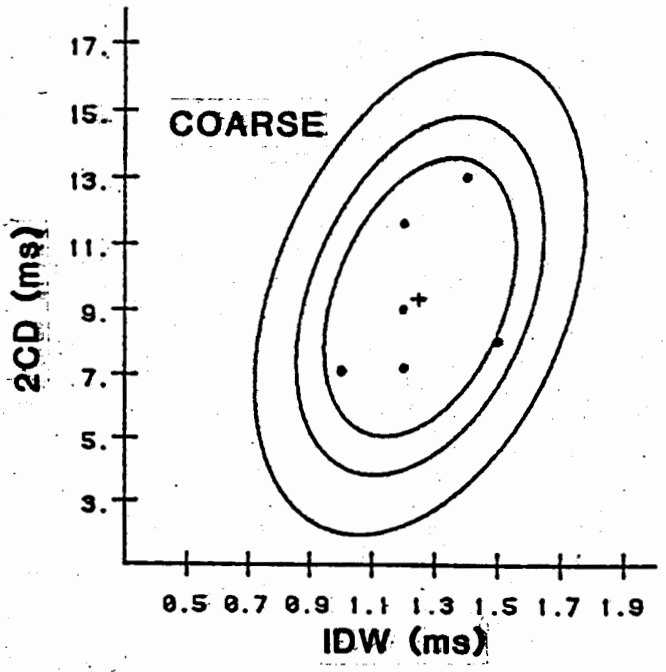

Figures 3.7 and 3.8 - Location of fine and coarse training set DALS in the IDW/2CD plane. Ellipses are contours of equal Mahalanobis distance from the mean point (+) for distances of d^2=5,7, and 9.

The discriminant line defined by equation (3-3) is the locus of all points that lie at equal Mahalanobis distance from the two clusters, that is, where $D_F^2 = D_C^2$. We could construct the discriminant graphically by plotting many contours of constant D^2 for the two clusters, marking the intersections, and then connecting them. This procedure is illustrated in Figure 3.9 where two sets of D^2 contours and their intersections are shown. We can derive an equation for the resulting curve by equating (3-4) and (3-5) and solving for a relation between 2CD and IDW. This results in the equation for a hyperbola:

$$2.26(IDW)^2 - 32.9(IDW) + 7.83(IDW)(2CD) - 22.3(2CD) + 1.31(2CD)^2 + 67.9 = 0 \qquad (3\text{-}6).$$

The resulting classification curve is shown in Figure 3.10 along with the training set points. Note that one of the fine training set points falls on the wrong side of the discriminant curve.

3.3.2 <u>Testing the Classifier</u> - The feature measurements on the test set waveforms (Figs. 3.4(A)-(F)) obtained from lung sound teaching tapes are listed in Table 3.2. Figure 3.11 shows these test points and the additional test points obtained from clinical recordings in relation to the discriminant curve. All are correctly classified. For completeness, Figure 3.11 also includes the training set points.

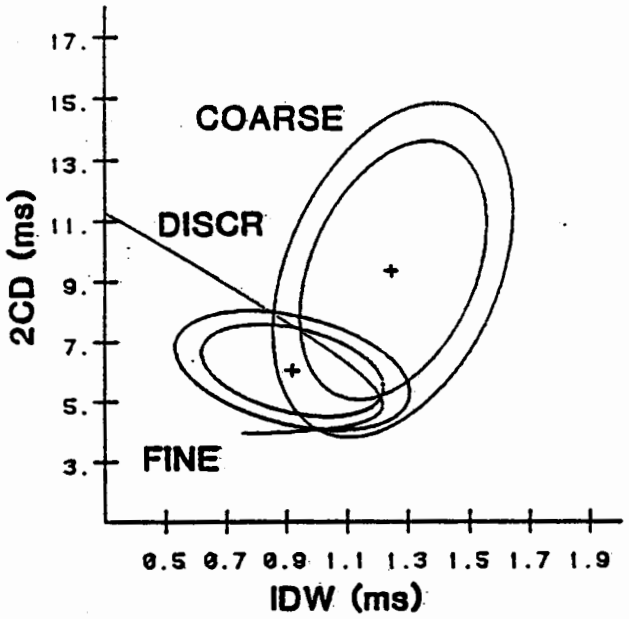

Figure 3.9 - Graphical construction of discriminant curve. The discriminant curve is the locus of points that are at equal Mahalanobis distance from the two clusters. Every point on the curve represents the intersection of a pair of ellipses. The ellipses shown are for $d^2=5$ (inner) and $d^2=7$ (outer).

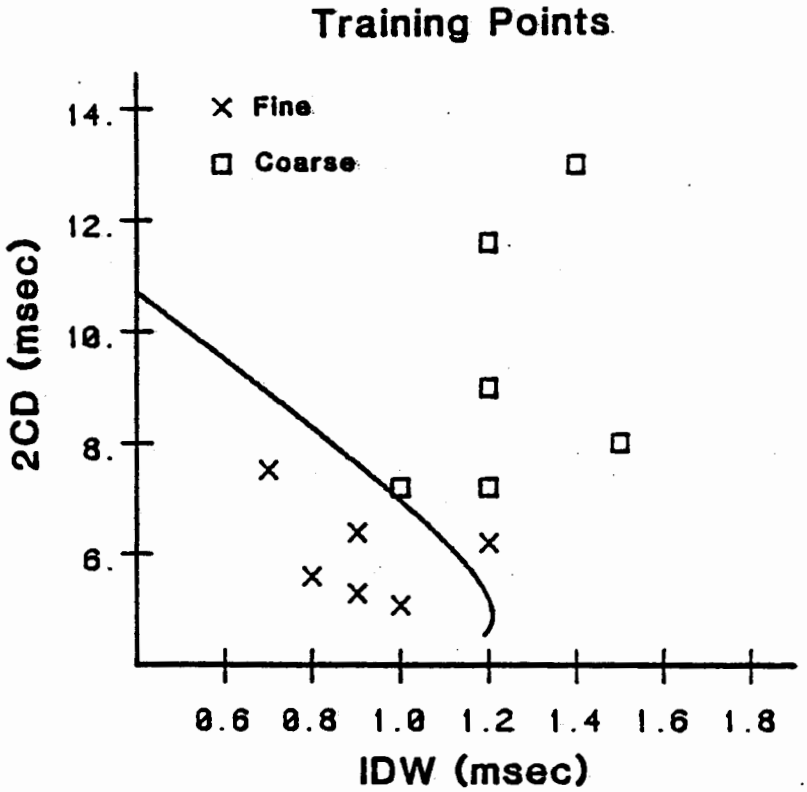

Figure 3.10 - Location of training set points with respect to the discriminant. Note that a fine training set point is misclassified.

TABLE 3.2

Test Set

Example-Source	Class	IDW	2CD
A - H*	C	1.2	7.7
B - H	F	.75	4.0
C - H	C	1.7	5.1
D - A*	C	1.2	5.5
E - A	C	1.5	6.2
F - A	F	0.5	4.8

(*) H - Humetrics Corporation Teaching Tape
A - American College of Chest Physicians Tape

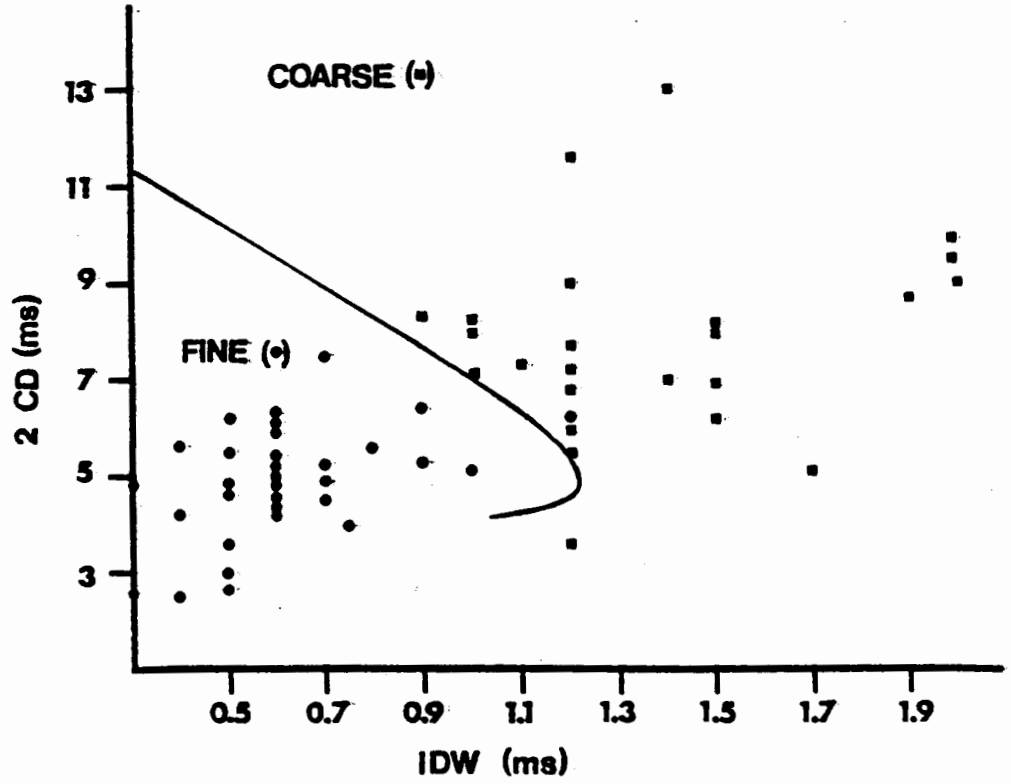

Figure 3.11 - Location of test and training points with respect to the discriminant curve. The one misclassified point belongs to the fine training set.

3.4 Discussion

It would be desirable to use these results in classification of DALS in the general population. The current classifier was derived from relatively few training DALS. Although the classifier was subsequently tested successfully using many other examples, several points need attention before the method could be recommended for wide use. Tests should be made using sounds recorded from diverse populations, and explicit evaluation of the effects of different transduction schemes should be undertaken. A model for this process would be (1) collection of DALS from diverse populations according to well defined sampling criteria, (2) use of standardized transduction and recording equipment, (3) subjective classification by a group of experienced physicians, and (4) selection and measurement of DALS by blinded observers according to defined criteria.

The current method was successful in classifying DALS obtained from independently produced tapes, and this is partial evidence of the method's insensitivity to variations in recording equipment. While the independent tapes were presumably "clear" instances of fine and coarse DALS and thus unlikely to be confusing, they were recorded using different equipment and categorized subjectively by the tape producers. It thus seems likely that the classification method is not overly sensitive to changes in recording equipment and that the subjective criteria used by the physician consultant in this study are typical.

Consideration should be given to adding medium DALS to the study. The proposed standard lung sound nomenclature of the American Thoracic Society does not include this category, partly due to the lack of objective methods for defining the phenomena. Given that some chest physicians are able to agree on what medium DALS sound like and given the successful development of an objective classifier for fine and coarse DALS, it seems likely that a system could be developed for categorizing fine, medium, and coarse DALS using waveform analysis.

One significant aspect of this work is that it allows the subjective element in classification to be removed. More precisely, it allows the subjectivity to be held constant, since we are duplicating a subjective judgment. The technique does, however, allow us to do something the physician with a stethoscope cannot do. While a physician may report that a breath contains both fine and coarse DALS, he or she is unable to identify particular complexes with any precision or to classify such stimuli individually. The method described in this chapter does precisely that, and it has made possible for the first time a study of the chest surface distributions of fine and coarse DALS as detailed in Chapter 4.

Chapter 4

The Chest Surface Distribution of DALS

4.1 Introduction

This chapter presents some observations of DALS made with two matched transducer channels applied simultaneously to the chest[1]. The original motivation for this study was the desire to learn more about the mechanism(s) producing DALS. Using the objective classification method of Chapter 3, it was possible to focus on individual fine and coarse DALS to learn whether differences in the distribution of their energy on the chest wall might point to differences in their mechanism or, perhaps, to differences in location within the lung of similar events producing the two varieties of noise. In particular, it seemed logical that a DALS complex might have a maximum amplitude in some small region on the chest, and that the amplitude would fall off as the point of observation moved over the chest away from the maximal region. It also seemed logical that DALS occur-

---

[1] Many of the actual recordings and waveform measurements presented in this chapter were performed in cooperation with E. Kunica, who reported them in an S.B. Thesis [Kunica (1980)].

ring in larger airways might be more widely observable since in the lung's binary branching structure a larger airway has more terminal units and thus more chest wall area dependent to it. This, however, was strictly supposition because the physical mechanisms responsible for generating DALS and the transmission characteristic of the lung had not been elucidated. No previous studies had been made of the chest wall distribution of individual DALS.

Some information about the surface distribution of DALS can be gleaned from clinical observations. Physicians often make note of the exact areas of the chest where DALS are heard. In some patients, DALS of uniform subjective quality may be widespread over the chest surface. In such instances the physician has no general way of knowing whether he or she is observing the same events at one site as at another. In other patients DALS may be heard with a stethoscope only in a small patch a few centimeters in diameter. From this observation it can be inferred that individual DALS probably have a rather limited area of observability. To learn whether any systematic differences in surface distribution could be observed among DALS with different waveform characteristics, two microphones were applied to the chests of patients with DALS.

4.2 Methods and Materials

DALS were recorded from the chests of twelve office and hospitalized patients who were selected for study by the

presence of DALS upon clinical auscultation with a stethoscope. The patients were not selected with respect to the nature of the disease state(s) present. The subjects varied in age from 50 to 80 years. The diseases diagnosed included chronic obstructive pulmonary disease, interstitial pneumonitis, interstitial fibrosis, and congestive heart failure. Recordings were made while the subjects were sitting upright and breathing with their mouths open. Sounds were recorded both during normal tidal breathing and during excursions from residual volume (RV) to total lung capacity (TLC).

Two microphones were applied to the chest simultaneously over the area where the DALS were best heard. The transducer channels were carefully matched as described in section 2.2.2 so that amplitude versus time plots for the two channels could be compared with respect to amplitude and timing of the DALS. The microphones were applied at two different separations. When the microphone cases were immediately adjacent, the center line separation was 6 cm. Recordings were also made at 12 cm separation in most patients. When possible, the microphones were attached by suction. Occasionally, chest surface conditions required the microphones to be hand held, but this did not produce serious artifacts.

At the time of digitization, the recorded 1 kHz standard tone signals were used to match the gains of the two channels of the playback equipment. The phase-matched

aliasing filters described in section 2.2.5 were used to minimize inter-channel time delay and waveform shape distortions. A simultaneous sample-and-hold circuit was not available in the analog-to-digital converter, so the two channels were sampled sequentially at a rate of 4000 point pairs per second. The time delay between conversions within each pair was less than 25 μs, which is a negligible time base error.

The sampled signals were plotted simultaneously on a time scale of 3300 mm/s and examined for the presence of DALS complexes in either channel. All DALS appearing in a given inspiration that were acceptable for analysis were identified in the plots. Acceptability was determined by ability to measure the waveform features IDW and 2CD by the method of section 3.2.1. Rejections resulted most often from overwhelming background lung sounds and from the occasional occurrence of a succeeding DALS complex that overlapped the one being measured. It was then noted whether each identified DALS complex in either channel was paired with one in the other channel. This pairing, or "association", thus required the presence in the two channels of complexes whose IDW and 2CD parameters were measurable. "Unassociated" DALS occurred with either no recognizable DALS complex at all in the alternate channel or with a recognizable but unmeasurable complex. When the ratio of peak amplitudes of the complexes in the two channels was greater than three, the smaller one often had

unmeasurable parameters because of background sounds.

As a last step, each identified, measurable complex was classified as fine or coarse using the (IDW, 2CD) discriminant method described in Chapter 3. A tally was made for one breath in each subject of how many DALS of each type appeared in both channels and how many appeared in a single channel. These counts were kept separately for the two microphone spacings. The totals for all 12 subjects were recorded for each separation in a four-fold table. The independence of the rows (fine/coarse) and the columns (associated or not) was tested using the chi-squared statistic [DeGroot (1975)] to learn whether the results were significant statistically.

4.3 Results

When DALS are divided into fine and coarse and each of these groups is subdivided into those appearing in one channel and those present in both channels, four categories result. Figure 4.1 shows an example from each category. Table 4.1 gives the numbers of DALS in each category found in each subject for the 6 cm microphone separation. Fourfold Table 4.2 summarizes these observations in all subjects. The chi-squared statistic for this table is 29.9 ($p<.0005$). Table 4.3 gives the same data for the 12 cm microphone separation. For this table chi-squared is 14.7 ($p<.0005$). Thus it is highly likely that the fine/coarse separation is associated with a difference in chest wall

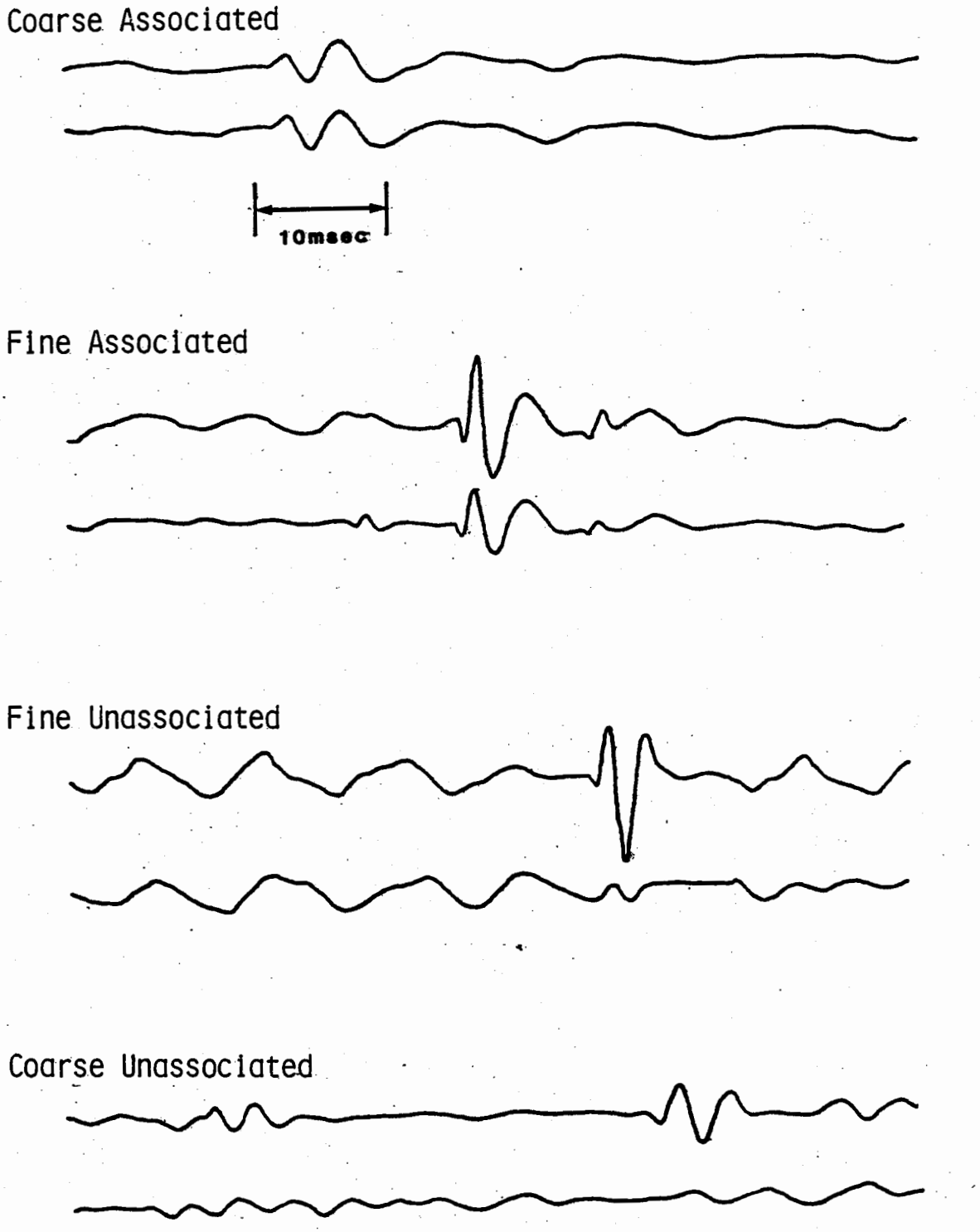

Figure 4.1 - Examples of degree of association between fine and coarse DALS observed at two adjacent transducers in patients.

Patient No.	Fine DALS		Coarse DALS	
	Unassoc.	Assoc.	Unassoc.	Assoc.
1	0	0	0	3
2	1	1	0	4
3	0	1	0	2
4	0	0	0	6
5	4	0	3	1
6	2	1	0	0
7	4	1	0	0
8	0	0	0	1
9	3	0	0	1
10	4	0	0	0
11	3	0	0	2
12	9	1	0	0

Table 4.1 - Relation between fine/coarse classification and observation at two microphones separated by 6 centimeters.

	Unassoc.	Assoc.	
Fine	30	5	
Coarse	3	20	
			58

$\chi^2 = 29.9$

$p \ll .0005$

Table 4.2 - Association versus waveform classification with 6 cm transducer separation (12 patients).

	Unassoc.	Assoc.	
Fine	18	1	
Coarse	4	9	
			32

$\chi^2 = 14.7$

$p < .0005$

Table 4.3 - Association versus waveform classification with 12 cm transducer separation (10 patients).

distribution.

Figures 4.2 and 4.3, for 6 cm and 12 cm separation respectively, present the same information in a different format. All observed DALS are plotted in the IDW/2CD plane, and each is identified as associated (boxes) or unassociated (x's). The fine/coarse discriminant line is also shown. It is clear that most of the associated DALS have coarse waveform properties, whereas most of the unassociated DALS have fine properties.

4.4 Discussion

The results of section 4.3 will be discussed in Chapter 6 and compared to the predictions of the DALS model presented in Chapter 5. The discussion here focuses on measurement problems and possible explanations for associated fine DALS and unassociated coarse DALS.

Measuring the waveform features consistently and deciding when DALS are associated requires some subjective judgments. To reduce variance and avoid bias, the measurements and decisions regarding association made by one of the two persons who recorded the sounds (E. Kunica or A. Murphy) were checked independently by the author. When disagreements were noted, they were resolved by discussion, and the measurement criteria were refined. The resulting method yields a binary (yes/no) decision regarding presence in both channels. In many instances, a DALS complex in one channel may be accompanied by deflections in the other chan-

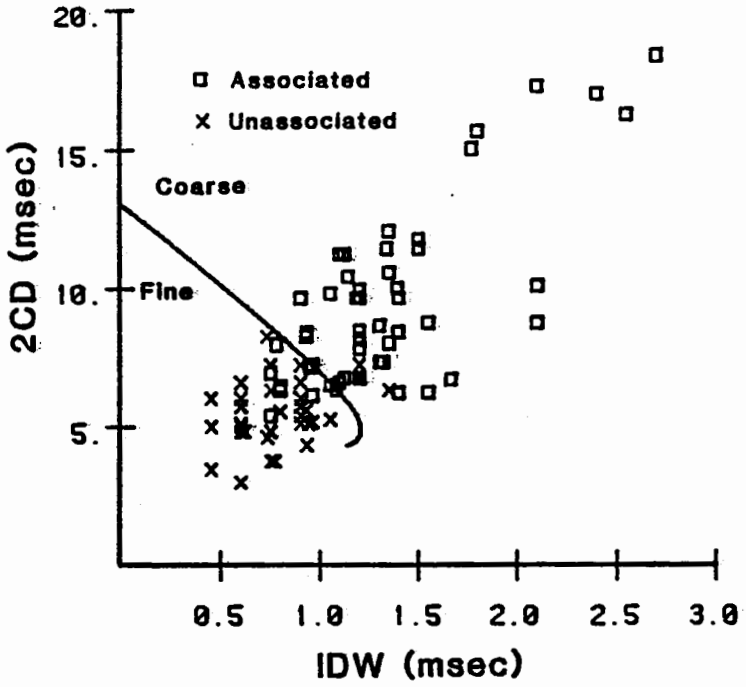

Figure 4.2 - Location in IDW/2CD plane of DALS observed at 6 cm transducer separation. Note that nearly all associated DALS had coarse waveform properties, while most unassociated DALS were fine.

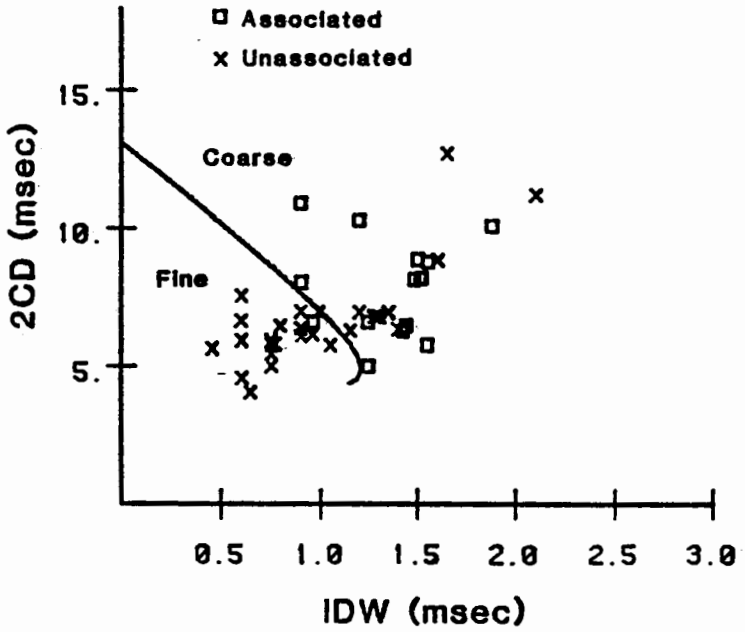

Figure 4.3 - Location in IDW/2CD plane of DALS observed at 12 cm transducer separation. With the transducers farther apart, only one associated point lies in the fine region. More coarse DALS were seen in only one channel at this wider separation.

nel that are too small to measure reliably, but which seem to have a definite association with the main complex. Figure 4.4 illustrates this phenomenon. Association is obviously not an innately binary variable. A correlation method might be capable of measuring association on a continuous scale.

Even if we could measure the waveforms with no uncertainty, the observations might still be confused by our ignorance of the precise location of the source of the DALS disturbance in relation to the location of the microphones on the chest wall. Figure 4.5 shows how this might explain some of the points in figures 4.2 and 4.3 that do not fit with the simple hypothesis that fine DALS are observable at only one microphone and coarse at both. If the source of a fine DALS were located in the underlying lung <u>between</u> the two microphones, it is quite conceivable that the disturbance would be observed at both transducers. Similar reasoning suggests that if the source of a coarse DALS were

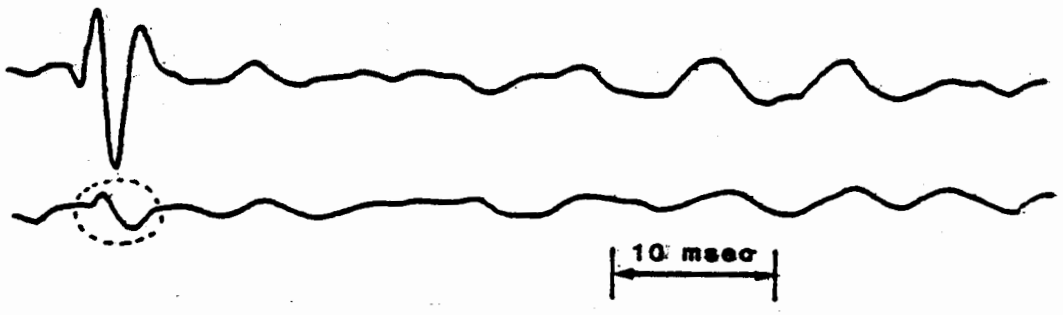

<u>Figure 4.4</u> - Example of DALS paired with a disturbance in the alternate channel that may result from the same source in the lung but which has unmeasurable IDW and 2CD.

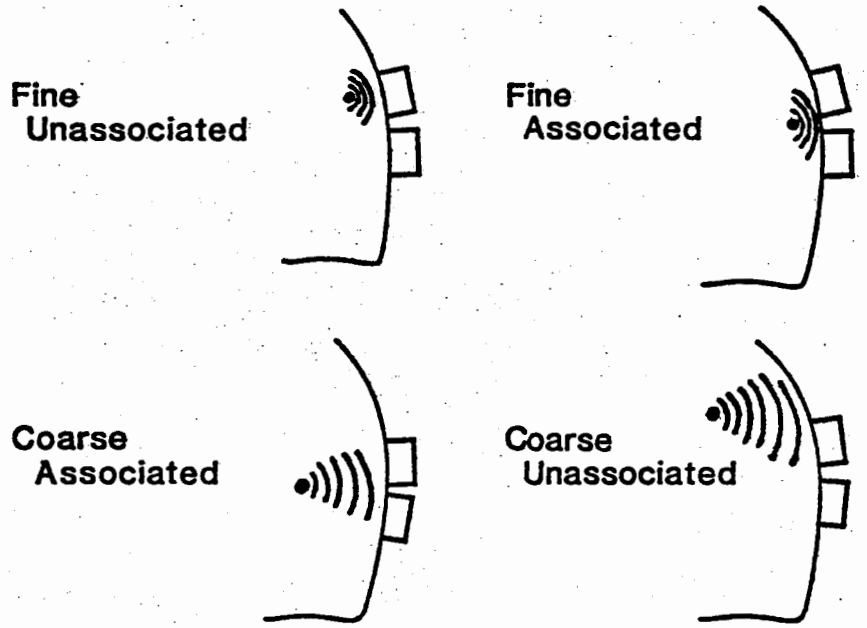

Figure 4.5 - Effect of source location on observation of DALS at two chest surface locations. The illustrations on the left show the usual observation of fine DALS on one microphone or coarse DALS at both. The illustrations on the right show how source location could explain observation of fine DALS at both sites or coarse DALS at only one site.

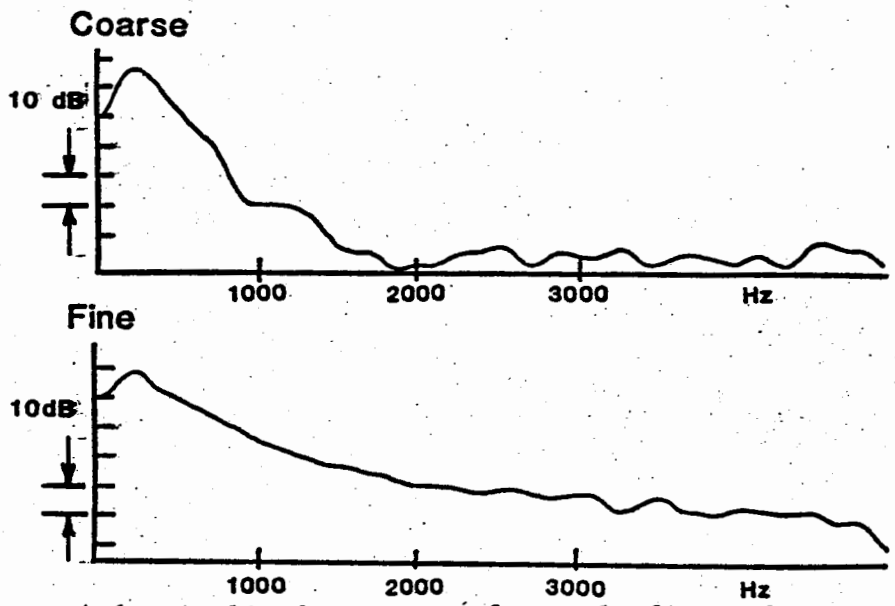

Figure 4.6 - Amplitude spectra of example fine and coarse DALS. The fine DALS have more high frequency content. The similar low frequency content of fine and coarse DALS makes it unlikely that coarse DALS are more widely transmitted because of some frequency-dependent transmission property of lung tissue.

located well to the side of one microphone, it might not be observable at both.

Figure 4.5 is drawn with the assumption that fine DALS occur closer to the chest and thus in smaller airways than coarse DALS. This conclusion does seem to follow from the observed difference in surface distribution. This might not be true if coarse DALS were preferentially transmitted. By this we mean that the two disturbances might be transmitted differently through the medium. If, for example, the medium had frequency dependent attenuation, we might imagine that one variety of DALS would be transmitted with much less attenuation, that is, preferentially. Our conclusion that coarse DALS occur in larger airways than fine DALS would be untrue if coarse DALS occurred in smaller airways but were preferentially transmitted because they occupied a different portion of the frequency spectrum than fine DALS.

Figure 4.6 shows the amplitude spectra of two of the training set DALS from Chapter 3. Note that the spectra have most of their energy in the band below 1000 Hz. The peaks are at about the same frequency. The primary difference is a less rapid fall in energy content of the fine DALS with increasing frequency. If the frequencies of vibration present in coarse DALS were preferentially transmitted, we would expect much of the energy in fine DALS to be transmitted in the same way because of the spectral similarity. Preferential transmission of coarse DALS is thus an unlikely explanation for the data presented in this chapter. Further

understanding of the results of Chapters 3 and 4 is provided by the physical model for the generation of DALS discussed in the next chapter.

Chapter 5

Modeling DALS as Quadrupoles in the Lung

5.1 Introduction

DALS are natural phenomena that occur in large numbers. If we assume that one in 1,000 people in a world population of three billion has 25 DALS in each of an average 12 breaths per minute, we estimate that 10^{12} DALS occur in the world every day. They are readily observed with inexpensive equipment and are widely interpreted as signs of disease. It seems obvious that their nature must be determined by the physical properties of the tissue from which they emanate. DALS thus have locked within them information, perhaps valuable information not readily obtained from other diagnostic tools. One key to releasing this information would be a detailed quantitative understanding of the physical mechanisms producing DALS. A quantitative predictive model for DALS has not been available, despite the efforts of Forgacs and others (see section 1.3.5), who have put forward qualitative explanations.

A possible quantitative model for DALS has recently been proposed by Fredberg [Fredberg and Holford (1981)]. The basic premise of the model is that DALS result from the sudden opening of a collapsed airway within the lung. This

idea is consistent with the previous observations and reasoning summarized in section 1.3.5, which suggest that a collapsed airway remains closed until the radial tractive forces built up as the lung expands during inspiration overcome the forces holding the airway shut. Forgacs believed that when the airway opened suddenly, an ''explosive equalization'' of pressure occurred between the upstream and downstream airspaces. While this explanation seems plausible, no detailed analysis of such a mechanism has been produced.

Fredberg's model rests on an alternative hypothesis, namely, that the DALS vibrations are simply the result of a sudden relaxation in the stress concentrated in the medium around the collapsed airway segment. Specifically, the model assumes that the stress field around a collapsed airway is essentially different from the field around the same airway in the open state. The model assumes (1) a particular form for the stress concentration, (2) a function to describe the relaxation source, and (3) a surrounding transmission medium that is a lossless, homogeneous, isotropic, linearly elastic, non-dispersive, infinite continuum. It is not the purpose of this chapter to describe the model in detail since the description is given elsewhere [Fredberg and Holford (1981)]. The basic equations and simulation methods are described here, and predicted waveforms, Fourier transforms, and spatial distributions are presented so the theoretical predictions can be compared with the data of

Chapters 3 and 4.

5.2 Methods

In this section, the theoretical basis of the DALS model is described, the equations for the pressure in the medium are given, and the methods for simulating the equations and investigating their spatial behavior are detailed.

5.2.1 **Theoretical Formulation of the Model** - The model represents the airway by its effect on the surrounding tissue. That is, the behavior of the airway is represented by static and dynamic changes in the stress field within the continuum in the neighborhood of the airway. When inspiration begins and the airway remains closed, a stress concentration builds up around the airway as a result of the tractive forces exerted by neighboring structurally interdependent tissue. These forces are opposed by the surface tension forces in the fluid lining within the collapsed airway that tend to keep it closed. Axial symmetry is assumed so that every force around the airway is balanced by an equal and opposite colinear force.

This distribution of radial forces around the airway is shown in Figure 5.1(a). We assume that the airway changes its shape in an axially symmetric way. For larger airways it might be more realistic to assume a flattened shape in the collapsed state. This configuration would still be modeled as a quadrupole source but without axial symmetry.

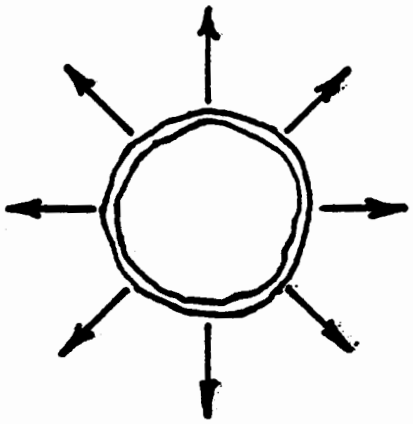

Figure 5.1(a) - Balance of radial tractive forces on airway exerted by surrounding tissue.

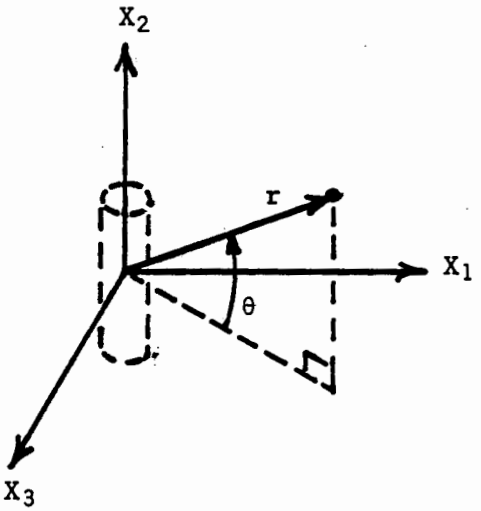

Figure 5.1(b) - Coordinate orientation with respect to the airway.

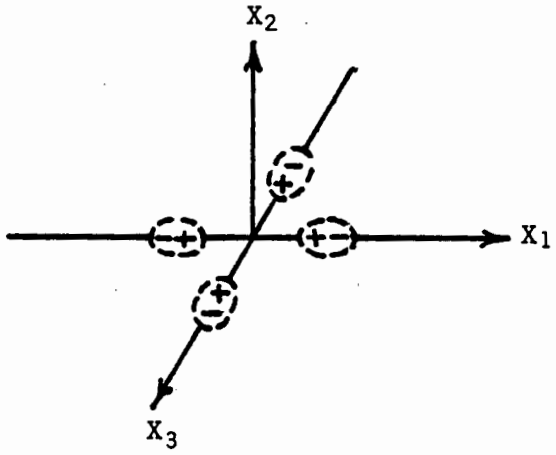

Figure 5.1(c) - Array of four point forces (quadrupole) equivalent to the force configuration of Figure 5.1(a).

For simplicity, axial symmetry was assumed for all airway sizes. Figure 5.1(b) shows the orientation of the rectilinear and polar coordinates with respect to the airway axis.

Since we are modeling the change in airway configuration by considering its effect on the stress field in the continuum, we are free to replace the continuous distribution of forces in Figure 5.1(a) with any other set of forces that produces an equivalent stress field. In particular, the force distribution can be represented by the four point forces shown in Figure 5.1(c). We assume that a stress concentration of magnitude σ_o exists in a region with volume Δv surrounding the airway. The parameters Δv and σ_o enter the equations as a product, $(\Delta v \times \sigma_o)$, which we can think of as the ''strength'' of the quadrupole source. For this configuration, the average normal stress at a point $\underline{x}$ in the medium is given by [Fredberg and Holford (1981)]

$$p(\underline{x},t) = -(\Delta v/12\pi)[3-4(c_T/c_L)^2]\ \{[s(t-r/c_L)/r^3 + \dot{s}(t-r/c_L)/(c_L r^2)][3\cos^2\theta-1] + \cos^2\theta\ \ddot{s}(t-r/c_L)/(rc_L^2)\} \qquad (5\text{-}1),$$

where Δv = volume of the region of stress concentration

c_T = transverse wave speed of the medium

c_L = longitudinal wave speed of the medium

s = stress source function

r = radius from the airway at the origin

$\cos^2\theta = (x_1^2 + x_3^2)/r^2$

$(\dot{}) \Rightarrow$ time differentiation.

The resulting field is symmetrical about the x_2 axis, which is aligned with the airway axis.

It was necessary to assume a function describing the time course of stress change when the airway opens. A simple smooth function that is symmetric about t=0 and depends on a single parameter, τ, was assumed.

$$s(t) = \sigma_o \left[\frac{1}{2} - \left(\frac{1}{\pi}\right)\tan^{-1}(t/\tau)\right] \qquad (5\text{-}2).$$

As τ varies, the abruptness of the change in stress s(t) is altered (Figure 5.2).

Equation (5-1) can be cast in dimensionless form by making the following substitutions:

$$\overset{*}{r} = r/(c_L\,\tau) \quad \text{and} \quad \overset{*}{\underline{x}} = \underline{x}/(c_L\,\tau) \qquad (5\text{-}3a)$$

$$\overset{*}{t} = t/\tau \qquad (5\text{-}3b)$$

$$(\dot{}) = (\,)'/\tau \qquad (5\text{-}3c)$$

$$K_p = \frac{\sigma_o(\Delta v)\,[3-4(c_T/c_L)^2]}{12\pi c_L^3(\tau)^3} \qquad (5\text{-}3d)$$

$$\overset{*}{p}(\overset{*}{\underline{x}},\overset{*}{t}) = p(\overset{*}{\underline{x}},\overset{*}{t}) \;/\; K_p \qquad (5\text{-}3e).$$

The non-dimensional pressure can then be expressed as a function of dimensionless time $\overset{*}{t}$ and position $\overset{*}{\underline{x}}$ by

$$\overset{*}{p}(\overset{*}{\underline{x}},\overset{*}{t}) = -\left[\frac{g(\overset{*}{t}-\overset{*}{r})}{\overset{*}{r}^3} + \frac{g'(\overset{*}{t}-\overset{*}{r})}{\overset{*}{r}^2}\right](3\cos^2\theta-1)$$

$$- \frac{g''(\overset{*}{t}-\overset{*}{r})}{\overset{*}{r}}\cos^2\theta \qquad (5\text{-}4),$$

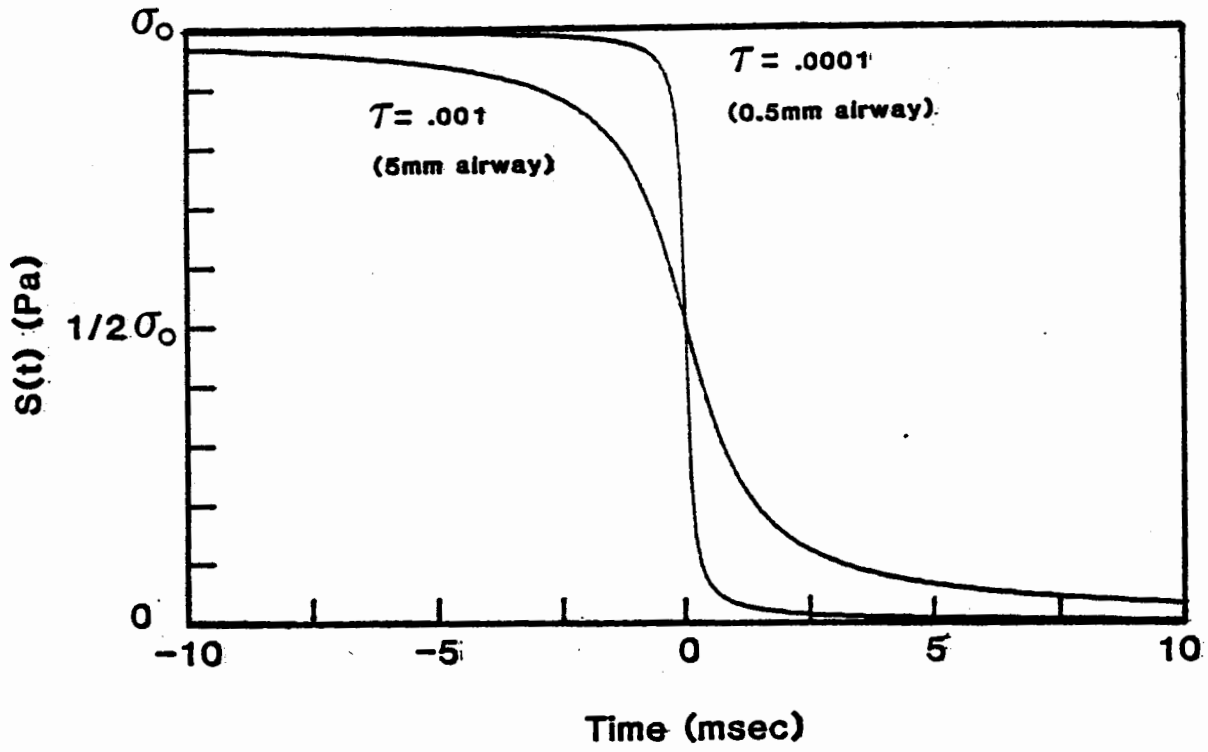

Figure 5.2 - Function s(t) describing stress change when a collapsed airway opens. The shape of s(t) depends on a single parameter, τ, which is assumed to be proportional to airway diameter.

where the source function and its time derivatives are

$$g(\overset{*}{t}) = \frac{1}{2} - \frac{1}{\pi}[\tan^{-1}(\overset{*}{t})] \qquad (5\text{-}5a)$$

$$g'(\overset{*}{t}) = -\frac{1}{\pi}\frac{1}{1+\overset{*}{t}^2} \qquad (5\text{-}5b)$$

$$g''(\overset{*}{t}) = \frac{1}{\pi}\frac{2\overset{*}{t}}{(1+\overset{*}{t}^2)^2} \qquad (5\text{-}5c).$$

Figure 5.3(a) shows these three source terms plotted as functions of $\overset{*}{t}=t/\tau$. The theoretical DALS waveform $\overset{*}{p}(\underline{\overset{*}{x}},\overset{*}{t})$ is composed of a weighted sum of these fundamental functions, the weights being powers of the radius $\overset{*}{r}$ and functions of the angle θ.

The first two terms of equation (5-4) fall off as $\overset{*}{r}^3$ and $\overset{*}{r}^2$ respectively. They are thus more prominent near the source in what is called the near field. The last term, which falls off only as $\overset{*}{r}$, is most important far from the source (far field). The transition region occurs at about $\overset{*}{r}=1$, i.e., when $r = (c_L\,\tau)$. Notice that the near field terms disappear completely when $\cos^2\theta = \frac{1}{3}$. At $\theta=90^\circ$, the far field term is zero, leaving only the near field. This means that the quadrupole field is more widespread broadside to the airway, i.e., when $\theta=0^\circ$. The spatial behavior of these equations and the effects of the individual parameters will be discussed further in Chapter 6.

The Fourier transforms of the functions in equations (5-5) are readily computed:

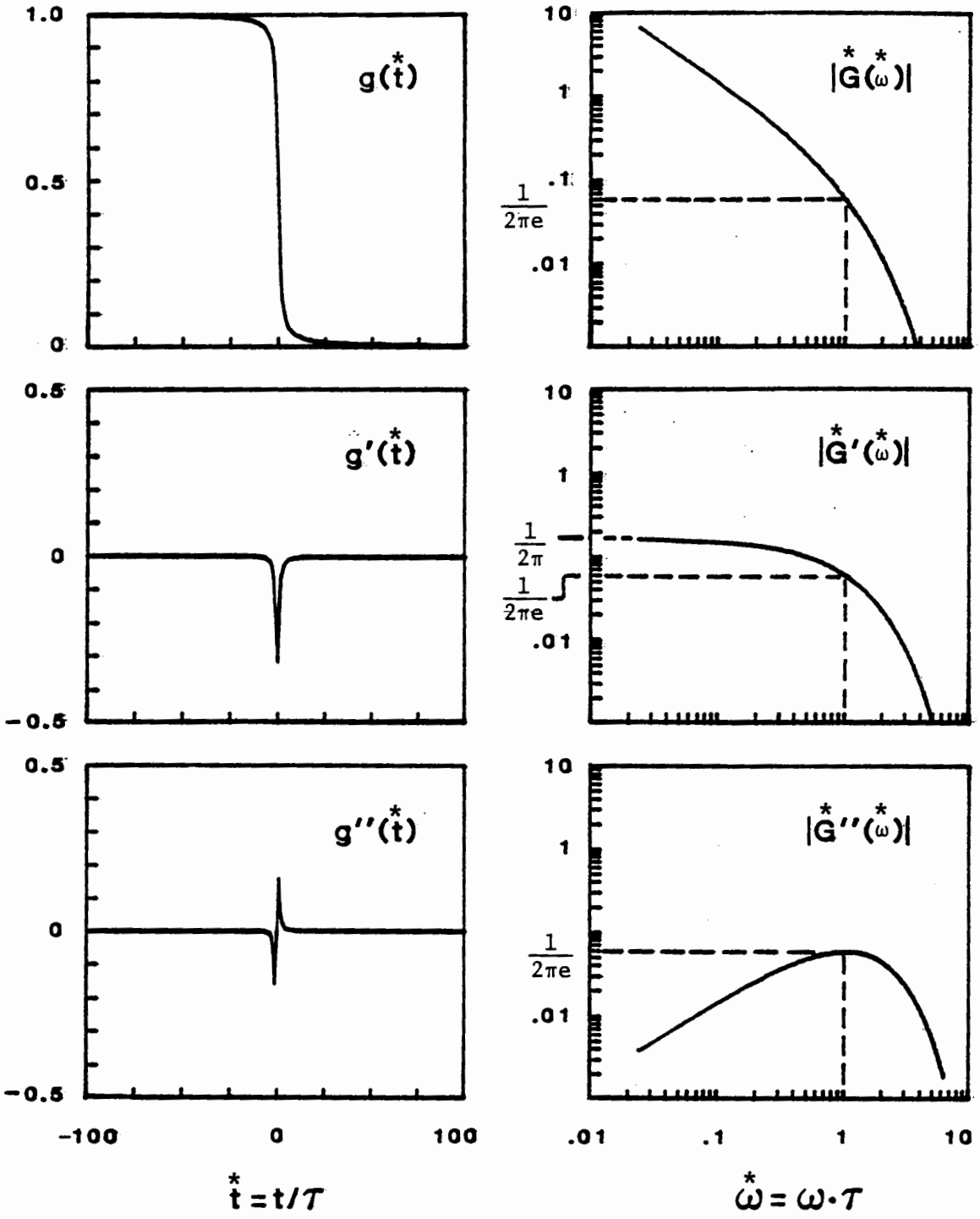

Figure 5.3(a) - Terms of stress relaxation source function plotted versus dimensionless time.

Figure 5.3(b) - Fourier transform magnitudes versus dimensionless frequency.

$$g(\overset{*}{t}) \longleftrightarrow \overset{*}{G}(\overset{*}{\omega}) = -\frac{1}{j\overset{*}{\omega}} e^{-|\overset{*}{\omega}|} + 2\pi u_o(\overset{*}{\omega}) \qquad (5\text{-}6a)$$

$$g'(\overset{*}{t}) \longleftrightarrow \overset{*}{G}'(\overset{*}{\omega}) = - e^{-|\overset{*}{\omega}|} \qquad (5\text{-}6b)$$

$$g''(\overset{*}{t}) \longleftrightarrow \overset{*}{G}''(\overset{*}{\omega}) = - j\overset{*}{\omega}\, e^{-|\overset{*}{\omega}|} \qquad (5\text{-}6c),$$

where $\overset{*}{\omega}=(\omega\tau)$ is the non-dimensional frequency variable, $\overset{*}{G}$ is $G(\overset{*}{\omega})/\tau$, and $u_o(\overset{*}{\omega})$ is the delta function.

The magnitudes of these functions are plotted in Figure 5.3 in normalized form. As expected, increasing relative amounts of energy at high frequency are present in the differentiated terms. All three transforms have magnitude of $(1/2\pi e) = 0.059$ when $\overset{*}{\omega} = (\omega\tau) = 1$. The transform $\overset{*}{G}(\overset{*}{\omega})$ corresponding to the undifferentiated stress relaxation source function approaches infinite magnitude at low frequency with a slope of -1 on the log-log plot. The transform $\overset{*}{G}'(\overset{*}{\omega})$ corresponding to the first time derivative of the source function approaches a constant value of $(1/2\pi)$ at low frequency. The third transform $\overset{*}{G}''(\overset{*}{\omega})$, which corresponds to the second time derivative of the source function, approaches a magnitude of zero at low frequency with a slope of +1. The actual theoretical Fourier transform for a particular DALS can be obtained by denormalizing the component transforms of equations (5-6) and combining their complex values with the proper weights depending on the position $\underline{x}$ with respect to the airway.

5.2.2 **Estimation of Parameters** - It is necessary to estimate the values of several parameters in equation (5-1).

Fredberg and Holford [1981] provide a detailed rationale for these choices. The shear wave speed estimate of 169 cm/sec is based on measured values [Lai-Fook (1977)]. The estimate of compressional wave speed, taken to be 3000 cm/sec, results from considering the stiffness of the gas and the density of lung tissue as dominant over the stiffness of the tissue and the density of the gas, respectively. The value chosen is consistent with actual measurements in excised animal lung preparations [Rice(1980)].

Note that the shear wave speed, c_T, enters equation (5-1) only in the term $[3 - 4(c_T/c_L)^2]$. For the values given here, replacing this term by [3.0] would cause an error in the resulting pressure amplitude of about 1%, which is much less that the precision of the model. This lack of dependence on the shear wave speed and the absence of terms delayed by c_T result from the calculation of average <u>normal</u> stress in the medium.

Since the density of the lung tissue decreases with lung volume, it is expected that the value of c_L will vary during the respiratory cycle. The range of variation may be about 2000-4000 cm/sec [Fredberg and Holford (1981)]. In the near field, this variation of c_L has only small effects on the shape and amplitude of the waveforms, and plots in this chapter are made for c_L = 3000 cm/sec. The effects of a time-varying c_L are discussed further in Chapter 6.

The strength of the quadrupole source is determined by the product ($\Delta v \times \sigma_o$), which has units of energy. Since

this product is a pure amplitude scale factor in equation (5-1), it was adjusted to produce simulated DALS with the right amplitude at reasonable distances from the airway to the surface (see Chapter 6). The quadrupole source strength was taken to be

$$(\Delta v \times \sigma_o) = 500\ d^2 \qquad (5\text{-}7),$$

where $(\Delta v \times \sigma_o)$ is in ergs and d is in mm.

We can see that this is a reasonable value for the product by considering appropriate magnitudes for Δv and σ_o individually. The level of stress change in the source region, σ_o, can be estimated by considering the surface tension forces within the collapsed airway. Since the radius of the meniscus at the interface between patent and closed airway regions would depend on airway diameter, the stress level varies inversely with the airway diameter. This follows from the Laplace relation for a hemispherical surface, which gives the surface tension stresses as 2T/r where T is the liquid surface tension and r is the radius of the meniscus. Macklem [1971] discussed the opening of small airways and used 40 dynes/cm as an appropriate value for T during inspiration. Using this value, and approximating the meniscus radius as half the uncollapsed airway diameter gives

$$\sigma_o = 160 / d \qquad (5\text{-}8),$$

where d is the airway diameter in mm and σ_o is in Pascals (N/m^2). A 1mm airway thus has a value for σ_o of 160 Pa, or about 1.5 cmH_2O. This is consistent with the overall

transpulmonary pressures during breathing, which range from about 1-10 cmH_2O.

With this value for σ_o, the effective volume, Δv, over which the source stress is concentrated is

$$\Delta v = 0.32\ d^3 \qquad (5\text{-}9),$$

where d is in mm and Δv in cm^3. This is equivalent to assuming that the stress is concentrated in a spherical region whose diameter is 8 times the airway diameter (Figure 5.4). The source strength product expressed in equation (5-7) could result from other values for Δv and σ_o. In particular, the stress level might actually be higher and the effective volume lower. However, the values assumed are physically reasonable based on the Laplace relation and the presumption that the stress ought to be concentrated within a few diameters of the airway.

Fredberg estimated the characteristic opening time of small airways by considering the effective inertance imposed by the surrounding medium upon a spherical void of diameter d embedded in the lung. Using this argument, the airway opening time is estimated to be between 0.1 and 1.0 ms for a 1mm airway, with τ being proportional to d. A value for τ of 0.2 ms was used in the simulation for a 1mm airway. Scaling of simulation parameters with airway diameter is summarized in Table 5.1.

5.2.3 <u>Calculation of Pressure Waveforms</u> - For a particular set of model parameters, the pressure at a given point

TABLE 5.1

Scaling of Model Parameters with Airway Diameter

Parameter	Value for 1mm Airway	Scaling with d
τ	.0002 sec	$\propto d$
ΔV	.32 cm^3	$\propto d^3$
σ_e	1,600 dynes/cm^2	$\propto d^{-1}$
c_T	169 cm/sec	constant
c_L	3,000 cm/sec	constant

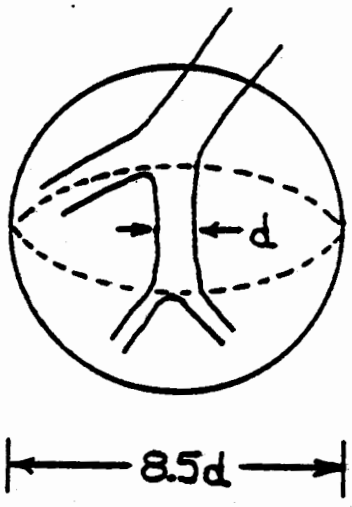

Figure 5.4 - Cross-section showing volume of stress concentration relative to airway size. Drawn 1 to 1 scale for a 5mm airway.

$\underline{x}$ was calculated at uniformly spaced time points using equation (5-1). The 0.1 ms time spacing used corresponds to sampling an analog pressure waveform 10,000 times per second.

As noted in Chapter 2, the air-coupled transducers used to measure DALS in patients introduce both high pass and low pass filter effects. In order to compare waveforms predicted by the model to data obtained from patients, the model pressure waveforms were filtered digitally to approximate the transducer effects as described in the following paragraph.

Based on the measurements of transducer effects described in section 2.1, the digital filter's frequency response was taken to be a four-pole Butterworth high pass filter with f_c = 200 Hz cascaded with a similar low pass filter with f_c = 1000 Hz. This response approximates the real transducer characteristic with respect to numbers of poles as well as corner frequencies. A 256-point finite impulse response (FIR) digital filter was obtained by the windowing method [Oppenheim and Schafer (1975)]. The filter was applied to the model waveforms using the fast convolution program FASTFILT described in section 2.4.3.

The resulting time and frequency domain characteristics of the digital filter and convolution process are shown in Figure 5.5. Figure 5.5(a) shows the unit sample response obtained by convolution with a unit sample. Figure 5.5(b) shows the response to a unit step. The frequency response

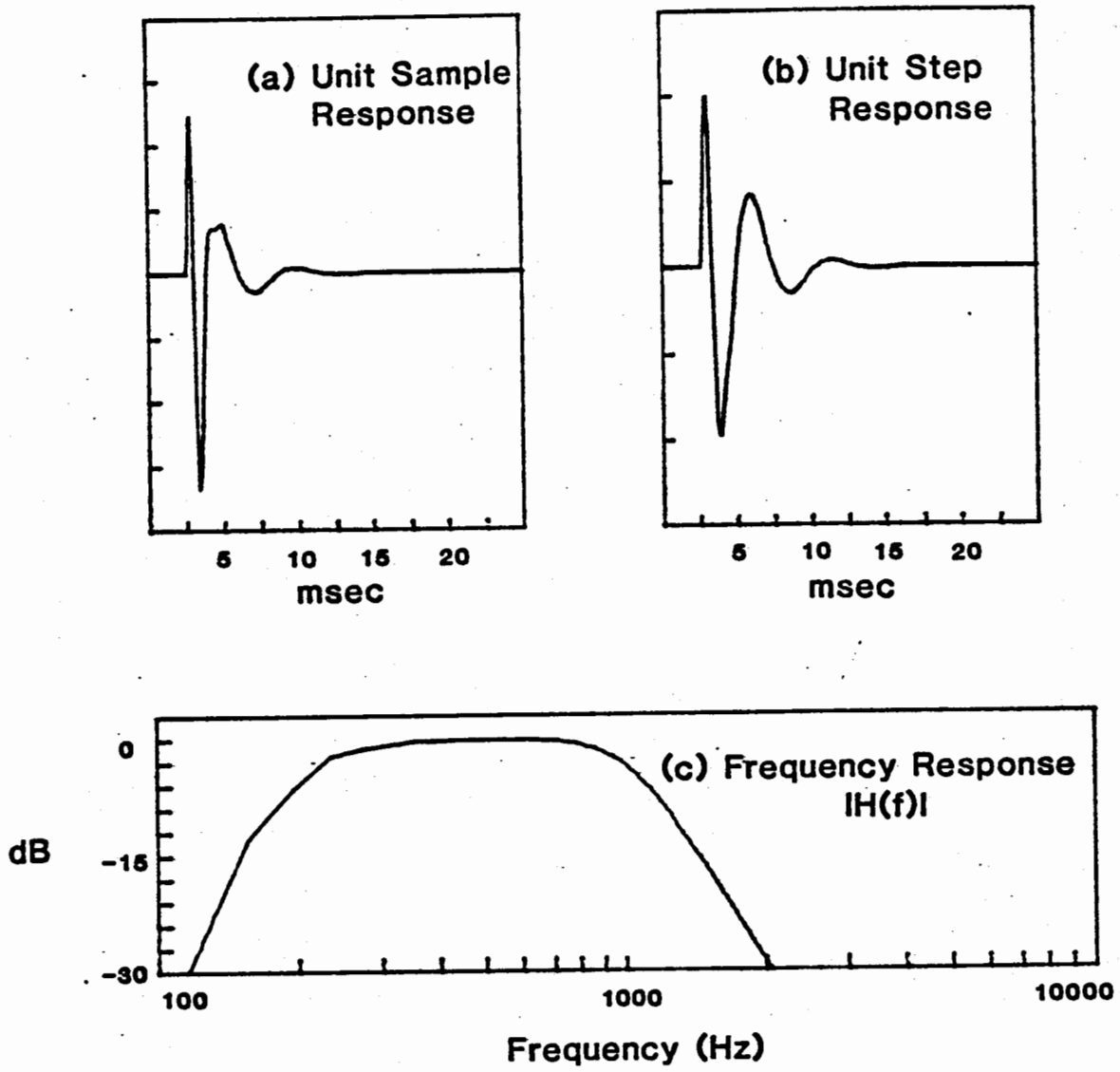

Figure 5.5 - Response of the digital filter used to simulate the effects of transducer filtering.

(a) Unit sample response
(b) Unit step response
(c) Magnitude of frequency response as measured by cross-spectral analysis with a broadband noise input.

was measured with program CCSE (section 2.4.2) by applying the filter to sampled noise using FASTFILT and calculating the transfer function between the input noise and the output signal. Figure 5.5(c) shows the magnitude of the frequency response, which exhibits the desired roll-offs at 200 and 1000 Hertz.

5.2.4 **Calculation of Intensity Contours** - The spatial properties of equation (5-1) were investigated by plotting contours of constant energy around the airway. To do this, the energy reaching a point $\underline{x}$ was needed,

$$e(\underline{x}) = \int_{-\infty}^{\infty} p_f^2(\underline{x},t)\, dt \qquad (5\text{-}10),$$

where p_f is the filtered pressure response. Elimination of the components at DC by high pass filtering combined with the transient nature of the source makes it possible to calculate $e(\underline{x})$ by a finite sum

$$e(\underline{x}) = \sum_{i=1}^{512} p_f^2(\underline{x},i) \qquad (5\text{-}11).$$

The sum was over 512 points because the unfiltered pressure response and the filter impulse response were each 256 points long. Convolving these two 256 point sequences together resulted in a 512 point sequence, which corresponds to a 51.2 ms segment of time.

Since the three-dimensional pressure field is cylindrically symmetric about the x_2 axis, which is aligned with the airway axis, the spatial nature of the field can be studied

in two dimensions by plotting contours of constant energy in one quadrant of the x_1-x_2 plane with x_3=0. The full three-dimensional set of constant energy contours can then be visualized as a rotation and reflection of the one-quadrant plots.

A constant energy contour was located by beginning a search along a radial line at some angle θ from the x_1 axis. The searching program used a combination of bisection, secant interpolation, and inverse quadratic interpolation strategies embodied in a routine called ZEROIN [Forsythe et al (1977)]. Once the desired energy point was located along the current radial line, θ was incremented, and the search was begun along the new radial line. In this manner the desired contour could be plotted for a particular range of θ, usually between 0 and 90°.

Contours were plotted with logarithmic spacing. The energies were normalized, somewhat arbitrarily, to a reference energy e_{ref} given by

$$e_{ref} = p_{ref}^2 \times t_{ref} \qquad (5\text{-}12),$$

where p_{ref} is 20μPa, the reference pressure (RMS) of a standard sound pressure level scale. The constant t_{ref} was taken to be 10 msec, the approximate duration of predicted and observed DALS. Contours were plotted for constant values of the normalized variable

$$E(\underline{x}) = 10 \log \frac{e(\underline{x})}{e_{ref}} \qquad (5\text{-}13).$$

5.3 Results

5.3.1 **Composition of DALS - Time Domain** - When the three terms of equation (5-1) are examined individually, the theoretical variations in composition among DALS emanating from airways of different diameter can be seen. Figures 5.6-5.8 illustrate this variation for three sets of model parameters believed to correspond to airway diameters of 1,3 and 5mm. Both the filtered and unfiltered pressure signals are presented so that the effect of the filter introduced to account for the transducer can be seen. For each airway the observation point $\underline{x}$ was at $\theta=0^{o}$ and at a value of r that yielded a filtered waveform p_{Tf} having a normalized energy $E(\underline{x})$ = 85dB. The resulting DALS have peak amplitudes of about 1 Pa, which is comparable to amplitudes observed in patients.

The unfiltered pressure waveforms are seen to differ in their relative content of the three component terms. The smaller airway DALS contain more of the differentiated source terms. This is most evident in the summed p_T as a difference in the leading edge of the step. For the 1mm case, there is a considerable overshoot (about 50%). The 5mm p_T shows no overshoot, and the step itself has a much larger transition time.

The right columns of Figures 5.6-5.8 show how the transducer filter modifies the basic component waveforms and how these filter responses combine to produce the observed complex p_{Tf}. More of the energy and shape of p_3 are seen to

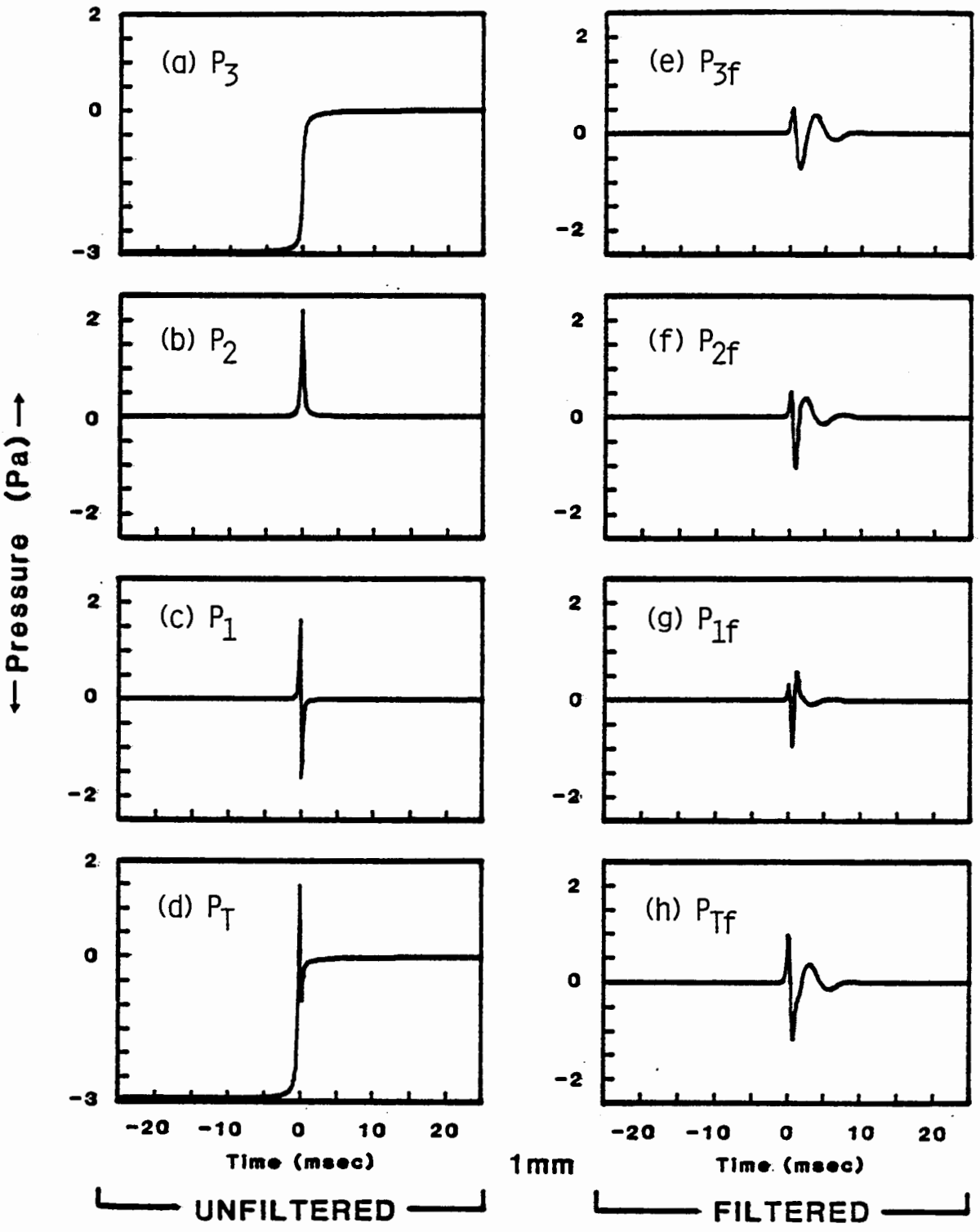

Figure 5.6 - Model DALS waveforms from a 1mm airway observed at r = 1.40 cm, θ = 0° where the energy is 85 dB. Parts (a-c) and (e-g) show the contributions of the three terms that fall off as r^3, r^2, and r respectively. Parts (d) and (h) show the total response, which is the sum of the three components.

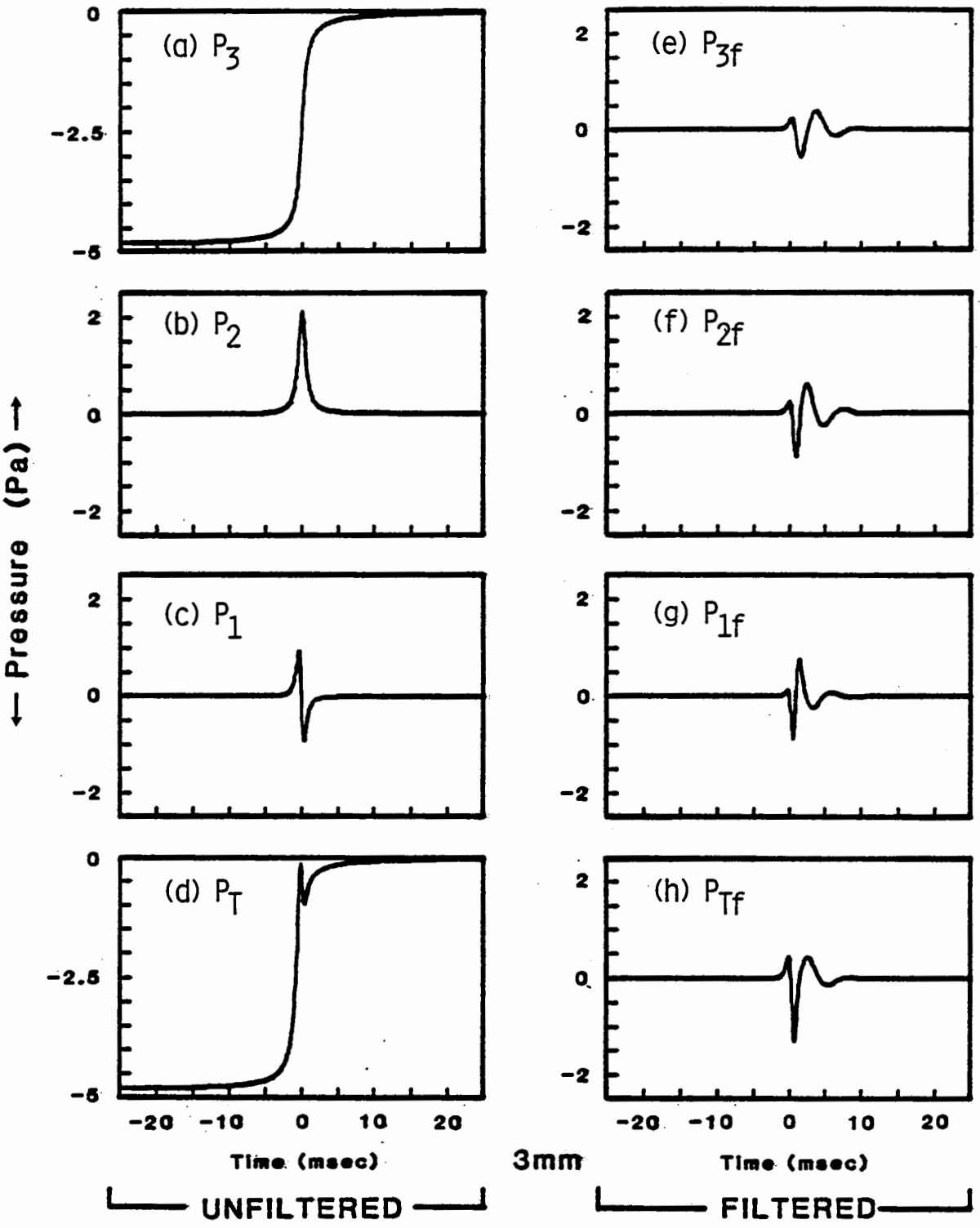

Figure 5.7 - Model DALS waveforms from a 3mm airway observed at r = 2.47 cm, $\theta = 0°$ where the energy is 85 dB. Parts (a-c) and (e-g) show the contributions of the three terms that fall off as r^3, r^2, and r respectively. Parts (d) and (h) show the total response, which is the sum of the three components.

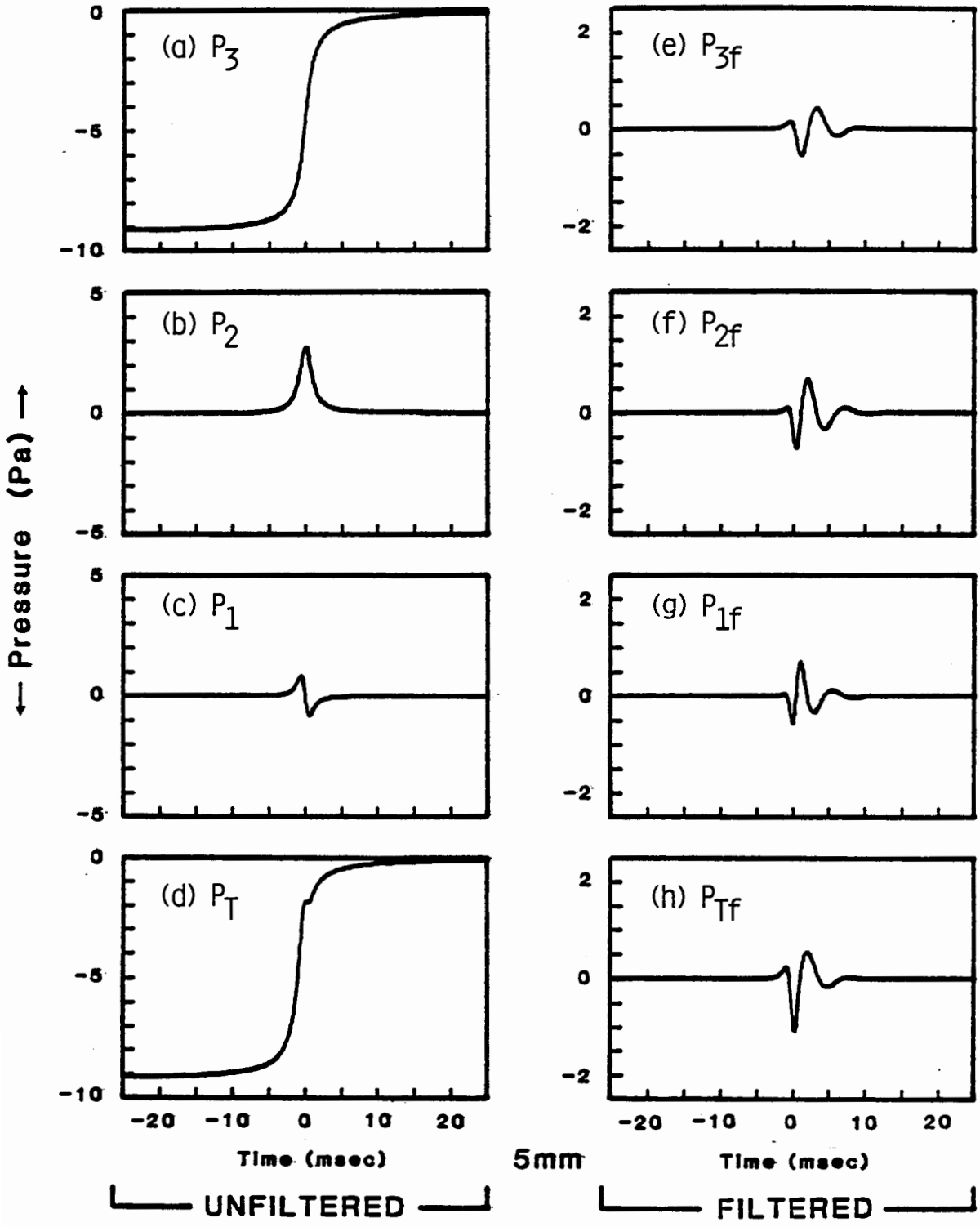

Figure 5.8 - Model DALS waveforms from a 5mm airway observed at r = 2.80 cm, θ = 0° where the energy is 85 dB. Parts (a-c) and (e-g) show the contributions of the three terms that fall off as r^3, r^2, and r respectively. Parts (d) and (h) show the total response, which is the sum of the three components.

be lost in the filter. Consistent changes are observed as one proceeds from the 1mm case to the 5mm case. The amplitude and sharpness of the initial deflection of p_{Tf} are greatest for the smallest airway. The small airway complex exhibits a noticeable transition from a ''fast'' wave front to a ''slow'' response.

5.3.2 **Composition of DALS - Frequency Domain** - The effects of the transducer filter can also be observed in the frequency domain. Figure 5.9 shows the component Fourier transforms of equations (5-6) for d = 1 and 5 mm, before and after filtering. The shapes of the unfiltered transforms are the same as the normalized plots of Figure 5.3, but the frequency axes have been denormalized so that they are appropriate to the two particular airway sizes. For the 1mm airway, $\overset{*}{\omega} = (\omega\tau) = 1$ when f = 796 Hz. This is the location of the peak of the term $|G'(f)|$ corresponding to the second time derivative of the source function describing stress relaxation. This peak for the 5mm airway is located at f = 159 Hz, below the low frequency cutoff of the transducer.

The effects of the filtering introduced by the transducer are different for the small and large airways. For the 5mm airway, the filter only modifies the low frequency content of the signal. Both low and some high frequencies are lost in the filter in the 1mm airway case, but the low frequency loss has the most effect on the time domain waveform.

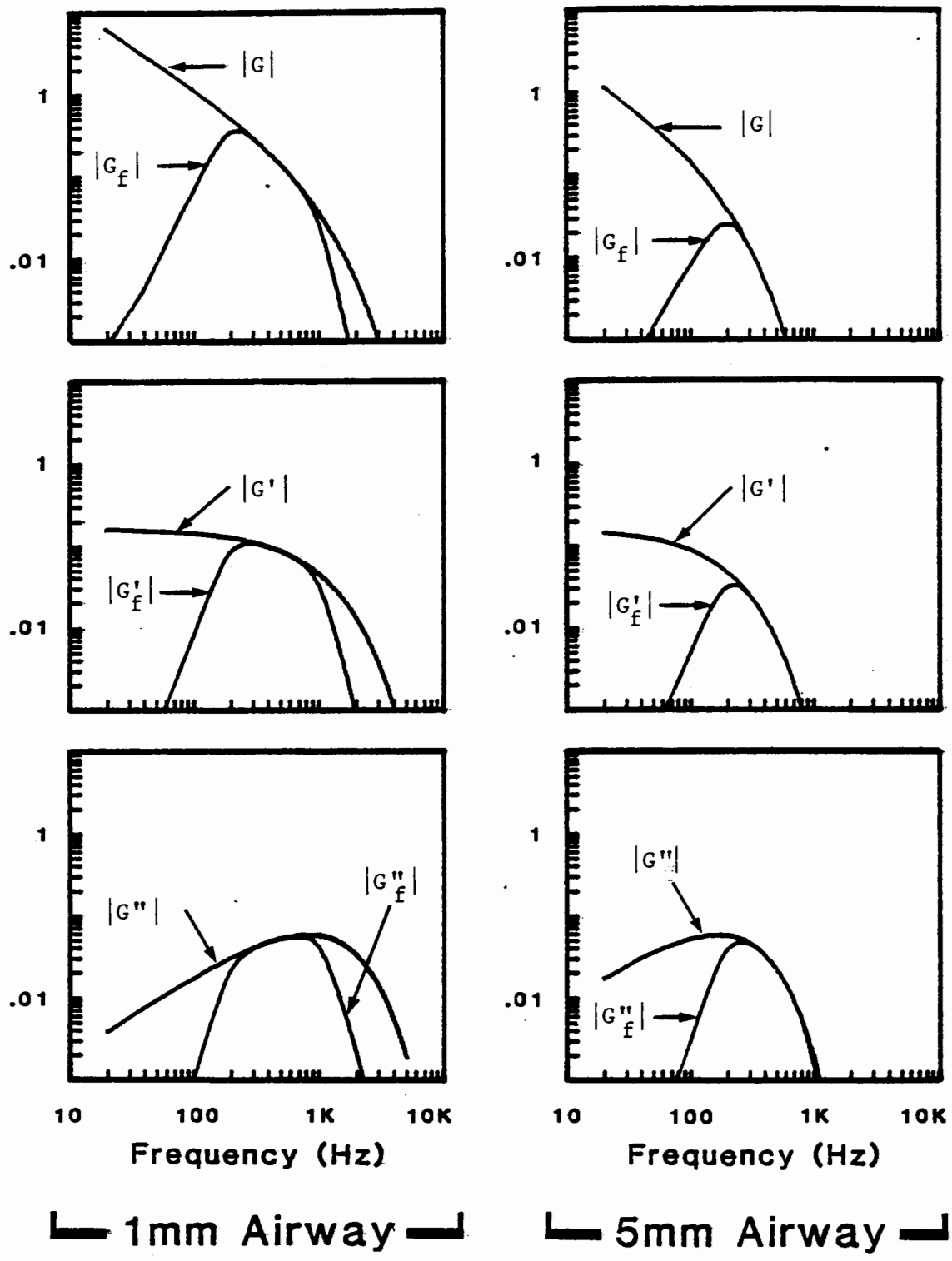

Figure 5.9 - The effect of the transducer filter on frequency components of model DALS from 1mm and 5mm airways. The top row shows the magnitude of the transforms of the undifferentiated source terms. The second and third rows show the first and second derivative terms.

5.3.3 **Iso-energy Contours** - The calculated constant energy contours for airway diameters of 1,3, and 5mm are shown in Figure 5.10. Each plot shows one quadrant of a plane that passes through the origin and contains the airway axis (that is, the plane defined by the equation $x_3=0$). The airway can be imagined to be located at the lower left corner of the plot with its axis vertical. Points at the right are thus located to the side of the airway, while points above the origin have an end-on view of the airway.

The distinct cusp is apparent in each set of contours. When r is approximately $(c_L \tau)$, the cusp becomes shallow and begins to disappear. For example, for the 3mm airway plot of Figure 5.10(b), $(c_L \tau)$ is about 1.8 cm. Note that the cusp of the 75 dB contour is located at about this radius and is much less indented than those of higher energy contours. Further progression in the loss of the cusp can be observed in Figure 5.10(a).

The similarity of the contours for different airway diameters is more readily seen in plots with logarithmic axes. Figure 5.11 show such plots for the same airways as seen in Figure 5.10. With logarithmic axes, it is possible to see more of the contours without squeezing together those occurring at small radii. The similarity in shapes is readily apparent.

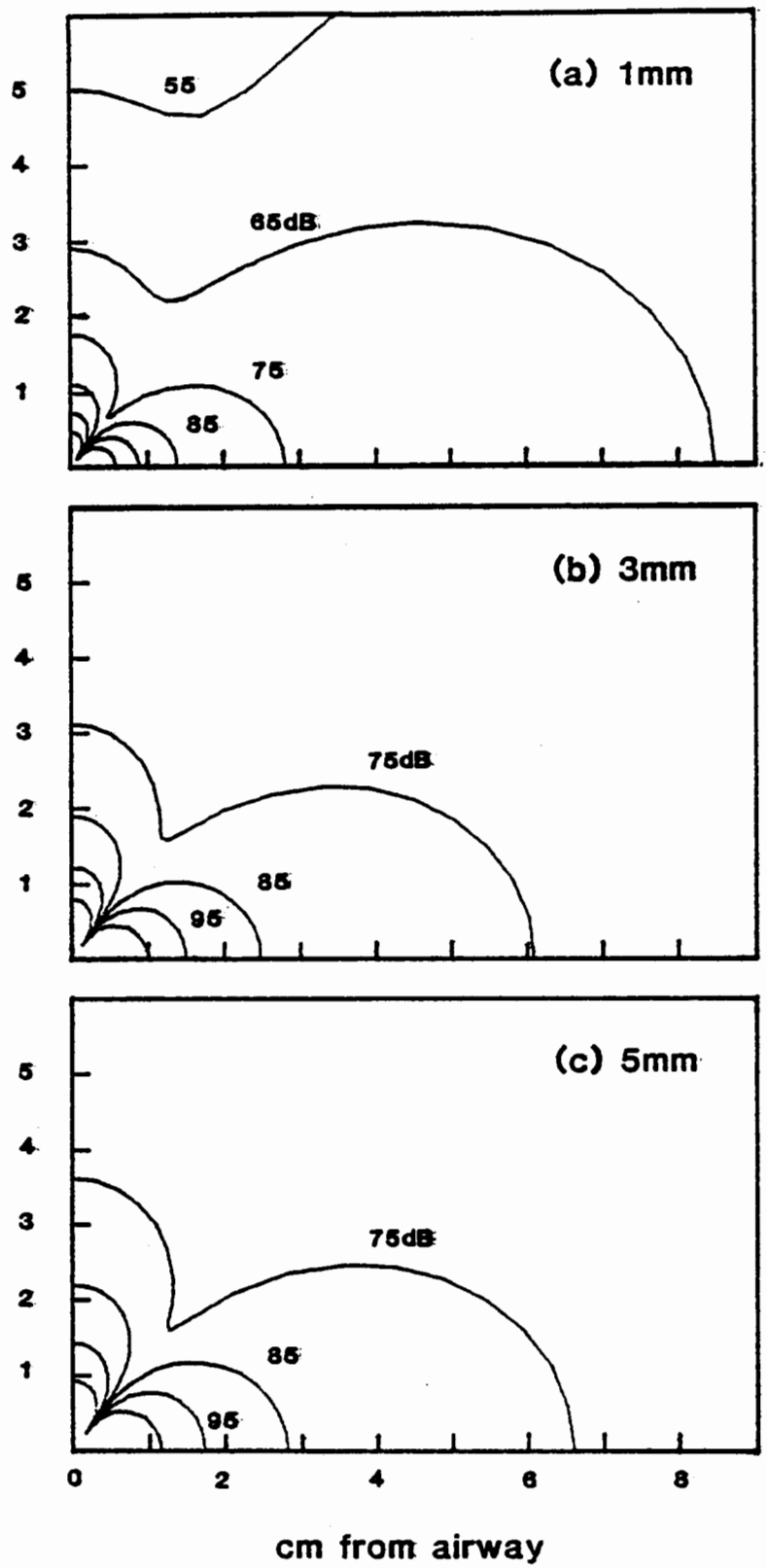

Figure 5.10 - Iso-energy contours for three model airway diameters plotted on natural-size centimeter scales.

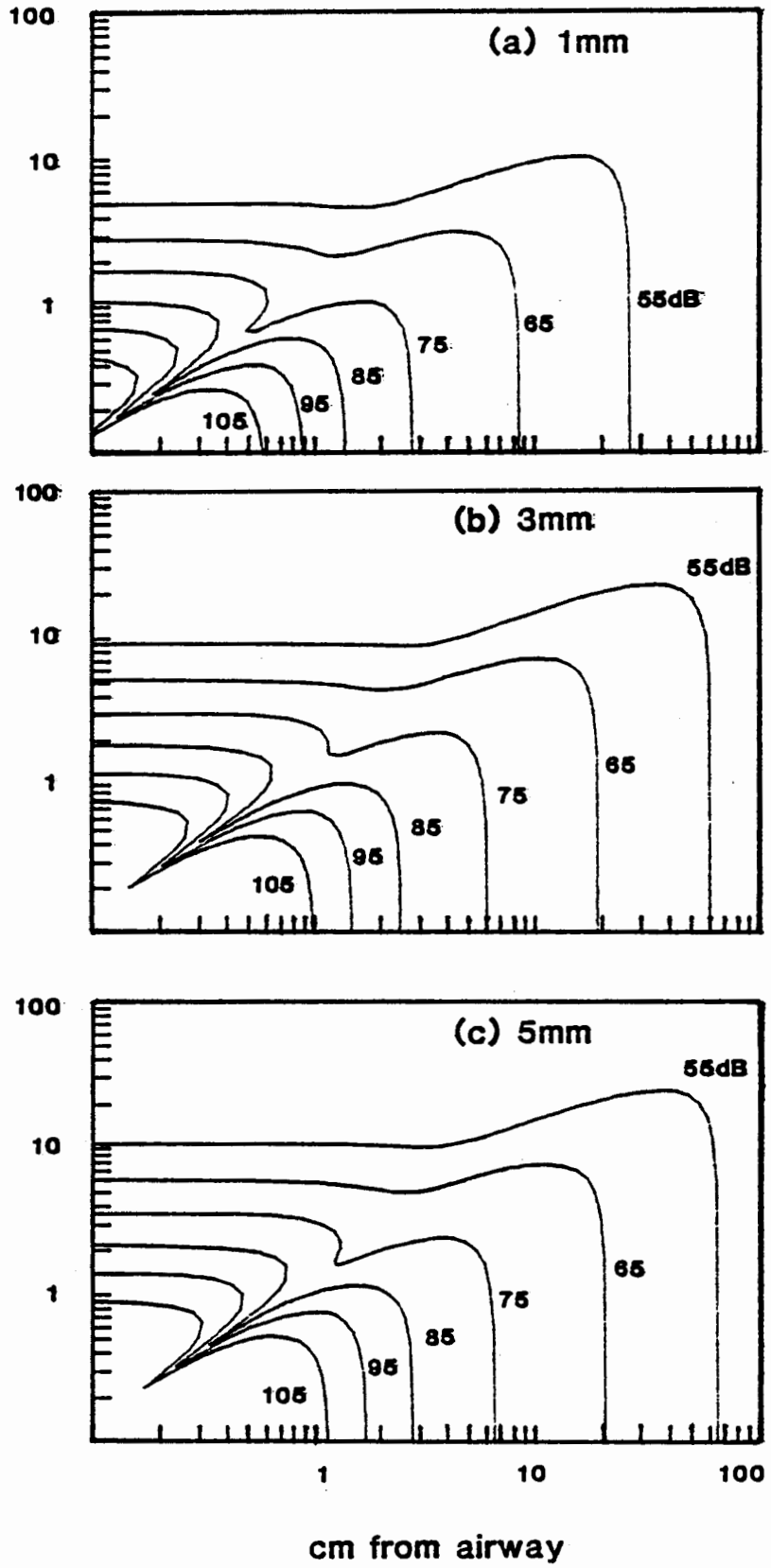

Figure 5.11 - Iso-energy contours for 1,3, and 5mm model airways plotted on logarithmic scales. The furthest contours are of theoretical interest only because they are located at distances exceeding the dimensions of the lung.

5.3.4 **Spatial Variations of Waveforms** - To see how the waveforms vary in shape and amplitude as the point of observation moves in relation to the source airway, we can move along a single iso-energy contour, along an arc of constant radius, and along a line of constant θ. Figure 5.12 shows twenty sample simulated DALS occurring at points located on the 85 dB iso-energy contour of a 1mm airway. The waveform shapes before the cusp at 54.7° are rather similar and have positive initial deflections, indicating that the disturbance begins coming toward the point of observation. The shapes past the cusp are also quite similar to one another and have a negative initial deflection.

Figure 5.13 shows samples along an arc of constant radius for a 1mm airway. The arc was taken with radius r=1.40 cm, which produces an 85 dB complex for $\theta=0^{\circ}$. There are significant variations in amplitude when we move at constant radius from 0° to 90°. The overall variation in energy between the complex at $\theta=0^{\circ}$ and the small ones near the cusp is about 15 dB, somewhat more than is observable in patients (see Chapter 6).

Figure 5.14 shows samples along the line $\theta=0^{\circ}$ for 1mm and 5mm airways. To facilitate both shape and amplitude comparisons, each DALS is plotted both at the same vertical scale as the others for its airway and also at a scale such that it nearly fills the box. The energy range is 20 dB, 5 dB on either side of the range reported in Chapter 6 as the range of observability in patients.

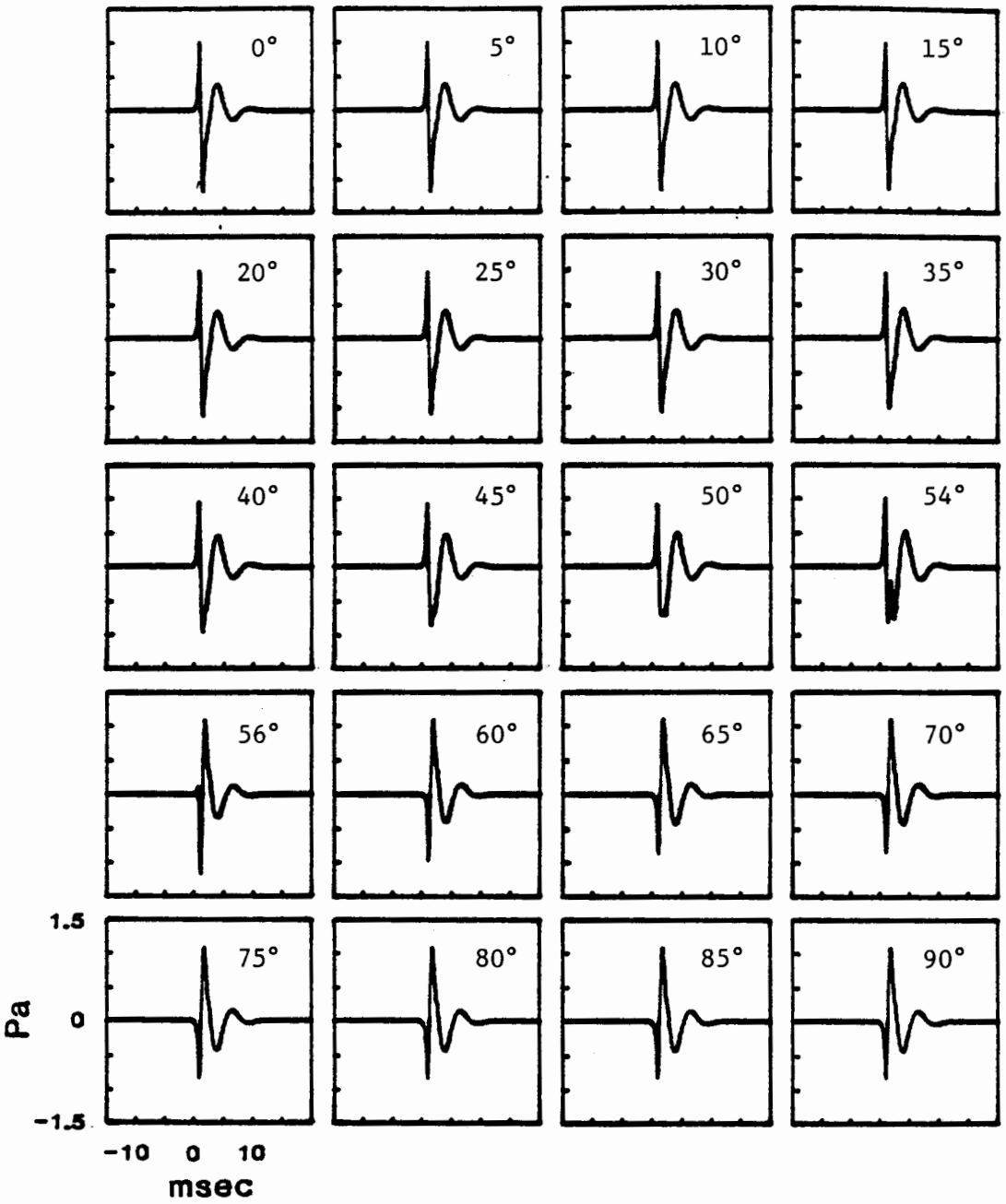

Figure 5.12 - Model DALS occurring along the 85 dB constant energy contour from a 1mm airway. Note the positive initial deflections before the cusp (54.7°) and the negative initial deflections at angles greater than the cusp angle.

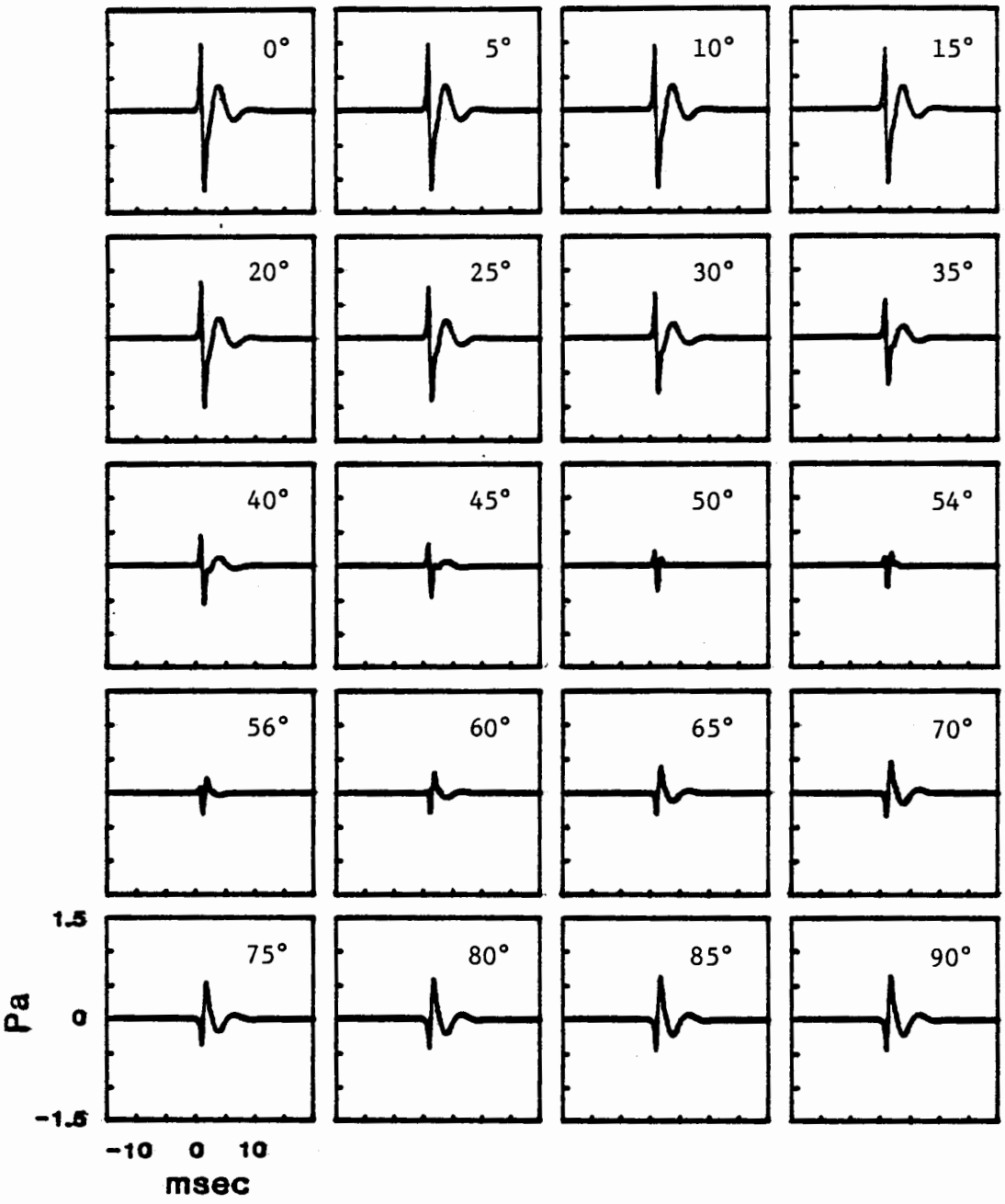

Figure 5.13 - Model DALS occuring along an arc of constant radius, r = 1.40 cm from a 1mm airway. The waveforms near the cusp angle (54.7°) have about 15 dB less energy than the complex at 0°, which has an energy of 85 dB.

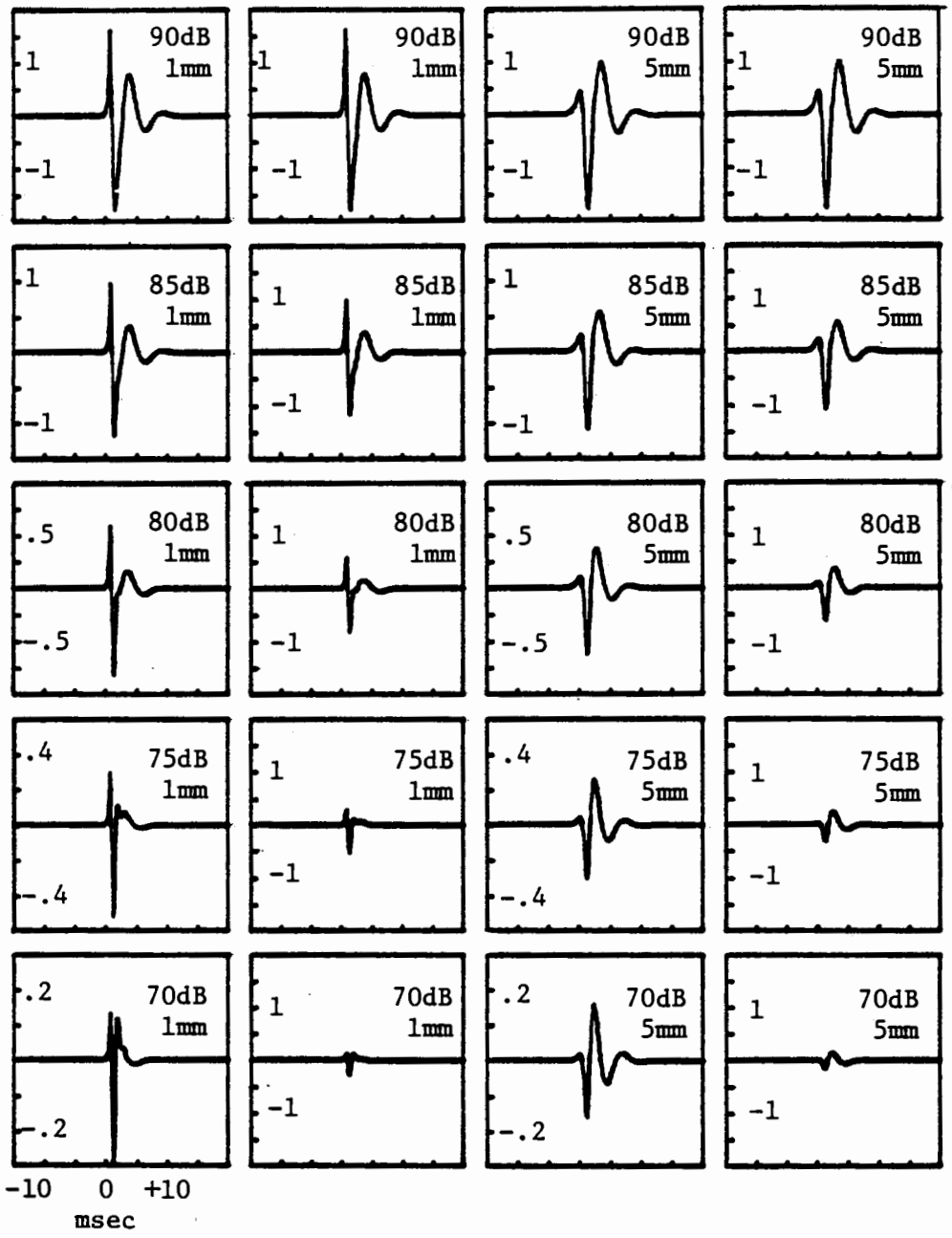

Figure 5.14 - Model DALS from 1mm and 5mm airways observed at points along the line where $\theta=0°$. Each row shows DALS of equal energy. Each complex is plotted twice in adjacent boxes with different vertical scales. All the plots in columns 2&4 have equal vertical scales to emphasize amplitude changes, while plots in columns 1&3 have different scales to facilitate shape comparisons. Vertical scales in Pascals are marked in each box.

In Figure 5.14 all the plots have the same horizontal scale. The first two columns are DALS from a 1mm airway. In the first column the plots are arranged in order of decreasing energy starting from 90 dB at the top to 70 dB at the bottom. To facilitate shape comparisons, each plot in column one has its own vertical scale. Notice that as we proceed away from the airway (down the page), the deflections become sharper, that is, the zero-crossing intervals become smaller. This sharpening occurs because $\overset{*}{r}$ starts at 1.83 for the 90 dB 1mm DALS and increases to 7.98 for the 70 dB DALS, a range of 4.4: 1. The second column of the figure shows the same DALS plotted at vertical scales that are all the same as the top 90 dB DALS. The 20 dB difference in energy corresponds to about a tenfold difference in peak amplitude.

Columns 3 and 4 of Figure 5.14 show DALS from a 5mm airway organized in the same way as columns 1 and 2 for the 1mm airway. For the larger airway, $\overset{*}{r}$ varies from 0.72 at the top to 3.87 at the bottom, a 5.4: 1 change. The height of the first deflection becomes increasingly reduced at lower energies, a fact which makes the larger airway DALS more difficult to measure in the presence of other signals.

5.4 Discussion

Many of the results of this chapter are better understood by considering distances from the airways on the normalized scale of equation (5-3a), $\overset{*}{r} = r/(c_L \tau)$. Table 5.2

gives the real and normalized distances from 1,3, and 5mm airways at which 85 dB DALS occur for $\theta=0^{o}$. In normalized units, the point of observation is 2.5 times as far away from a 1mm airway as from a 5mm airway. This is just the reverse of the relation between the real distances in centimeters. Examining equation (5-4), we can see that the small $\overset{*}{r}$ associated with the 5mm airway emphasizes the undifferentiated terms. For this particular example, equation (5-4) becomes for $\theta=0^{o}$

$$1mm: \quad -.16\overset{*}{g} - .37\overset{*}{g}' - .43\overset{*}{g}'' \qquad (5-14a)$$

$$5mm: \quad -.50\overset{*}{g} - .39\overset{*}{g}' - .22\overset{*}{g}'' \qquad (5-14b),$$

where the second equation has been divided by 5 to account for the difference in the factor K_p, which scales inversely with the diameter. Inspection of Figures 5.6 and 5.8 reveals precisely this relation between the individual terms for the two airways. Thus, measuring on the distance scale that determines the shape of DALS, we observe large airways from a <u>closer</u> vantage point. The closer we are to the source, the more the unfiltered pressure waveform resembles

<u>Table 5.2</u>

Relation between real and normalized distance from the airway to the 85 dB iso-energy contour.

d_{aw} (mm)	r_{85dB} (cm)	$c_L \tau$	$\overset{*}{r}_{85dB}$
1	1.40	0.60	2.33
3	2.47	1.80	1.37
5	2.80	3.00	0.93

the stress relaxation source function itself. We will return to this subject in Chapter 6. The remainder of the discussion here focuses on some problems and limitations of the model and simulation process.

In formulating the basic equation for the pressure in the medium the source was assumed to have only a quadrupole component without any monopole or dipole contributions. Omitting the dipole component seems physically reasonable since it corresponds to an external force acting on the medium. The monopole term corresponds to net volume injection at the source, and this may indeed occur when the airway opens. The magnitude of this effect is unknown at this time. The philosophy adopted was to start with the quadrupole term alone and determine the accuracy of the resulting model's predictions. As we will see in Chapter 6, these predictions are as yet more extensive than the available data.

There is no fundamental reason to believe that the lung tissue behaves as a lossless, non-dispersive transmission medium. The magnitude of departures from the ideal assumptions is not known. It does seem reasonable to ignore dispersion of the compressional waves because the point of observation is only on the order of one wave length from the source. At a wave speed of 3000 cm/s and a frequency of 500 Hz, the wave length is 6 cm.

The medium was also assumed to be infinite in extent, whereas the lung itself is finite and enclosed by the chest

wall. We assume that the chest wall blocks the motion of the lung normal to it, but allows free motion in the transverse direction. For this configuration, the method of images allows us to replace the chest wall by an infinite continuation of the medium with an image source. The transducer response should thus be viewed as the superposition of disturbances from the actual source airway and the image source. Since this would result in only a factor of two amplitude change, it was neglected in comparison to the uncertainties in parameter estimation, which are discussed below.

The model used is quite simple in its assumptions of a quadrupole source and an ideal medium. But even for this simple model estimation of appropriate values for the several parameters is a significant problem. Values for the velocities c_L and c_T were based on measured properties of lung tissue, and the value for c_L compares favorably with Rice's measurements. As noted in section 5.2.2, however, this value may be somewhat dependent on lung volume. The effect of this variation needs to be evaluated.

The surface tension stress, σ_o, was based on well known estimates of the surface tension, T, of the fluid airway lining material on inspiration. The radius of the meniscus, however, is uncertain and has to be estimated. It was taken to be the same as uncollapsed airway radius, but it seems quite reasonable that it might be smaller than that.

The exact form of the function describing the time

course of stress relaxation affects the predicted waveforms. The current model assumes a source disturbance characterized by a single time constant. The function used is symmetrical about t=0, which implies that the dynamic behavior of the stress at the airway is the same before and after the opening event. In particular, we assume that the function has no overshoot and ringing. This seems overly simplistic, but there is no current justification for a more complicated model of the time course of stress relaxation. An appropriate range of values for the source function parameter, τ, was estimated by considering the natural frequency of the accretion mass imposed by the surrounding medium and the elastance of the airway. Changing the parameter τ affects the normalized time, frequency, and space variables. It is thus an important determinant of the model's predictions with respect to temporal waveforms, frequency content, and spatial distribution of the disturbance. The implications of our lack of precise knowledge of the value of τ and the other model parameters for a particular airway are discussed below.

Because of the uncertainties in parameter estimation, the predictions of the model for a particular set of parameters can not be absolutely associated with a particular airway diameter. However, each of the parameters was assumed to scale in a particular way with airway diameter (Table 5.1), and these scaling laws are more easily justified than the exact constants of proportionality. Thus, the predic-

tions of the model should really be interpreted in terms of relative airway size. When better estimates or measurements of the parameters are available, the connection with absolute airway sizes may be made. It is also possible that better parameter estimates will reveal significant shortcomings in the model's formulation.

The exact nature of the filter used to simulate the effects of the transduction process affects the shapes of the predicted waveforms. It seems reasonable to suspect that significant variations in chest wall mechanical properties would change the observed shape of DALS. The mechanical interaction between the transducer and chest wall needs more study if the filtering effect is to be quantified more precisely.

It is not surprising that attempting to estimate parameters in a living structure as complex as the lung is rather difficult. Even so, the predicted waveforms are quite similar to observed DALS. Further, the model provides a basis for interpreting and integrating the clinical observations presented in Chapters 3 and 4. The predictive ability of the model with respect to such data is an important test of its correctness.

Chapter 6
Comparison of Model Predictions and Real Observations

6.1 Introduction

To learn whether the DALS model presented in Chapter 5 is compatible with the clinical observations of Chapters 3 and 4, we need to examine the model's predictions regarding waveform shapes and chest surface distribution patterns for a range of airway diameters. Since the model predicts the pressure at any point in the 3-dimensional medium, we can compute the iso-energy contours and waveform shapes on any plane that we have chosen to approximate the chest wall. The validity of our comparison between the model's predictions and real observations rests partly on realistic placement of a chest wall plane. Section 6.2 shows how we can estimate the distance of the plane from the airways as well as its average angular orientation.

Having located the plane, we will "project" iso-energy contours onto it so we can see the model's prediction of the energy distribution of DALS on the chest wall. To compare these energy distributions to the observations of Chapter 4, we need to know the energy range between the largest DALS seen in patients (high energy) and the smallest DALS (low

energy). At the low energy end of the range, we are not so interested in visibility of the DALS as in measurability of their parameters, because measurability in both channels was used as a criterion for association of DALS at two chest sites. By returning to the two microphone data of Chapter 4, we can estimate the range of measurability directly (section 6.2.2).

Knowing the energy range of real DALS measurable on the chest, we will examine both the shapes and surface distributions of the model's DALS and compare them to the findings of previous chapters. Section 6.3 shows the results of varying the model's parameters from small to large airway sizes and measuring the (IDW, 2CD) parameters of the resulting waveforms. We will see that the model's waveforms span about the same range of parameters as real DALS classified auditorily as fine and coarse. Section 6.4 shows how the IDW/2CD plane classification connects to the measurement of surface distribution for sets of model parameters corresponding to small and large airways. The resulting predicted connection between fine/coarse waveform parameters and DALS measurability at two microphones is discussed in section 6.5.

To avoid confusion between properties of real DALS and those of modeled DALS, we will reserve the adjectives fine and coarse for DALS from patients. DALS waveforms produced by the model will be referred to as class F when their (IDW, 2CD) parameters fall into the fine region and as class C

when their parameters fall into the coarse region.

6.2 Prediction of Chest Wall Distributions

6.2.1 **Amplitudes of DALS in Patients** - Few measurements of DALS amplitudes have been reported. As noted in section 1.2.4, Wooten and Waring [1972] observed in a pediatric population DALS with peak pressures of up to 0.5 Pa in their air coupling chamber, which had a volume of 3.3 cm^3. They reported only this maximum number, which corresponds to a peak pressure of about 2.0 Pa in the 0.8 cm^3 chamber used in the present work.

Figures 6.1 and 6.2 show example tracings of fine and coarse DALS encountered in patients. Amplitude calibration was performed as described in section 2.2.6. Each of the figures shows the resulting amplitude scale. In Figure 6.1, which shows fine DALS, the largest complex has a peak amplitude of about 1.0 Pa, while the smallest DALS whose IDW and 2CD can be measured has a peak amplitude of 0.32 Pa. As will be shown later in this chapter, this 10 dB range of measurability is typical. The range of observability is larger. Note the very small deflections with recognizable DALS shapes, which can be seen but not measured according to the IDW/2CD criteria. The largest DALS in Figure 6.2 has a peak amplitude of 1 Pa, while the smallest measurable complex has a peak of 0.45 Pa.

The source strength parameter, ($\Delta v \times \sigma_o$), of the model

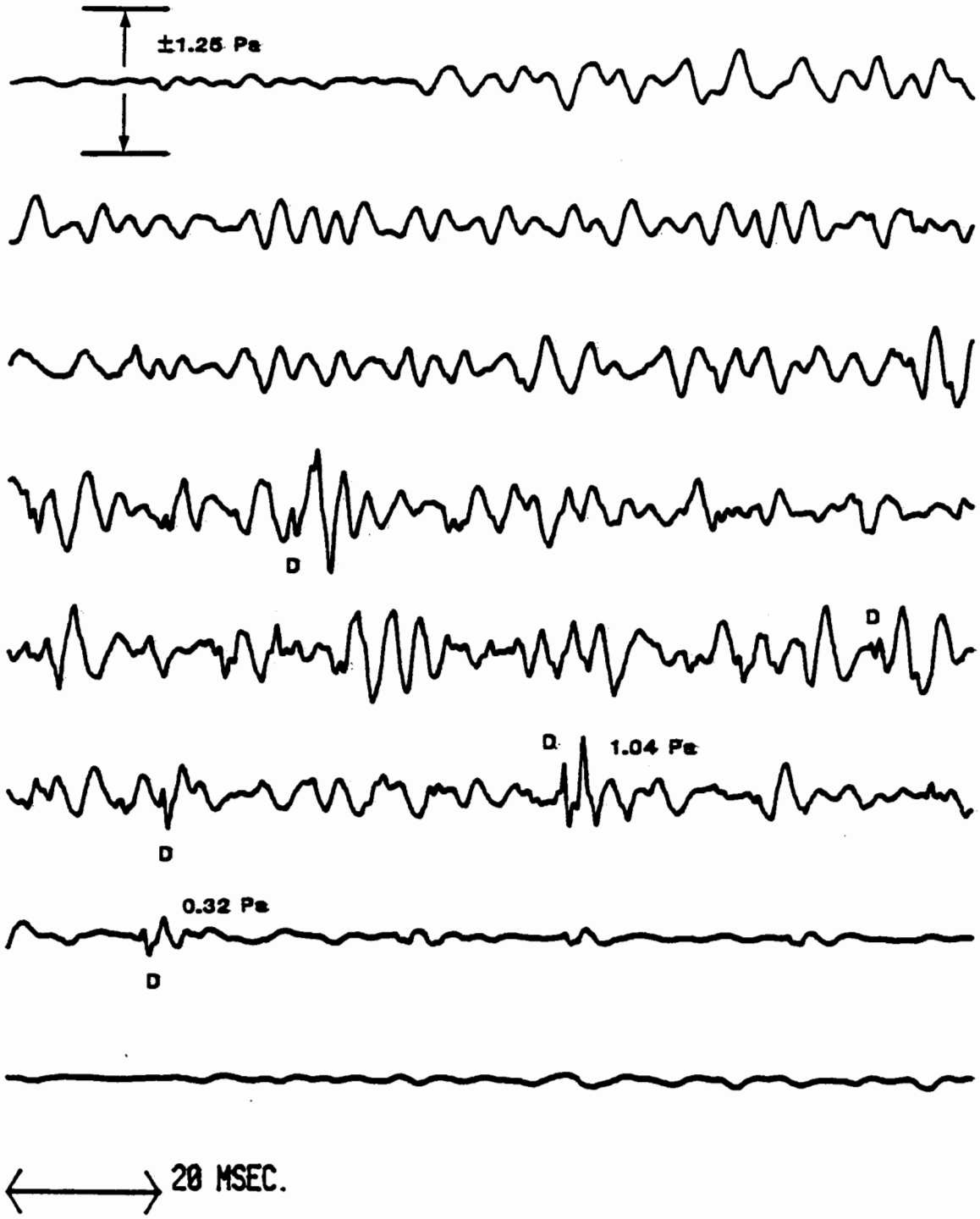

Figure 6.1 - Amplitude versus time plot of inspiratory sound from a patient with fine DALS, some of which are marked (D). The plot begins at upper left, and one line follows another like printed text. The calibrated amplitude scale is ± 1.25 Pascals. The peak amplitudes of two DALS are marked; they show a 10 dB difference.

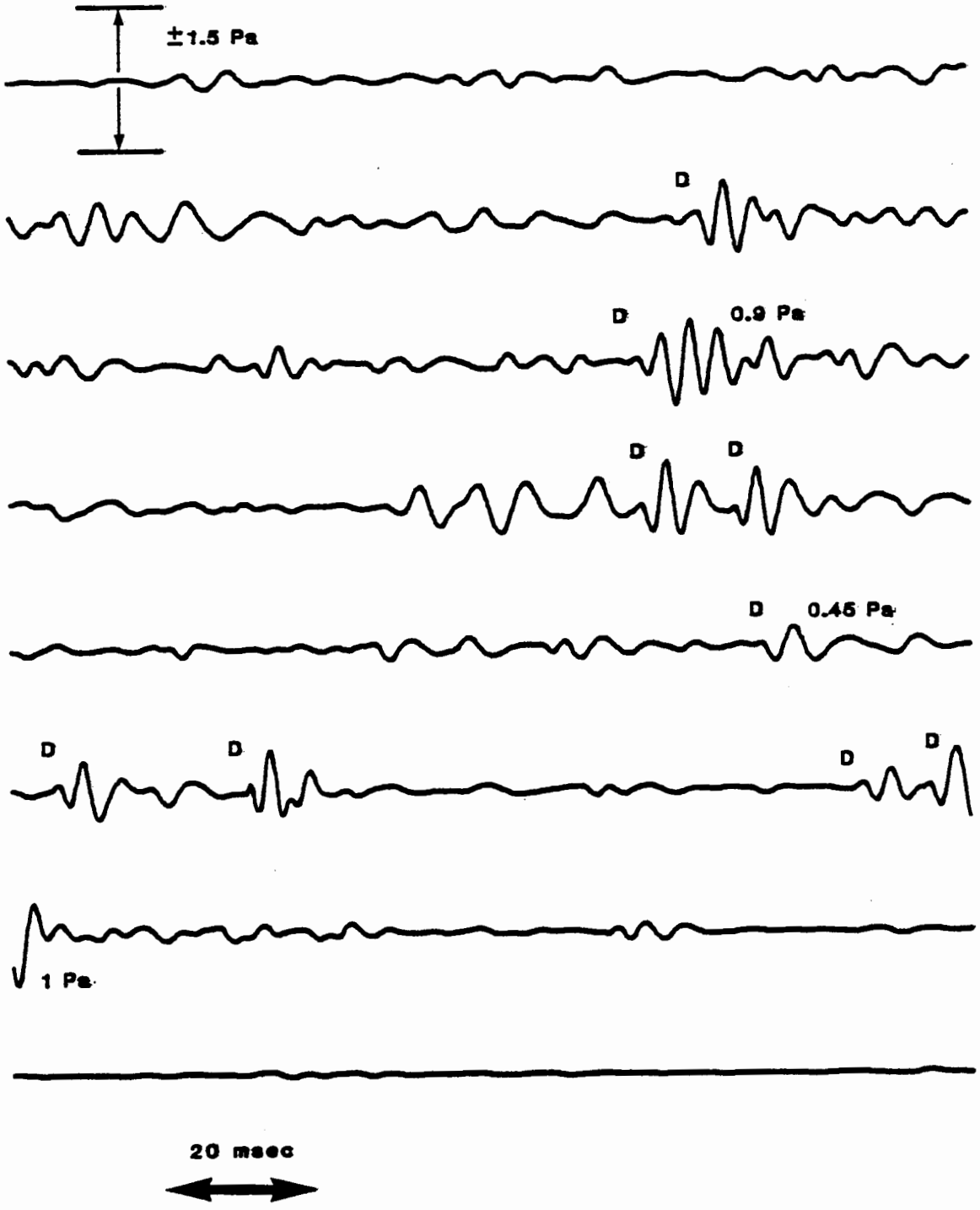

Figure 6.2 - Amplitude versus time plot of inspiratory sound from a patient with coarse DALS (marked D). The calibrated amplitude scale is ± 1.5 Pascals. The peak amplitudes of three DALS are marked.

was adjusted to produce DALS with energies of 85 dB at a distance of about 3 cm from a 5mm airway. This distance to the surface was estimated by bronchogram measurements. Bronchograms are x-rays taken of the chest with contrast medium in the airways. DALS with 85 dB energy have peak amplitudes of just over 1 Pa.

6.2.2 **Energy Range of Measurable DALS** - The tracings made for the two-microphone data of Chapter 4 were examined to learn what the average range of measurability was in a larger number of patients. The peak amplitude of each measurable DALS in the 12 patients was noted and was taken as a measure of waveform energy. The validity of this method for measuring energy was investigated by examining the relation between amplitude and energy for the model's waveforms. We wish to determine whether the energy is approximately proportional to amplitude in spite of changes in the details of the waveform shapes. Figure 6.3 shows the results. Part (a) of Figure 6.3 shows waveform energy of modeled DALS plotted versus distance from the airway at $\theta=0^{\circ}$ for 1mm and 5mm airways. Figure 6.3(b) shows peak amplitude versus distance for the same airways. In Figure 6.3(c) energy and peak amplitude are plotted against each other. From these plots it was concluded that for modeled DALS the difference in peak amplitude was an acceptable measure of energy difference, and we will assume the same relation in real DALS.

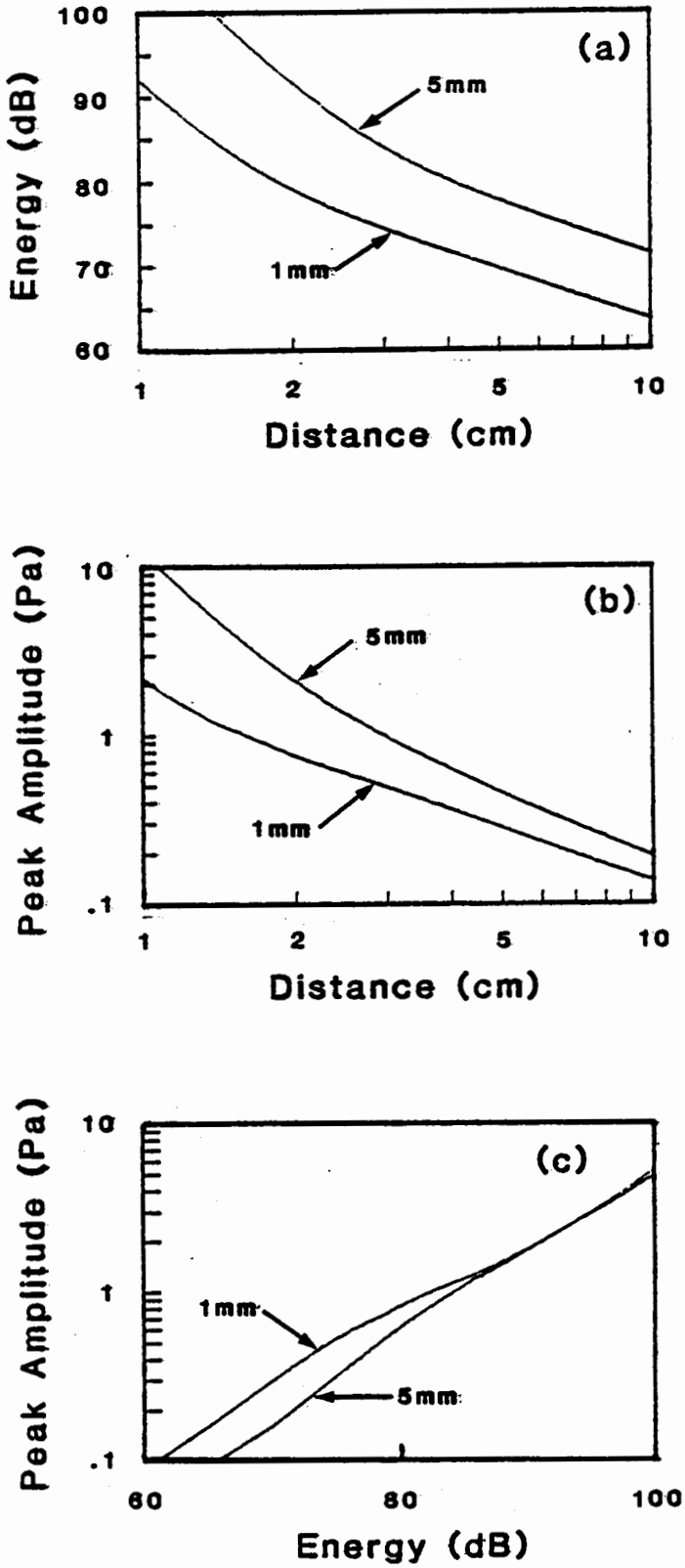

Figure 6.3 - DALS energy and peak amplitude for model airways with 1mm and 5mm diameters. (a) Energy of DALS waveform vs. distance from airway. (b) Peak amplitude vs. energy.

The histograms of Figure 6.4 are estimates of the distributions of energy difference between DALS at two microphones separated by 6 cm. One histogram shows the distribution of the energy difference between DALS whose IDW and 2CD were both measurable. The other histogram shows the distribution of the energy difference between pairs of DALS only one of which was measurable. In many of the cases where only one channel had a measurable complex, no recognizable DALS was present in the other channel. In these cases an energy difference of 20 dB was assigned for the purpose of plotting the histogram.

For the 6cm microphone spacing, the total number of associated DALS measured was 25 pairs (Table 4.2). Between DALS in these pairs, the mean energy difference was 5.7 dB. A total of 33 unassociated DALS were seen. Of these 33, 12 occurred with a recognizable complex in the alternate channel that did not have measurable (IDW, 2CD) parameters but <u>did</u> have measurable amplitudes. For these 12 DALS, the mean energy difference between the two channels was found to be 12.2 dB. When we add in the (33-12) = 21 instances when no recognizable complex was seen in the alternate channel and assign an energy difference of 20 dB, the average energy difference for unassociated DALS becomes 17.1 dB (N=33). The midpoint between the means of the two distributions is then either (5.7 + 12.2)/2 = 9 or (5.7 + 17.1)/2 = 11, which are both on the order of 10 dB. The histograms are seen to cross at about 10 dB as well. It was thus decided to use an

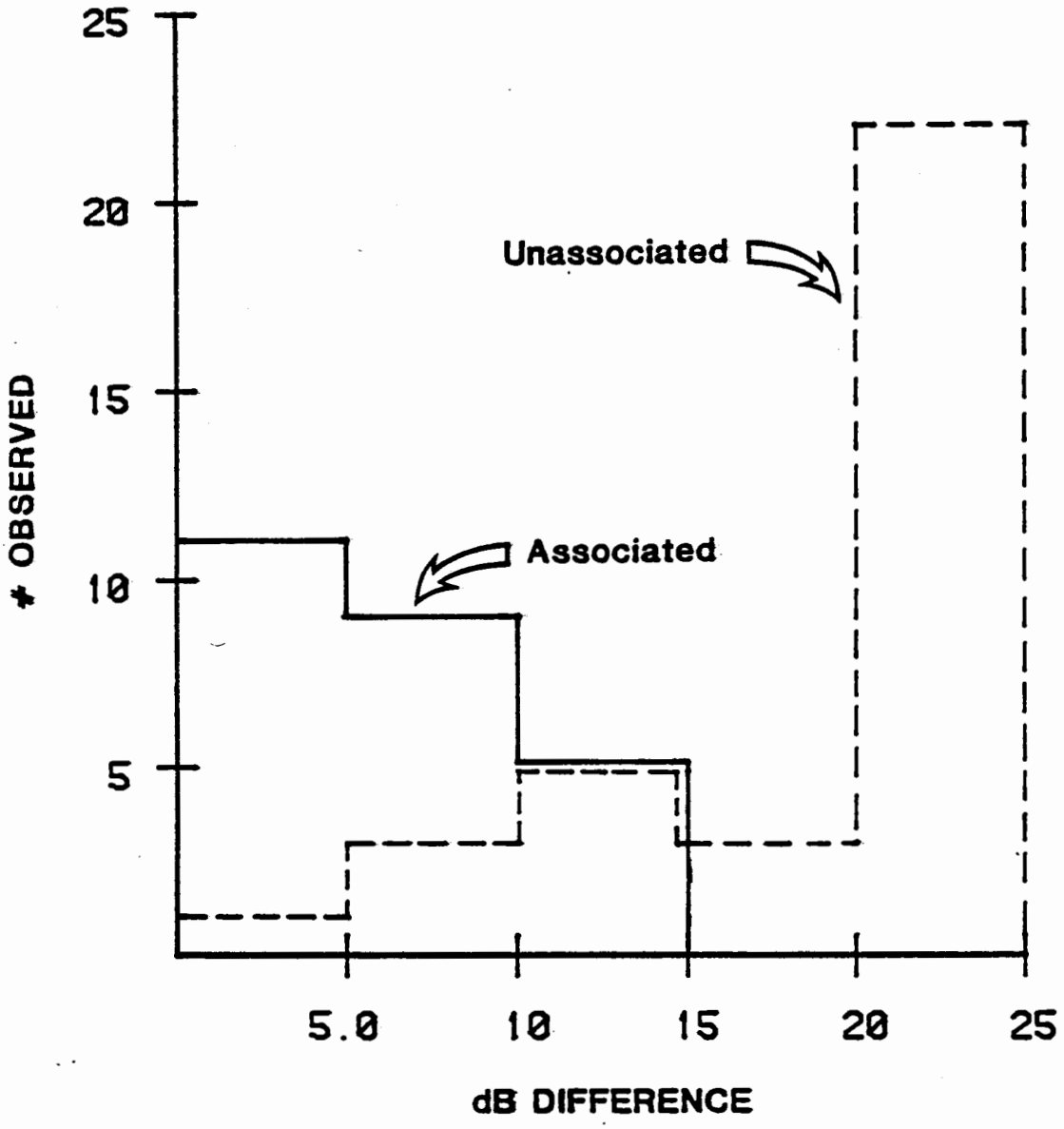

Figure 6.4 - Sample distributions of energy difference between DALS at two microphones. The histogram with solid lines shows the energy difference in dB between measurable DALS appearing at two transducers separated by 6 cm. The histogram with dotted lines shows the dB difference when a complex whose IDW and 2CD could be measured appeared at only one microphone. When no recognizable DALS could be seen in the second channel, an energy difference of 20 dB was assigned.

energy span of 10 dB to approximate the range over which DALS are measurable on the chest wall.

Using a nonparametric test for difference in distribution, we can test the hypothesis that the associated and unassociated DALS really have different underlying distributions of energy difference between the two channels. The Mann-Whitney rank sum method is such a test [DeGroot (1975)]. Applying the rank sum test to the energy differences of the 33 associated DALS and 12 unassociated DALS recognizable in both channels yields a z-score of 3.5 ($p<.001$). This result means that there is less than one chance in 1000 that the two observed histograms arose by chance from identical underlying distributions.

The results of this and the preceding section tell us first that we should locate our imagined chest wall plane such that the largest model DALS observable on the plane have energies of 85 dB. Second, to estimate the size of the region corresponding to measurable DALS, we should go from the 85 dB central point out to the 75 dB contour, a span of 10 dB. We still need to know in what direction from the airway to locate the chest wall plane. Studying the initial deflections of real DALS tells us the proper direction as described in the next section.

6.2.3 **Sign of Initial Deflection** - Recall from Chapter 5 that model DALS have positive initial deflections when the point of observation is to the side of the airway and

negative initial deflections when observed at points near the airway axis. Thus, by noting the direction of initial deflections in real DALS we can see where to locate the model's chest wall projection planes. The signs of the initial deflection of the DALS complexes were noted for all the patient data from the two microphone study. Of the 90 DALS measured at both microphone separations in 12 patients, 78 had an initial deflection that was negative.

Since the transduction-recording-playback-analysis chain involves a number of possible sign inversions, the actual equipment used to acquire and analyze the two microphone data was checked in the following way. A microphone was attached to the forearm and tapped lightly. The resulting signal was recorded and analyzed. Figure 6.5 shows the resulting complex, which has a <u>negative</u> first half cycle. This tells us that compression of the air chamber

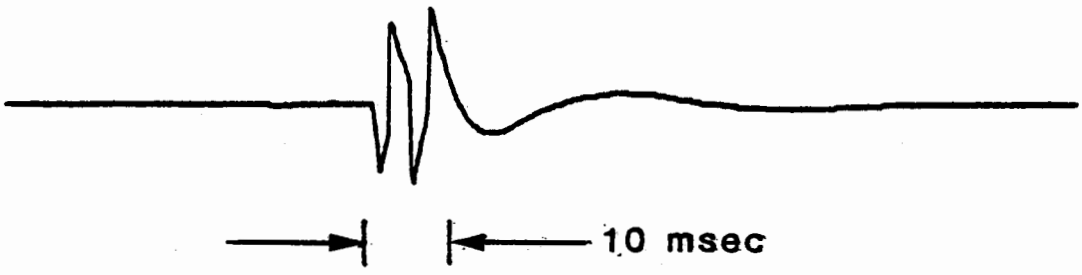

<u>Figure 6.5</u> - Microphone response to tapping on the case. Since the force on the back of the case compresses the air in the chamber, negative initial deflections in patient data are interpreted as first half cycles of the chest moving toward the microphone. The microphone was placed on the arm for this experiment. The point of interest is the direction of the initial deflection rather than the details of the response.

produces a negative change in microphone output. Since the pressure in the chamber is in phase with the chest wall deflection, we conclude that for this set of equipment the predominantly negative initial deflections observed in patients indicate that the first cycle of chest wall movement for DALS is usually toward the microphone. Since such deflections are observed in the model's waveforms at points located to the side of the airway, the chest wall projection plane should be located near $\theta=0^{o}$. Having considered the appropriate range and angle for the projection surface, we now proceed to the projection methodology.

6.2.4 **Calculation of Iso-Energy Contour Projections** - Having decided where to locate the chest wall plane, we can use the model's equation for pressure in the medium to tell us what the model waveforms and energy values are for any point on the chest plane. Since it is convenient for the chest wall plane to have its own coordinate system, we need to derive a transformation between chest wall coordinates and the airway-centered coordinates of the model. In particular, we need to know the values for the r and θ variables in equation (5-1) for any given point on a chest wall plane. Figure 6.6(a) shows the coordinate transformation problem involved in calculation of iso-energy contours on a chest wall plane. Recall that the origin of the (x_1,x_2,x_3) coordinates is at the airway with the x_2 axis aligned with the airway axis. The location of the chest

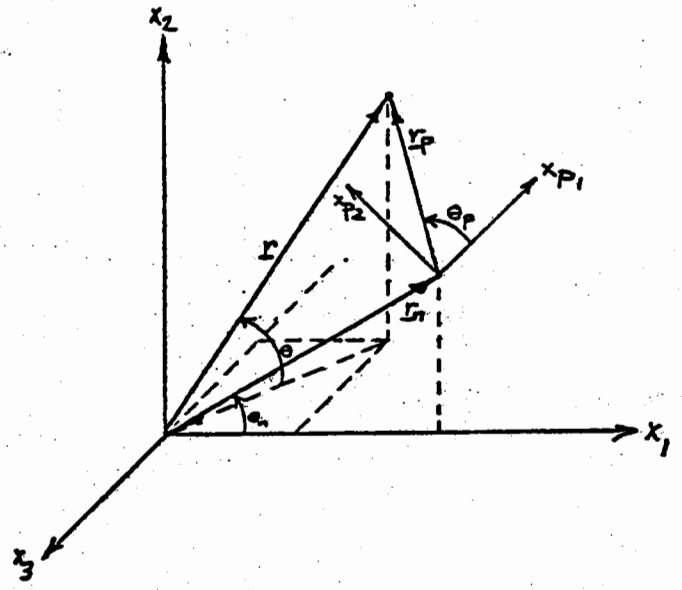

Figure 6.6(a) - Coordinate transformation geometry. The airway is located at the origin of the (x_1, x_2, x_3) system with its axis vertical. The chest wall projection plane system (x_{p1}, x_{p2}) is located in a plane whose normal is $\underline{r}_n$. For convenience, $\underline{r}_n$ lies in the x_1-x_2 plane. The point at which the pressure is desired is located at $\underline{r} = \underline{r}_n + \underline{r}_p$.

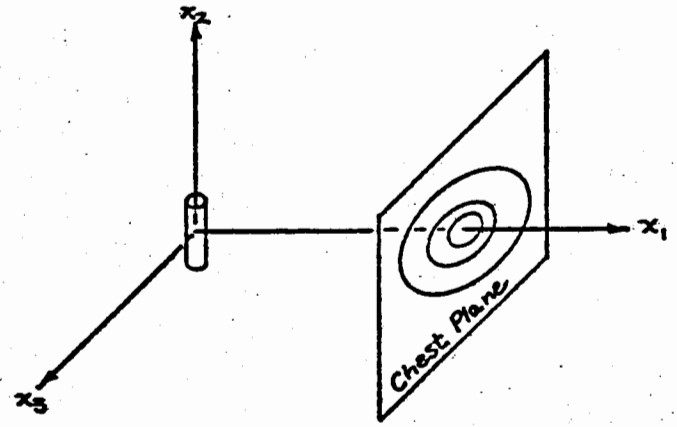

Figure 6.6(b) - Orientation of model airway with respect to projection plane and resulting chest surface iso-energy contours.

wall projection plane is specified by the vector $\underline{r}_n$, which is the normal to the plane. Because of the cylindrical symmetry of the problem, we can confine $\underline{r}_n$ to have an x_3 component of zero without loss of generality.

In the projection plane we define a new coordinate system (x_{p1},x_{p2}) such that x_{p1} is aligned with the negative x_3 axis. In deriving the transformation, it is convenient to define unit vectors pointing along the coordinate axes: $\underline{u}_1$, $\underline{u}_2$, $\underline{u}_3$, $\underline{u}_{p1}$, and $\underline{u}_{p2}$. Then

$$\underline{u}_{p1} = -\underline{u}_3 \qquad (6\text{-}1a)$$

and $$\underline{u}_{p2} = -\sin\theta_n \underline{u}_n + \cos\theta_n \underline{u}_2 \qquad (6\text{-}1b),$$

where θ_n is the angle between $\underline{r}_n$ and the x_1 axis, so that

$$\underline{r}_n = r_n \cos\theta_n \underline{u}_1 + r_n \sin\theta_n \underline{u}_2 \qquad (6\text{-}2).$$

Similarly, we define $\underline{r}_p$ to be the vector from the origin of the projection plane coordinate system to the point of interest in the plane. θ_p is then the angle between $\underline{r}_p$ and the $\underline{x}_{p1}$ axis, so that

$$\underline{r}_p = r_p \cos\theta_p \underline{u}_{p1} + r_p \sin\theta_p \underline{u}_{p2} \qquad (6\text{-}3).$$

Then the vector $\underline{r}$ from the airway coordinate origin to the point of interest is just

$$\underline{r} = \underline{r}_n + \underline{r}_p = r_1\underline{u}_1 + r_2\underline{u}_2 + r_3\underline{u}_3 \qquad (6\text{-}4),$$

where

$$r_1 = r_n \cos\theta_n - r_p \sin\theta_p \sin\theta_n \qquad (6\text{-}5a)$$

$$r_2 = r_n \sin\theta_n + r_p \sin\theta_p \cos\theta_n \qquad (6\text{-}5b)$$

$$r_3 = -r_p \cos\theta_p \qquad (6\text{-}5c).$$

Equation (5-1) defining the pressure requires $r=|\underline{r}|$ and θ, which is the angle between $\underline{r}$ and its projection in the

x_1-x_3 plane. For computational reasons, θ is defined by its inverse tangent

$$\theta = \tan^{-1}\left[\frac{r_2}{(r_1^2 + r_3^2)^{1/2}}\right] \qquad (6\text{-}6).$$

The distance r can be calculated as

$$r = (r_n^2 + r_p^2)^{1/2} \qquad (6\text{-}7).$$

With this formulation, it is possible to use the contour searching program described in section 5.2.4 directly. The contour search takes place in the projection plane with the coordinate transformation being performed before evaluation of the pressure waveform and energy. Figure 6.6(b) shows the orientation between the airway, chest plane, and the resulting contours.

Figures 6.7-6.10 show the resulting predicted chest wall iso-energy contours for airways diameters of 1,2,3, and 5 mm. Each projection plane was located such that the 85 dB contour was just visible in the middle. The distances used for 1,2,3 and 5mm airways to the chest plane are 1.35, 2.05, 2.47, and 2.80 cm respectively. Recall that the distance to the 5mm airway was set, while the other distances result from requiring 85 dB energy in the center of the contours. Between the 85 and 75 dB contours lies the region of measurability, i.e., the area over which DALS with measurable IDW and 2CD parameters are predicted to occur. This corresponds to the average 10 dB range in energies of measurable DALS in patients (section 6.2.2).

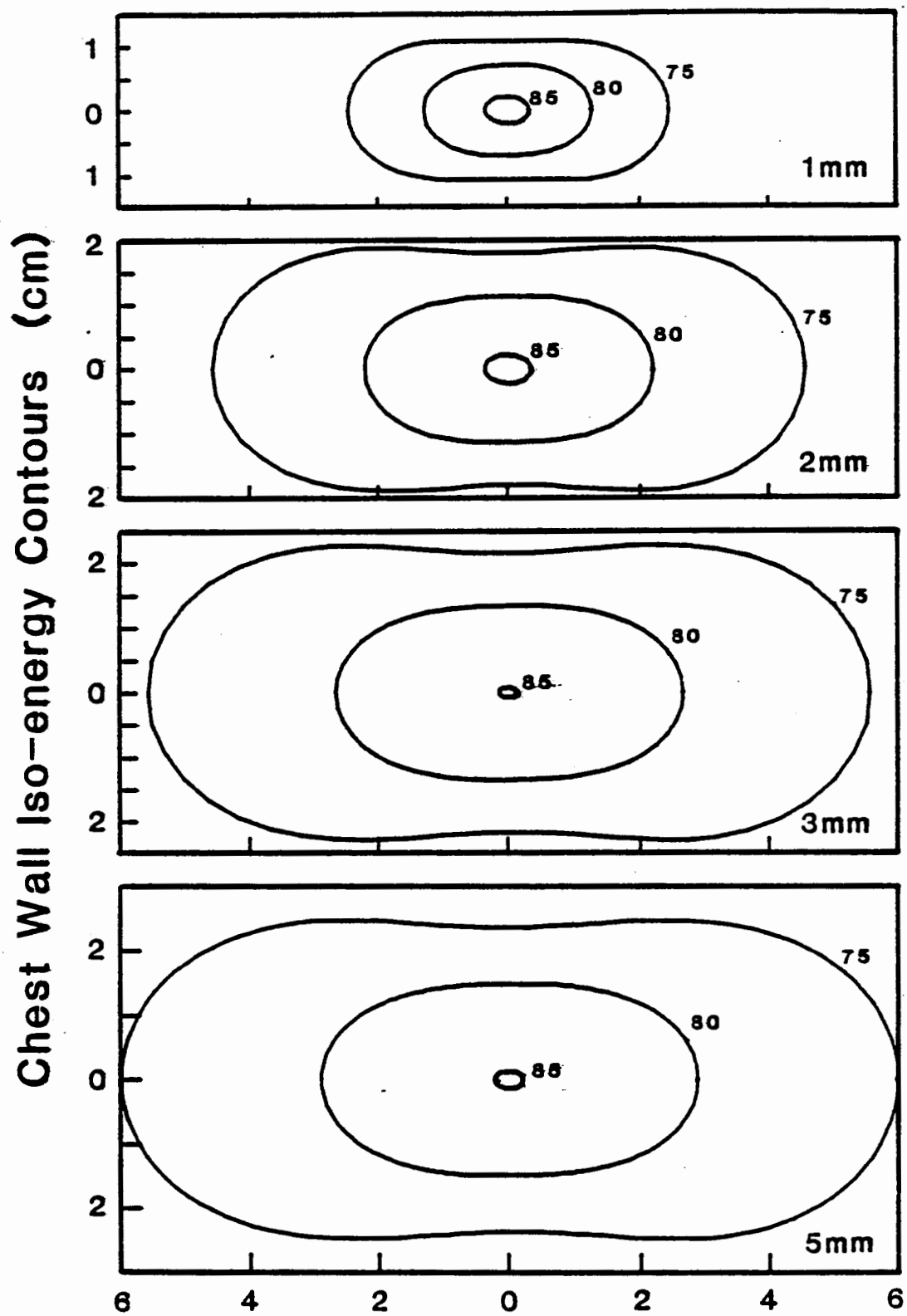

Figures 6.7 - 6.10 - Predicted chest wall iso-energy contours for model airways. The projection planes are located 1.35, 2.05, 2.47, and 2.80 cm from 1,2,3, and 5mm airways respectively. The area inside the 75dB contour is an estimate of the region where DALS would be measurable.

6.3 Comparison of Real and Predicted DALS Waveforms

If the model of Chapter 5 is correct, its predicted waveforms should closely resemble real DALS collected from patients. This correspondence depends on the correctness of (a) the formulation of the model and its equations, (b) the estimation of parameters and their dependence on airway diameter, and (c) the closeness with which the simulation's filter approximates the actual characteristic of the chest wall/transducer system. The simulator filter was designed to approximate the effect of the air-coupled electret microphones described in Chapter 2. Therefore, only real DALS recorded with such a microphone are presented in this section.

By measuring the IDW and 2CD of model waveforms in the same way we measured real fine and coarse DALS, we can see where in the IDW/2CD plane the model's DALS fall. Recall that we refer to model DALS falling on the fine side of the discriminant line as "class F" and those lying on the coarse side as "class C." We can see what region of the classification plane the model DALS occupy for different model airway sizes and waveform energies. We will display several pairs of DALS, one real and one modeled, that fall near each other in the IDW/2CD plane. This will allow visual comparison of the complete shapes of the complexes.

Figure 6.11 shows the location in the IDW/2CD plane of model DALS waveforms observable on the chest wall from various model airway diameters. An estimate of the region

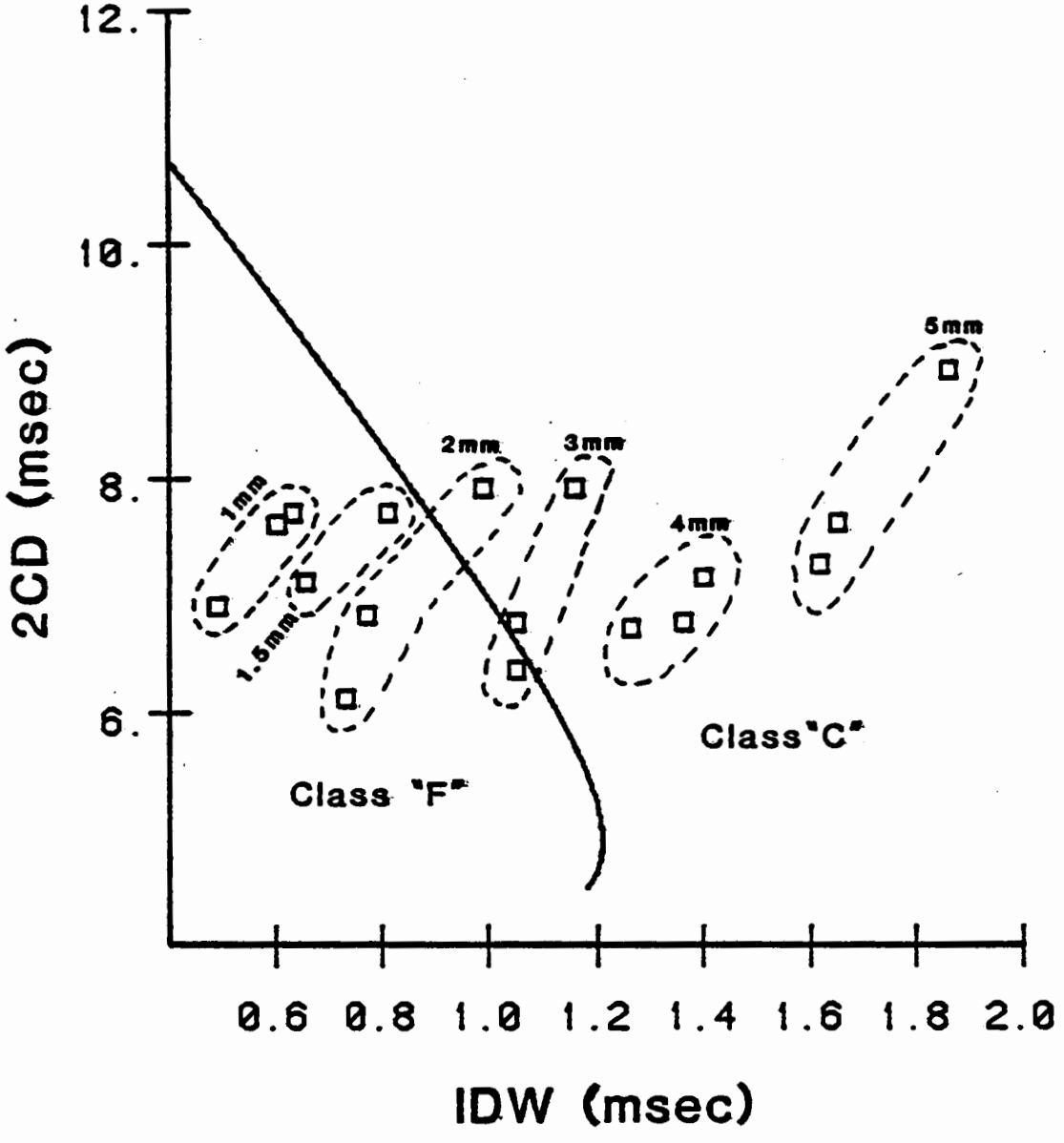

Figure 6.11 - IDW/2CD plane loci of DALS obtained from the model.

The dotted lines are rough estimates of the area of the plane in which lie DALS from airway diameters of 1mm through 5mm. The boxes are the measured parameters of DALS appearing in the region of measurability in chest wall projections for each airway size.

of the IDW/2CD plane containing DALS from a particular airway size was obtained by measuring the parameters of predicted DALS that fell in the 75-85 dB measurability region in the contour projections. The dotted lines in the figure are rough estimates of the loci of model DALS observable on the chest from airways located such that the angle θ_n of the projection plane with respect to the airway coordinates is 0^o.

The loci may be somewhat larger if we vary θ_n and plot the locations of DALS found on other projection planes. The data in Figure 6.11, however, suffice to make the point that the model's predicted waveforms for airway diameters from 1mm to 5mm fall in the same range of IDW and 2CD parameters occupied by real DALS that are classified as fine and coarse. We observe that the crossover from class F to class C occurs for the 2mm case, where the locus of predicted DALS falls about half on one side of the discriminant line and half on the other. The largest model airway producing only class F DALS is seen to be of 1.5mm diameter. The smallest model airway producing only class C DALS is about 3mm in diameter.

The right column of figure 6.12 shows model DALS for five different sets of airway parameters. Comparison DALS were obtained from patient data by noting the position of a model complex in the IDW/2CD plane and selecting a real DALS whose IDW/2CD parameters were nearly equal to those of the theoretical waveform. Horizontal scales are the same and

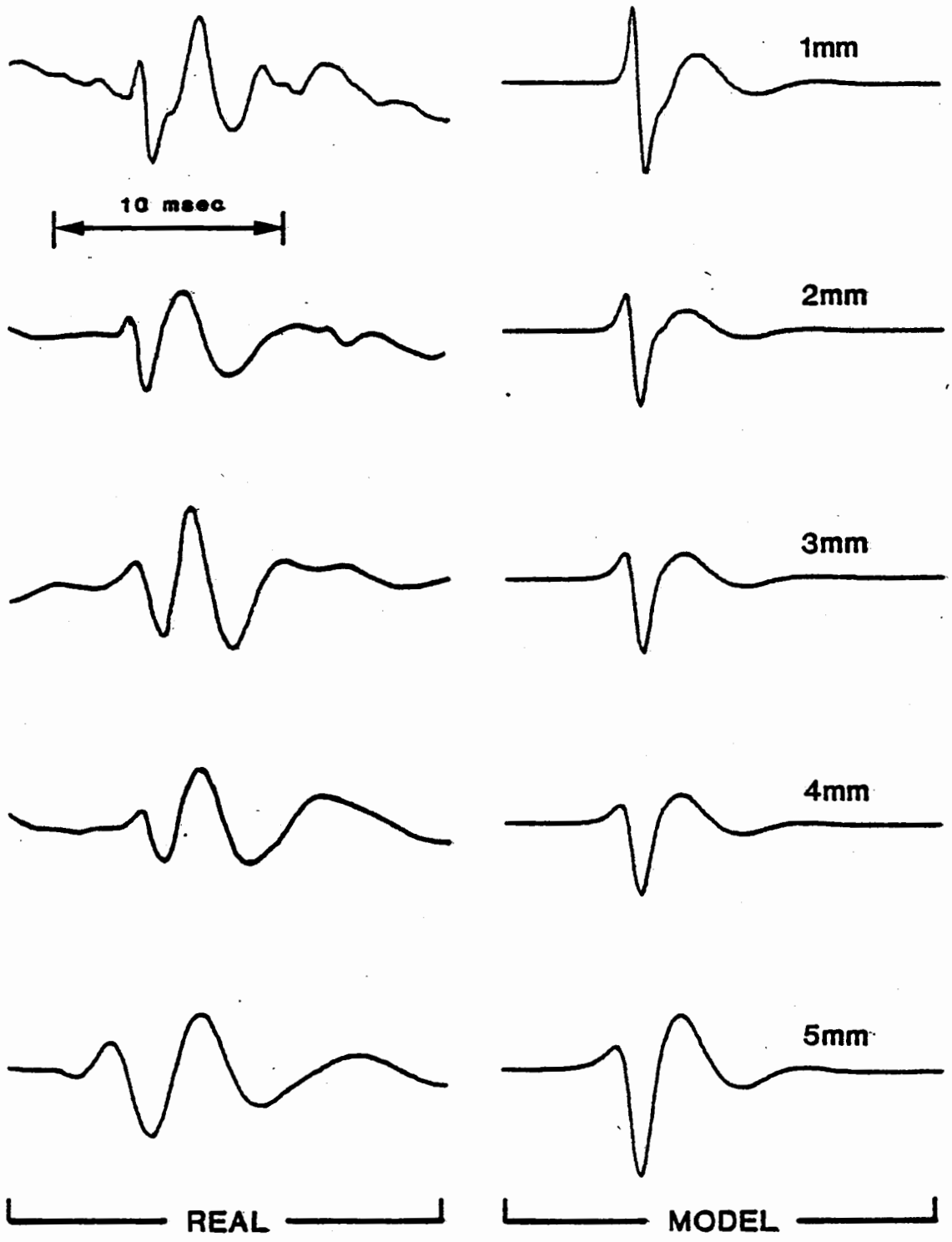

Figure 6.12 - Comparison of shapes of real and modeled DALS.

The predicted DALS in the right column correspond to airway diameters of 1-5 mm observed at an 85 dB chest wall contour. The real DALS on the left were selected from patient data by matching their IDW and 2CD parameters as closely as possible with their paired theoretical complex.

vertical scales were equalized to avoid visual confusion.

It is apparent from the figure that the model waveforms are not perfect matches for the observed DALS, even though their zero crossing intervals are similar. This is not surprising since a variety of waveform shapes is observed in patients for a particular set of (IDW, 2CD) parameters. Moreover, the real DALS are usually observed in the presence of background breathing noises, which are added to the pattern we see. Some of the shape differences may be due to deficiencies in the model or the digital filter that simulates the transducer. These issues are discussed further in section 6.5.2.

Waveform shapes in the two columns are generally similar. The 1mm airway model DALS and its comparison waveform have remarkably similar initial shapes. The biggest differences between real and predicted are in the later parts of the waveform. The real DALS tend to decay in amplitude less quickly than the predicted (see section 6.5.2 for discussion).

It is difficult to criticize the quadrupole model itself based on these comparisons because the shape of the predicted DALS is so dependent on the exact nature of the filter used to simulate transducer effects. Since our knowledge of the mechanical properties of the chest wall-transducer system is as yet imperfect, it is difficult to design with certainty a filter that realistically modifies the predicted pressure waveform. To further assess the

correctness of the model's temporal waveforms, it will be necessary to measure the properties of the air-coupled transducer system more adequately or to use transducers having less complicated interactions with the chest wall. Actual blocked force or free velocity (non-contact) transducers should greatly simplify the analysis of chest wall effects. The spatial energy distribution predictions are less dependent on transducer effects, and we consider them next.

6.4 Predicted Surface Distribution of DALS

Based on observations in patients, previous sections have reasoned that measuring the extent of the model's 75 dB energy contour in the chest wall plane gives a good estimate of the area over which measurable DALS could be observed. In this section we discuss the predicted connection between the size of the chest wall distribution and the waveform classification of the DALS observed within that region. We can directly compare the model's predictions to the finding in Chapter 4 that fine DALS, considered individually, were usually not measurable simultaneously at microphones separated by 6 cm, whereas coarse DALS were nearly always measurable at both transducers.

In Figure 6.13 the horizontal and vertical dimensions of the model's 75 dB energy contour are plotted for airway diameters from 0.5mm to 5mm. The patterns are elliptics whose horizontal axis is about twice as long as the vertical

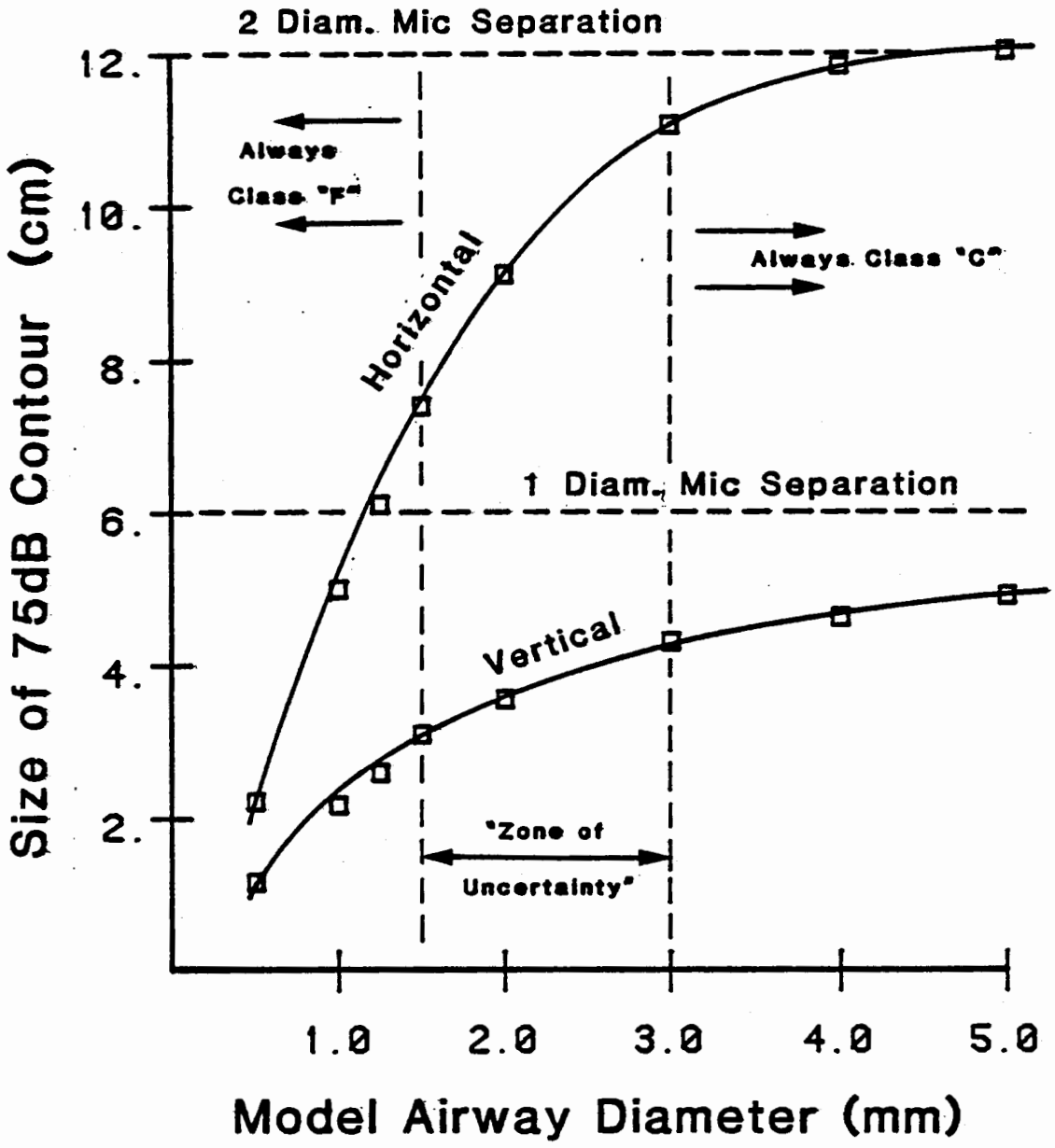

Figure 6.13 - Length of axes of elliptic 75 dB iso-energy contour on the chest plane versus model airway size.

The horizontal and vertical dimensions of the 75 dB contour in a chest wall plane like those in Figures 6.7-6.10 are plotted versus airway size. The vertical dotted lines show the airway sizes that bound the "zone of uncertainty" where DALS waveform parameters cross the discriminant line from class "F" to class "C". DALS that lie in the region where only class "F" parameters are found have chest wall contours that would not allow measurement at transducers separated by 6 cm. For model airway diameters greater than 3mm, the DALS are always class "C", and the chest wall contours are large enough to allow simultaneous observation at two transducers.

axis. In the figure, dotted horizontal lines at 6 cm and 12 cm represent the two microphone spacings of Chapter 4.

Note that the horizontal width first crosses the 6 cm line for a model airway diameter of 1.25 mm. For both the microphones to "see" the disturbance from this airway, they would have to be placed on the chest wall with the line connecting their center points aligned directly over the horizontal axis of the elliptic energy contour. This would require the airway itself to be precisely perpendicular to the microphone center line. Further, small lateral displacements of the transducers with respect to the energy contour would move one or the other of the microphones off the region of measurability. Thus, it seems unlikely that DALS from an airway this small would very often be measurable simultaneously at the two sensors.

As model airway size increases, the vertical axis of the elliptic grows longer, thereby increasing the likelihood of measurement at two microphones by decreasing the effect of airway rotation with respect to the transducer center line. The increasing horizontal size of the patterns reduces sensitivity to lateral displacement of the transducer pair.

Vertical dotted lines in Figure 6.13 show the results of the previous section regarding the diameters of model airways that are predicted to produce only class F or only class C DALS waveforms. We have seen that for small quadrupole model airway diameters the resulting DALS have (IDW,

2CD) parameters similar to those of real fine DALS. Figure 6.13 indicates that the chest wall distributions of these model DALS from small airways are such that they would not be simultaneously measurable at two transducers separated by 6 centimeters. As model airway diameter increases, we come to a zone where the predicted DALS may sometimes be observable at two sites 6 cm apart. In this zone, model DALS appearing at two sites may be both class F, both class C, or one class F and one class C. For large model airway diameters beyond the zone of uncertainty, only class C DALS are predicted. The chest wall distributions are then large enough that measurability at sites separated by 6 cm is quite likely. Further, the model predicts that if we separate the transducers by 12 cm, the observability of class F DALS at both sites should fall to zero, and class C DALS should be barely measurable at both sensors.

Figure 6.14 shows the IDW/2CD plane locations of all the DALS observed at one or both transducers separated by 6cm for the 12 patients of Chapter 4. Boxes in the figure represent DALS that were observed at only one transducer, while dots show DALS that ccurred at both sites. The two DALS in such a pair are connected by a dotted line so that the magnitude of the difference in their parameters is visible. A similar diagram was presented in Chapter 4, but we have now added the locations of model DALS for reference.

Recall that Figure 6.13 exhibits a zone of uncertainty where (1) some class C DALS may be measurable at only one

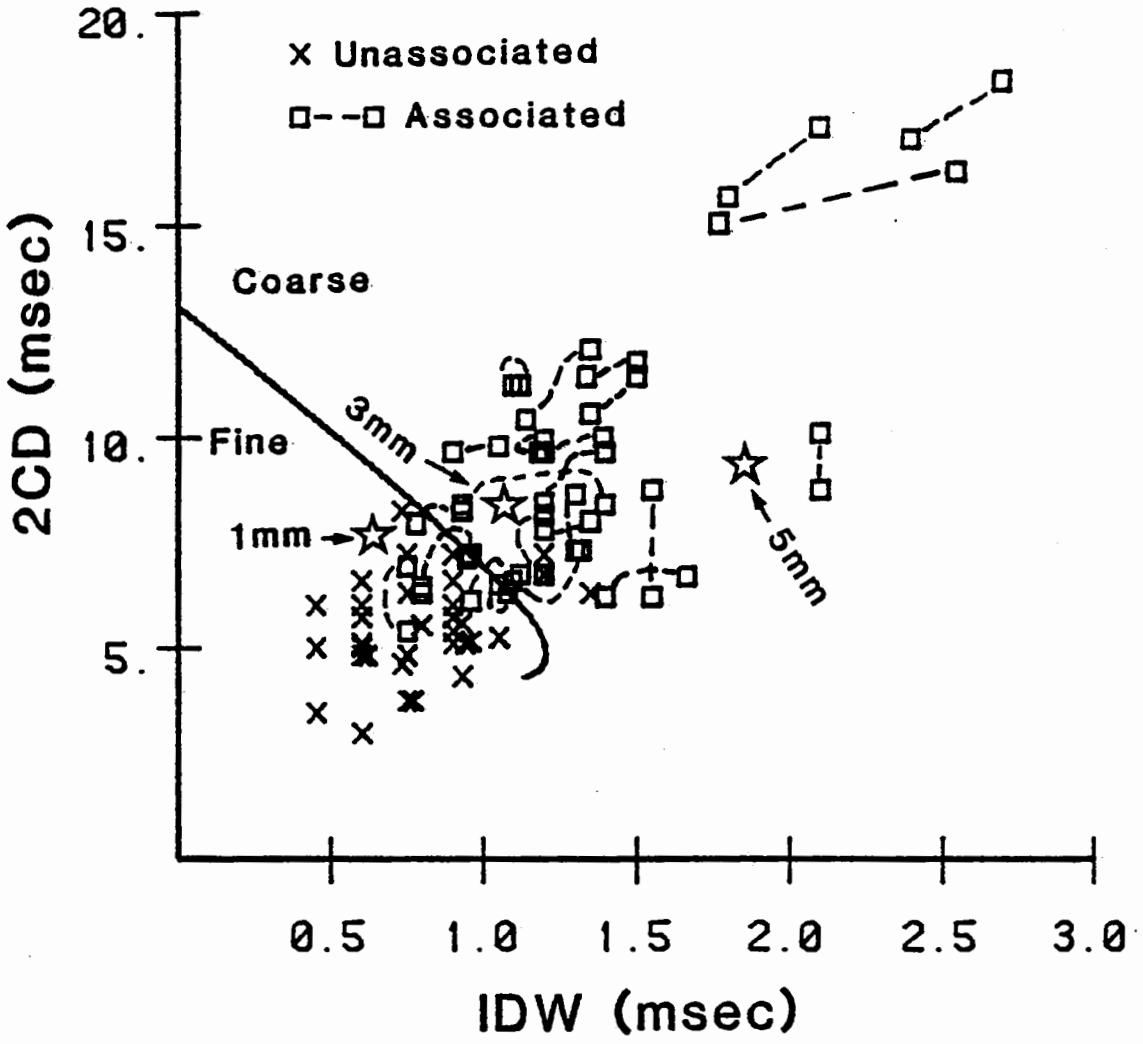

Figure 6.14 - Location of two-microphone data in IDW/2CD plane.

The X's show DALS measured at only one microphone. The boxes connected by dotted lines show the pairs of DALS measured simultaneously at two microphones 6 cm apart. The locations of model DALS from 1, 3, and 5mm airways are marked with stars.

microphone, (2) some class F DALS may occur at both, and (3) some pairs may be one class F with one class C. All these effects are observed in Figure 6.14. The boxes lying on the coarse side of the discriminant are real unassociated coarse DALS. The connected dots on the fine side are real associated fine DALS. There are three instances where one dot of a pair is on the fine side and the other lies on the coarse side. Finally, we note that the region of medium model airway diameters referred to above as the zone of uncertainty is the same range of airway diameters in which the model's waveforms move from class F to class C. In this sense, the model's zone of uncertainty maps to the region of the discriminant line in the IDW/2CD plane. If the model is correct, real unassociated coarse DALS and real associated fine DALS should be located close to the discriminant line, and this <u>is</u> the case for the data collected from patients.

6.5 Discussion

We set out to evaluate the quadrupole model for DALS by comparing its predictions to measurements of the amplitudes, shapes, and spatial distributions of DALS waveforms. In this section, the results of each aspect of the comparison are summarized.

6.5.1 **Amplitude: Real vs. Predicted** - We adjusted the source strength parameter of the model to produce model DALS whose amplitudes match the amplitudes of real waveforms.

This adjustment limits the scope of the conclusions we can draw about the correctness of the model in predicting the amplitude of DALS. In this section we will examine the model's prediction of the relative amplitudes at the chest wall among DALS from various airway sizes. In the model we have not constrained the relative amplitudes of DALS from different airways. We have simply set the amplitude for a particular airway size. The amplitudes for other airway sizes are determined by the form of the equations.

In discussing the predicted scaling of chest wall amplitude with model airway size, it is helpful to think in terms of the normalized pressure expressed in equation (5-4). Recall that the waveform shape is the same when $\dot{r}^*$ and θ are constant. The amplitude for a particular $\dot{r}^*$ is determined by the constant K_p, which scales inversely with model airway diameter. This means that if we observe two airways with differing diameters at the same value of $\dot{r}^*$ and θ for each, the amplitude will be smaller for the larger airway by a factor equal to the airway diameter ratio. Thus, to get the same amplitude we need to go closer in $\dot{r}^*$ units to a larger airway. This changes the model's waveform shape by emphasizing the g term relative to the g' and g'' terms, and the g' term relative to the g'' term. For the same amplitude, then, a larger model airway produces a ''coarser'' waveform.

Morphometric studies of the lung show that airway size is related to the amount of lung volume that is served by

the airway. The distance to the pleural surface from airways of a particular size varies within individuals and between individuals, and we expect this variability to be exhibited as variation in the amplitudes, shapes, and surface distributions of DALS from a particular airway size. The mean distance from the surface to an airway of diameter d is found to be proportional to $d^{2/3}$ [Fredberg and Holford (1981)]. With this information we can predict the variation in amplitude for model DALS from different airways.

Suppose the distance to a 5mm airway is related to the distance to a 1mm airway as

$$r_5 = 5^{2/3} r_1 \qquad (6\text{-}8).$$

We can see the relation between predicted amplitudes at the surface from model airways with these diameters by inspecting Figure 6.3(b). Taking the logarithm of both sides of (6-8) gives

$$\log r_5 = \log 2.9 + \log r_1 \qquad (6\text{-}9).$$

By shifting the 5mm curve in Figure 6.3(b) leftward by log(2.9), we can see the predicted peak amplitude relation at the surface. This translation is shown in Figure 6.15(a). In the region of interest between distances of 1.4 and 3 cm, the two curves show a peak amplitude difference of about a factor of two. Since these curves represent model airway diameters whose waveforms vary from class F to class C, we conclude that the model predicts that peak amplitude on the chest surface should not vary much as the location in the IDW/2CD plane changes. This is consistent with the

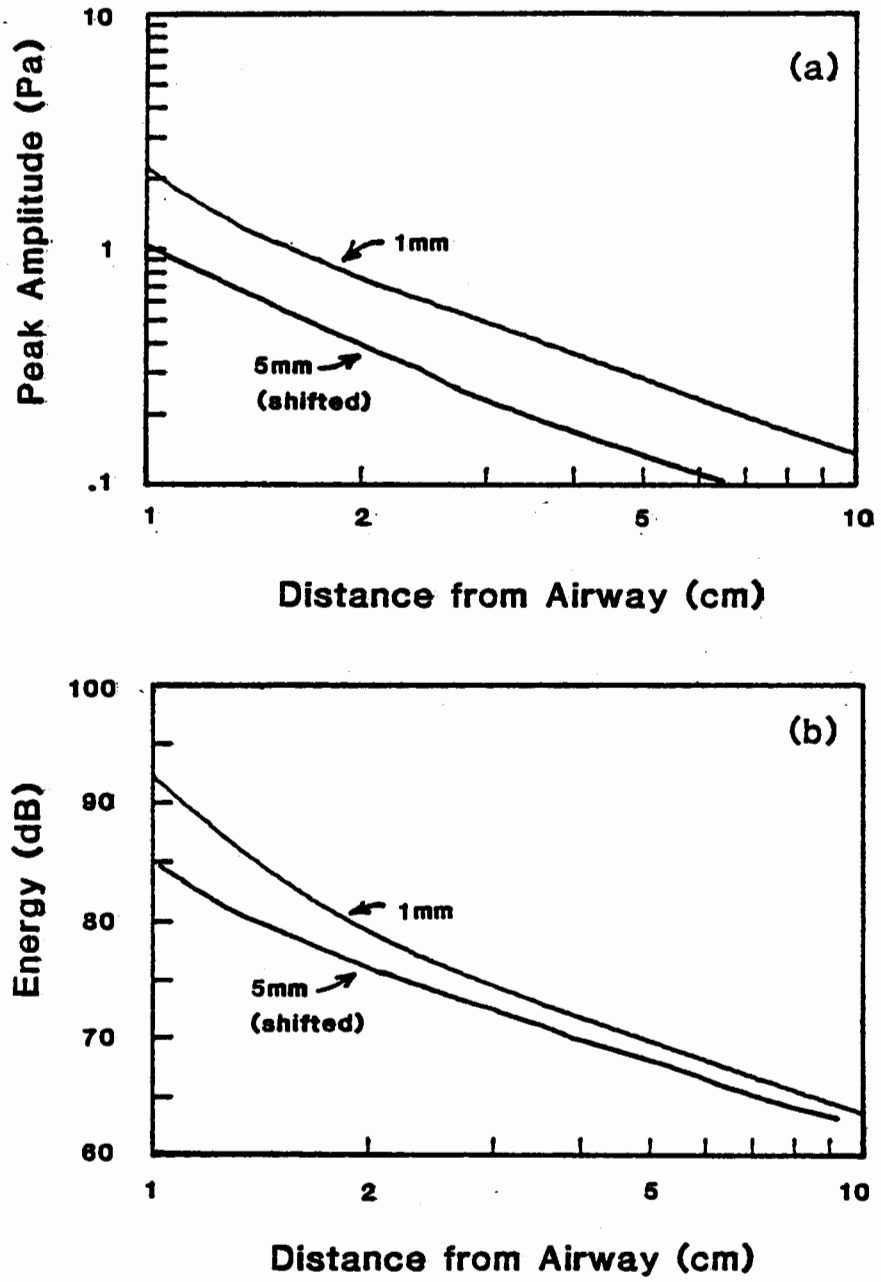

Figure 6.15 - Peak amplitude and energy at the chest surface assuming the distance to the airway is proportional to d to the 2/3 power. The distance scales are labeled for a 1mm airway. Values for the 5mm airway are obtained by multiplying by 2.9. Energies at the surface in the 75 to 85 dB range are within 2-4 dB for small and large airways.

general observation that fine and coarse DALS in patients occur with similar maximum amplitudes.

In deciding where to locate model chest wall projection planes, we assumed that equal energy DALS, not equal amplitude DALS, were to be observed at the central point of the projected contours. In assessing the derivation of chest wall contour spread versus model airway size, it is thus important to see how Figure 6.3(a) behaves when we shift the 5mm curve to account for the $d^{2/3}$ relation in distance to the surface. Figure 6.15(b) shows the result. Note that the two contours only differ by 2-4 dB in the region of interest between 75 and 85 dB. Our assumption of equal energies at the chest for model airways at average depth seems justified.

6.5.2 **Shape: Real vs. Predicted** - The shapes of real and modeled DALS were illustrated and discussed in section 6.3. We noted there that the shape of the predicted amplitude versus time waveform depends on the characteristic of the filter used to simulate the transduction process. Based on measurements and analysis of the transducer/chest wall interaction, we believe that a high pass filtering effect is present along with a low pass effect. As previously noted, the high pass filter has more influence on the resulting shape. This is due to the relatively large low frequency content of the predicted pressure waveforms.

We do not know whether the assumption of frequency

independent transmission is appropriate for the lung in the band of interest. It seems quite possible that filtering effects take place in the lung itself, and these would have a part in determining the shape of observed DALS. The presence of such effects in the lung is suggested by Figure 6.14, where we note that model DALS show considerably less variation in two-cycle duration than the observed DALS. The 2CD of the model's waveforms is largely determined by the fixed corner frequency of the high pass filter.

Our assumption of four-pole Butterworth high-pass and low-pass characteristics is probably justified with respect to numbers of poles, which determine asymptotic roll-off rates. However, the particular locations of the poles are unlikely to be evenly spaced as in the Butterworth case. Future study may show that the high pass filter should have more peaking in its frequency response, and this might make the model DALS look a bit more like their real counterparts in Figure 6.12. These possible explanations for differences in shape between real and predicted waveforms need to be evaluated before questioning the quadrupole model itself.

6.5.3 **Chest Wall Distribution: Real vs. Predicted** - Our knowledge of the actual chest surface distribution of an individual DALS is rather crude, i.e. low resolution. We have made simultaneous measurements at distances no closer than 6 centimeters. Clearly, measurements at closer transducer spacings will be necessary to validate or disprove the

model's predictions in detail. We concluded in section 6.4 that the model's predictions are consistent with the finding that real fine and coarse DALS are distributed differently on the chest wall. The observation of such a difference at 6 cm transducer spacing was suggested by Figure 6.13. Since a number of deductions and educated guesses were involved, it seems appropriate to review the process by which Figure 6.13 was generated in order to assess the strength of its prediction.

The first step was the formulation of the quadrupole model and its equations. Values were needed for several parameters of these equations, and these were taken from previous work or estimated. The effective volume of stress concentration was treated differently as noted below. Predicted pressure waveforms were digitally filtered as previously discussed. To calculate chest wall distributions, the location of an imagined chest wall had to be fixed for each airway size. This was accomplished by setting the distance for <u>one</u> airway size by measurements on bronchograms. Chest wall distances for other airway sizes were then determined by the assumption that equal energy DALS should appear at the central point of each chest wall contour. We have seen that this assumption is nearly equivalent to assuming a $d^{2/3}$ law for airway depth vs. diameter as found by morphometric studies. Thus, the chest wall plane locations are physically reasonable, both absolutely and relatively.

The model's source strength, ($\Delta v \times \sigma_o$), was adjusted to produce a DALS at the central point of the 5mm airway contours that had 85 dB energy, which corresponds to maximum amplitudes seen in patients. This arbitrary adjustment, however, did not affect the changes in shape or the energy contour spread of model DALS in the chest wall plane. Thus, the predicted connection between airway diameter, waveform shape, and surface spread is a result of the form of the equations and the assumed scaling of parameters with airway size.

6.5.4 **Airway Size: Model vs. Real Lung** - Throughout this report, airway diameter in millimeters has been used to characterize plots for different sets of model parameters. It should be noted that our knowledge of the actual airway diameter corresponding to a set of parameters is imprecise. This means that instead of concluding that class F and class C DALS come from 1-5mm airways, we should conclude that they come from airways having about a 5:1 diameter ratio. Likewise, we should conclude that the chest surface distribution of DALS is greater from larger model airways, but we cannot yet determine the precise airway size from measuring the contours in patients.

The model's prediction of measurability at two transducers separated by 6 cm for class C, but not for class F, DALS is more robust than the uncertainty about airway diameter might make it appear. What the model actually predicts

is that for some airway diameter the time waveforms go from class F to class C, and at this same airway diameter the chest wall spread becomes large enough to allow the two site measurement. This is precisely what was observed on the chests of patients. While we do not interpret this as a critical test of the quadrupole model, it is nonetheless an important test, and the similarity between predicted and observed results is unlikely simply to be fortuitous.

6.6 Conclusions

1. The qualitative assessment of fineness/coarseness used by physicians to describe discontinuous adventitious lung sounds can be objectively reproduced by simple waveform measurements.

2. A difference in chest surface distribution of different types of DALS can be observed using multiple transducers. Individual coarse DALS are seen to be more widespread than individual fine DALS. This is interpreted to mean that coarse DALS come from deeper in the lung and, therefore, from larger airways.

3. Fredberg's quadrupole model is a plausible explanation of the DALS phenomenon based on available data. The model's waveforms are reasonable approximations to the shapes of DALS. The model's prediction of nearly equal chest surface energies for different airway sizes is supported by the available (somewhat meager) data. The model correctly

predicts the connection between fine/coarse waveform properties and chest surface distribution.

6.7 Summary of Recommendations for Further Work

1. The objective classification scheme developed here for DALS uses only the two categories fine and coarse. The model predicts--and the observed DALS exhibit--a continuous gradation of waveform parameters from very fine to very coarse. Many physicians use the word medium to describe DALS that are between fine and coarse. It seems natural to speculate that these would fall somewhere in the middle region of the IDW/2CD plane near the discriminant curve. This hypothesis could be tested rather easily.

It may be found that medium DALS have some other waveform property that distinguishes them, such as a more or less damped response. Such detailed differences in wave shapes may also be found to correlate with clinical adjectives like "dry", "wet", "bubbling", and "sticky." Aside from the possibility of objectifying the definitions of these qualities, studying them may yield further insights into the origin of DALS and into the properties of the lung that determine their nature.

2. Transduction of lung sounds needs more study if attempts to verify models are to be fruitful. Chest wall impedance needs to be measured for actual transducer interface geometries so that the mechanical interaction between the

body and the instrumentation can be better understood. The development of a mechanical equivalent circuit for a particular type of transducer would allow correction for its effects. This might require measuring chest wall properties in each subject to estimate circuit element values.

Currently available transducers are too large to be used in studying the details of the surface distribution patterns of DALS. Verifying the model's predictions about the shapes of these patterns will probably require development of smaller transducers. Such miniature transducers might be applied in an array to ''map'' the vibration pattern of an area of the chest.

3. Better parameter measurements and estimates are needed to refine the model's predictions and to enable more precise verification of its fundamental form. None of the parameters is easily measured because the lung is a complex living structure. The wave speed c_L may be the easiest to measure. This needs to be done for human lung tissue at various lung volumes. Better values for σ_o, the surface tension-related source strength parameter, might result from study of airway collapse configurations. The variable τ that was used to parameterize the source function describing stress change was estimated by considering inertial and elastic forces acting on airway walls. A more detailed study of these forces and their variations with airway size would refine the estimates of τ.

4. Observation of the effects of intentional physiological parameter variations should be a good way to check the formulation of the model. For example, changes in the intrapulmonary gas composition should have little effect on observed DALS. This is easily checked. Introduction of agents that modify surface tension should change the source strength predictably. This could certainly be tried in excised specimens.

Appendix A

BASICS OF RD

Lung Sounds[1]

Raymond L.H. Murphy, Jr., M.D., S.D., M.P.H.
Director, Pulmonary Department
Faulkner and Lemuel Shattuck Hospitals;
Associate Professor of Medicine,
Tufts University School of Medicine
Boston, Massachusetts

Stephen K. Holford, S.M.
Bioengineer, Faulkner Hospital;
Research Associate in Medicine,
Tufts University School of Medicine
Boston, Massachusetts

INTRODUCTION

Auscultation of the chest is a rapid and inexpensive way to obtain information in a variety of diseases of the lung. The usefulness of lung sounds has been limited, however, because terminology has been confusing and the variability among observers has been considerable. Moreover, there is inadequate understanding of the basic mechanisms of production of the sounds, and few rigorous studies of the clinical and physiologic correlations of the acoustic events in the chest have been reported. Nevertheless, clinicians regularly use the stethoscope in their routine practice to obtain information about the status of a patient's health. Despite difficulties in communication, it is likely that useful information is obtained. Perhaps this is because, as pointed out by Laennec when he first listened to lung sounds, they are easier to recognize than to describe. The use of modern techniques to record and analyze sound has allowed clarification of some of the previous confusion. The following discussion will focus on basic aspects of lung sounds and their common clinical correlations in an attempt to summarize the concepts necessary for understanding the role of auscultation in routine clinical practice.

[1] This work was supported in part by the Institute of Occupational and Environmental Health and by Grant HL23318 from the National Heart, Lung and Blood Institute.

DESCRIPTION OF LUNG SOUNDS

Normal Breath Sounds

In healthy individuals, lung sounds have a characteristic quality that varies with the area of the chest where they are heard. Over the large airways, a tubular quality is normally present; such sounds are called "bronchial" or "tracheal breath sounds." They contain a wide range of frequencies extending from the threshold of audibility to more than 1,000 Hertz (Hz). The sound heard over the chest at a distance from the airways has a lower pitch and a frequency content that is maximal between 100 and 300 Hz, with little energy content over 500 Hz. Although the exact origin of this sound is unclear, it is called "vesicular," from the Latin word for small vessels. The vesicular sound is heard over all areas of the lungs except where large airways are close to the surface. Sounds heard over the large airways are relatively louder than the vesicular sound. The difference is particularly noticeable during expiration. The expiratory phase heard over the trachea has a longer duration than the expiratory phase heard at a distance from the large airways, and is usually separated from the inspiratory phase by a silent pause. The characteristic prolonged, loud expiratory phase usually allows separation of the bronchial or tracheal sound from the vesicular sound.

In normal persons, the bronchial sound is heard over the trachea or in the midline in the upper anterior chest, both to the right and to the left of the sternum. It is also heard in the right upper anterior chest and on the back between the scapulae (figure 1). Bronchial breath sounds heard at the base of the lungs are abnormal. They are usually due to better transmission of the centrally generated bronchial sounds to the periphery. More efficient transmission is caused by consolidation, as from pneumonia. Areas of the chest intermediate between those where bronchial sounds are heard and those where vesicular sounds are heard have sounds that are a mixture of the bronchial and vesicular qualities. These sounds have been referred to as "bronchovesicular." Variability among observers is particularly high in interpretation of these sounds, and, until their precise characteristics have been clearly defined, it is better to avoid the term.

Adventitious Sounds

Most adventitious sounds can be categorized as either "continuous" or "discontinuous." Although there are no established criteria, continuous sounds usually last more than 0.25s

PUBLISHED BY AMERICAN THORACIC SOCIETY —
MEDICAL SECTION OF AMERICAN LUNG ASSOCIATION

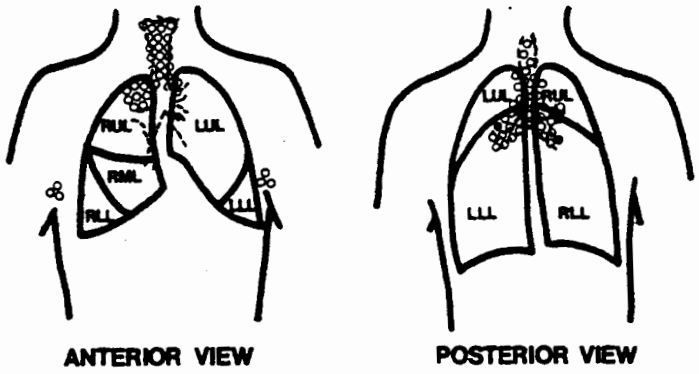

Fig 1. Areas of the chest where the lung sounds in normal persons may have a tubular quality are indicated by circles (O). The relation to the underlying large airways is apparent.

and frequently have a musical quality. These sounds are called "rhonchi" when low pitched and "wheezes" when high pitched. Discontinuous sounds occur in brief bursts, similar to the popping sound of bubbles or the crackling sounds of a fire, and they are called "crackles," "rales," or "crepitations." The discontinuous sounds (crackles) are divided into fine and coarse. Coarse crackles are louder, lower pitched, and slightly longer in duration than fine crackles. Another category of sound, which has both continuous and discontinuous aspects, is the pleural friction rub. It is heard in association with diseases of the pleura and is generally described as having a leathery or grating quality. This is usually heard during both inspiration and expiration.

Time-expanded waveform analysis of lung sounds allows differentiation of the typical sounds just described (1). The method consists of recording the sounds, putting them into a computer memory, and then visually displaying them on a two-dimensional plot with amplitude of sound on the Y-axis and time on the X-axis. On the final plots, the time axis is "expanded" or magnified by playing the sound back slowly from the computer memory. This is equivalent to running a chart recorder, such as that of an electrocardiographic machine, many times faster than the conventional rate. This allows visualization of details of the waveforms not easily seen at slower speeds. Normal tracheal and vesicular sounds are illustrated in figures 2A and 2B. The louder, longer expiratory phase of the tracheal sound is readily recognized, as is the pause between inspiration and expiration. In the vesicular sound, no clear demarcation between inspiration and expiration is observed. When crackles are heard clinically, "discontinuous" deflections, usually less than 10 milliseconds in duration, can be seen on the tracing. They are marked "C" in figure 2C. When continuous adventitious sounds are heard, they produce much longer abnormal deflections, as illustrated in figure 2D. Within the broad categories of continuous and discontinuous, further differentiation can be made by examination of the waveform. Fine crackles (rales) can be differentiated from coarse ones by a narrower initial deflection width, a shorter duration, and the lower amplitude of the sound. The higher pitched wheeze shows more deflections per unit time than the lower pitched rhonchi. This objective method of analysis has allowed construction of a table of equivalents for lung sounds (table 1).

Although it may be difficult or even impossible to achieve general agreement on preferred terms for given sounds, concentration on the acoustic characteristics has permitted improved communication among investigators, which should eventually lead to a more uniform nomenclature.

MECHANISMS OF PRODUCTION OF LUNG SOUNDS

As the gases move through the airways during respiration, vibrations from within the gas or from the walls of the airway are transmitted through the lung tissue to the chest wall. At the chest wall, these vibrations are superimposed on the larger excursions of inspiration and expiration. Due to the remarkable sensitivity of our auditory apparatus, a stethoscope allows us to sense chest wall vibrations, whose amplitude may be 10^{-6} meter or less.

The vibrations in the lung that we eventually interpret as sounds can arise from a number of phenomena. None of the generating mechanisms has yet been explained in detail, but there is enough agreement among investigators to allow us to describe the outlines of the mechanisms for normal and abnormal lung sounds.

Normal Sounds

In most of the conducting airways of the lung, gas flow is described as laminar. This smooth flow is replaced by turbulent, unsteady flow in large airways. The vibrations of the gas in the large airways are transmitted to the walls of the airway and thence to the surface of the chest, and they are also transmitted as airborne sound, both toward the mouth and toward the periphery. As the sound travels toward the periphery and the chest wall, it is progressively filtered and attenuated. By filtering, we mean that components of the sound occurring at different frequencies (or pitches) are transmitted differently. In fact, the transmission path acts as a low-pass filter, which means that it preferentially passes low-frequency sounds. This phenomenon is easily demonstrated by listening over the periphery of the lung while a subject speaks. The muffled sounds are hardly intelligible.

It is believed that this filtering phenomenon accounts for the differences in frequency content between tracheal or bronchial sounds and sounds heard over the periphery of the lung (vesicular or distal sounds). Some investigators still argue that sound is generated in the periphery, even though the flow rates are theoretically so low that turbulence is unlikely. The argument for peripheral generation of sound rests largely on the observation that regional differences in the intensity of vesicular sound at the chest wall are correlated, to a degree, with variations in regional air flow measured with radioactive gas techniques (2). An alternative explanation for the regional differences in sound is that the turbulent energy in the large airways may be convected with the air flow, and that regions with a larger share of the total flow also receive a larger fraction of the airborne sound.

Bronchial Breathing

When the transmission path to the surface of the chest is altered by consolidation of the lung, the filtering effect is decreased, so that we hear sounds over the periphery that are similar to those over large airways. This is accompanied by alteration in the transmission of voiced sounds, which are

heard more clearly over regions of consolidation.

Adventitious Sounds

Adventitious sounds are believed to result from abnormal motions of airway walls or materials within the airways during breathing. In contrast, normal sounds result largely from vibrations within the gas itself.

Continuous Sounds—Wheezes and some rhonchi are believed to be generated by a regular vibration, or oscillation, of the airway wall at one or more sites in the chest. This oscillation draws its energy from the air flow itself. Forgacs (3) observed that the pitch of a wheeze is relatively independent of gas density. This means that wheezes are not produced in the same way as the note of an organ pipe, in which a column of air vibrates and the pitch of the note depends both on the length of the pipe and on the density of the gas in the pipe. Forgacs also found that he could generate wheeze-like noises in excised bronchus by blowing air through the specimen and using compression to generate external pressure. The tone produced could be varied over eight octaves by manipulating the flow and the degree of compression.

Thus, it seems likely that wheezes and some rhonchi occur when air passing through a narrowed airway at high

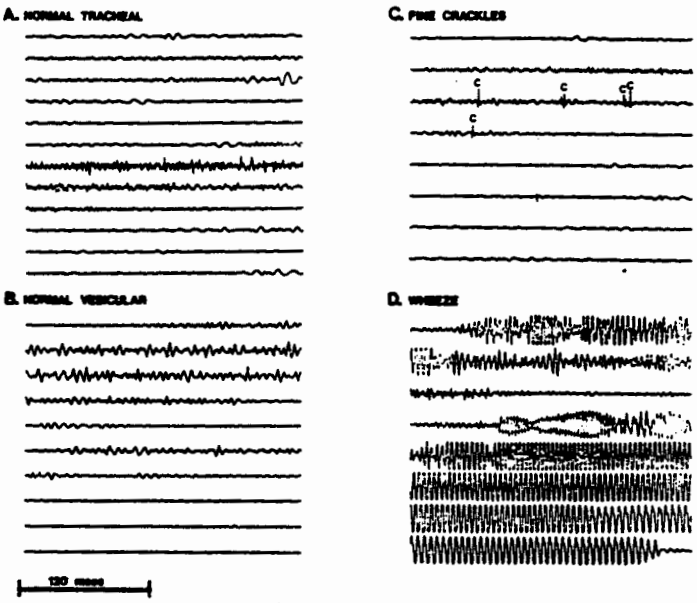

Fig. 2. *Time-Expanded Waveforms of Lung Sounds.* The time-intensity plots in this figure are made from tape recordings of lung sounds stored in a computer memory and then visually displayed on a two dimensional plot, with amplitude or intensity on the Y axis and time on the X axis. The time axis of the plot is "expanded" or magnified by playing back slowly from the computer memory. Figures 2A and 2B illustrate normal tracheal and vesicular sounds. The louder, longer expiratory phase of the tracheal sound is readily recognized as is the pause between inspiration and expiration. When crackles occur, they produce intermittent ("discontinuous") deflections superimposed on the normal vesicular pattern (marked C in figure 2C). Figure 2D shows a "continuous" deflection produced by a wheeze replacing the normal waveform.

TABLE 1

Acoustic Characteristics	Waveform	Recommended ATS* Nomenclature	Terms in Some Textbooks	British Usage	Laennec's Original Term
Discontinuous, interrupted explosive sounds Loud, low in pitch	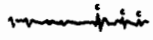	Coarse crackle	Coarse rale	Crackle	Rale muqueux ou gargouillement
Discontinuous, interrupted explosive sounds Less loud than above and of shorter duration; higher in pitch than coarse rales or crackles	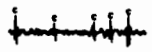	Fine crackle	Fine rale	Crackle	Rale humide ou crepitation
Continuous sounds Longer than 250 msec, high pitched; dominant frequency of 400 Hz or more, a hissing sound		Wheeze	Sibilant rhonchus	High-pitched wheeze	Rale sibilant sec ou sifflement
Continuous sounds Longer than 250 msec, low pitched; dominant frequency about 200 Hz or less; a snoring sound		Rhonchus	Sonorous rhonchus	Low-pitched wheeze	Rale sec sonore ou ronflement

* American Thoracic Society

While the terms used to name the categories of lung sounds vary widely, the categorization scheme itself has changed little since Laennec. The most recent names recommended for adoption by the American Thoracic Society and terms used by others are shown here, accompanied by acoustic descriptions and examples of typical sound waveforms for each category.

Table reproduced with permission from "A Simplified Introduction to Lung Sounds" by R.L.H. Murphy, published by Stethophonics, P.O. Box 122, Wellesley Hills, MA 02181.

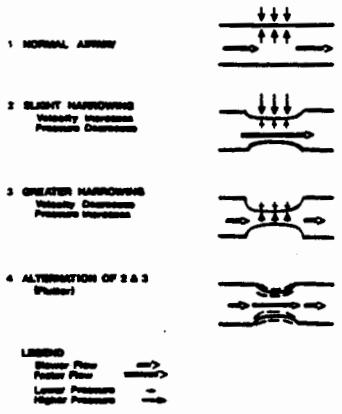

POSTULATED WHEEZE MECHANISM

Fig. 3. The stability of the airway wall depends upon a balance between internal air pressure and external forces and on the mechanical characteristics of the airway itself (1). When a narrowing of the lumen occurs, the air velocity must *increase* through the constricted region to maintain a constant mass flow rate. According to Bernoulli's principle, this leads to a decrease in air pressure in the constricted region, thus allowing external compressive forces to further collapse the airway (2). When the lumen has been reduced so much that the flow rate decreases, the process begins to reverse itself as the pressure inside the airway begins to increase and reopen the lumen. When conditions are right, the airway wall "flutters" between open and nearly closed states and produces a continuous sound whose amplitude, pitch, and duration depend on the airflow and mechanical parameters involved.

velocity produces a decrease in the gas pressure in the airway at the region of constriction. Bernoulli's principle relates the local velocity of the gas to local pressure in such flow. As the velocity of the gas increases at the constriction, the pressure decreases. If allowed by the other forces acting on the airway, collapse will continue progressively until there is a substantial resistance and the flow is decreased. Then, the internal pressure increases and the lumen enlarges. This alternation of the wall of the airway between almost closed and almost open can continue as long as the flow rate is high enough.

Low-pitched continuous sounds are often associated with production of sputum, and it is believed that a sputum flap vibrating in the airstream may produce rhonchi that clear after the patient coughs.

Discontinuous Sounds—Crackles are discrete vibrations that result from the sudden release of energy stored in elastic or surface forces within the lung. Although no quantitative physical models for the generation of crackles have yet been developed, it seems likely that more than one generating mechanism will be found. The coarse, discontinuous sounds occurring in pulmonary edema or other conditions in which fluid is found in the airways are probably caused by rupture of fluid films or bubbles. Such crackles often occur during both inspiration and expiration.

Forgacs has argued rather convincingly that crackles occurring in diseases such as pulmonary fibrosis or early congestive heart failure are not a result of air bubbling through fluid. His observations support instead the hypothesis that crackles in these diseases result from the sudden release of energy stored in the lung after delayed opening during inspiration of airways that had closed at the end of the previous expiration (figure 4). He bases his arguments on the often strikingly repetitive occurrence of crackles during succeeding inspirations, even after a cough. These crackles rarely occur in expiration and are often localized over dependent areas of the lung, where gravitational stress predisposes the airways to collapse at low lung volumes. Air bubbling through fluid would be expected to cause a noise during both inspiration and expiration. The pattern would probably change after a cough had redistributed the fluid.

CLINICAL CORRELATIONS OF ABNORMAL LUNG SOUNDS

Despite the fact that the stethoscope has been used for more than a century and a half, the clinical correlations of lung sounds are imprecisely known. In part, this is a result of the confusing terminology, and in part because there have been few careful investigations of the sounds. The following comments, then, represent an impression based on a review of the literature and the direct experience of the authors rather than a definitive statement of well-substantiated fact.

The character, intensity, and duration of the inspiratory and expiratory sounds over the chest can be readily recognized in normal persons. As mentioned previously, large airway sounds should be heard only over the areas mentioned before (see figure 1). Bronchial sounds heard elsewhere indicate disease, usually because the lung tissue has become consolidated and transmits the central airway sounds more clearly to the periphery than does normal, air-filled lung tissue.

Adventitious or added sounds are the most readily detected indicators of an abnormal state of the lungs. Even when adventitious sounds are not present, however, it is likely that in disease there are many variations from the normal character of the bronchial and vesicular sound, but only a few are widely recognized because of the difficulties in verbal description. Coarse breath sounds, for example, refer to sounds in which the lower frequencies are accentuated and some of the higher frequencies are lost. They are common in bronchitis, especially in children. A variety of other terms exist, such as cavernous, amphoric, conchal, and cogwheel, but these terms are currently not of great clinical importance.

Before attempting to summarize auscultatory findings in specific pulmonary conditions, it will be helpful to discuss the general associations of the four major classes of sounds mentioned previously. Continuous sounds usually reflect abnormalities of the airways; discontinuous sounds, abnormalities of the parenchyma and/or the airways. High-pitched continuous sounds (wheezes) are associated with narrowing of central airways, such as that caused by bronchospasm, edema of the airway lining, mucous plugging, and foreign bodies or tumors. When the high-pitched continuous sound is confined to inspiration or is accentuated during inspiration, it is called

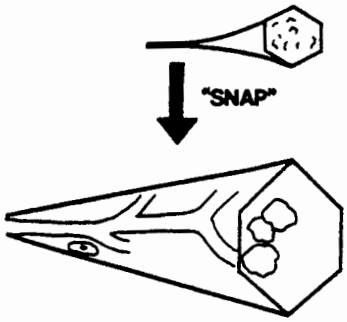

Fig. 4. Discontinuous lung sounds (crackles, rales) probably result from more than one physical mechanism. This figure illustrates the concept of an airway remaining closed for a portion of inspiration and then opening suddenly to produce a crackle. The lung downstream of the site of collapse remains underexpanded until upstream air pressure and external tractive forces on the collapsed walls overcome the surface tension of the material on the airway wall. The airway may then open suddenly, allowing a rapid equalization of pressure between the upstream and downstream airspaces. It remains uncertain whether the crackle sound itself results from this air pressure equalization or from the bursting of a film of surface material as the collapsed segment opens, or from a combination of the two sources.

"stridor." This is a common correlate of a large airway obstruction such as a foreign body or tumor. Lower pitched continuous sounds are usually associated with secretions in the airways and often change markedly after cough and expectoration. Fine discontinuous sounds, especially when high pitched and accentuated at end-inspiration, are most commonly associated with interstitial fibrosis. Similar sounds are also heard in early congestive heart failure and the early stages of pneumonia. Coarse discontinuous sounds commonly occur in advanced stages of pulmonary edema and in pneumonia, conditions in which it is likely that fluid or secretions are present in the airways. Pleural friction rubs indicate distortion of the normal anatomy of the pleural surface, usually by inflammation.

Atelectasis
When a portion of the lung is partially collapsed, as is common after upper abdominal surgery, fine crackles and bronchial breathing are often heard. These crackles might result from reopening of closed airways and congestion of lung parenchyma, leading to increased transmission of sounds.

Pneumonia
In its early stages, classic lobar pneumonia is associated with fine crackles and decreased breath sounds. These sounds probably result from poor entry of air and associated partial atelectasis. As the lung tissue becomes consolidated, the crackles disappear or decrease, and bronchial breathing occurs. As the pneumonia resolves, many discontinuous sounds are heard, most commonly coarse crackles. These adventitious sounds often change in character after coughing, but usually do not clear entirely.

Viral pneumonia is characterized by a discrepancy between the roentgenographic and auscultatory findings. A diffuse abnormality may be visualized on the radiograph when few or no adventitious sounds are present. The converse also occurs.

Pneumothorax
A dramatic decrease in the intensity of lung sounds occurs in complete pneumothorax. Lesser degrees of pneumothorax may be more difficult to detect with a stethoscope.

Pleural Effusion
In pleural effusion, lung sounds are decreased in intensity on the affected side. Dullness to percussion helps to distinguish this state from pneumothorax.

Pulmonary Edema
The most characteristic finding in acute pulmonary edema is the presence of numerous coarse discontinuous sounds with a bubbling quality. Initially, these are heard only at the lung bases; as the condition progresses, they are found increasingly further up on the chest. According to most studies, the correlation between these sounds and radiographic findings is poor. Significant evidence of pulmonary edema can be present in the absence of auscultatory findings. Most studies indicate that the roentgenogram correlates more closely with hemodynamic measurements.

Chronic Obstructive Lung Disease
Patients with chronic bronchitis tend to have noisy chests. Low-pitched continuous noises (rhonchi) are common and frequently change in character after coughing. Wheezes are also heard, particularly at end-expiration, which is often prolonged. The inspiratory sound is characteristically accentuated at the mouth (4). Discontinuous sounds (crackles) are heard at the lung bases and tend to begin with the beginning of inspiration (5). They are few in number and are often heard only over a small region of the chest.

The cardinal feature of emphysema is a decrease or even absence of lung sounds. The inspiratory sound at the mouth is also decreased. This point has been reported to help in the differential diagnosis of pure emphysema and bronchitis (4). In practice, the two diseases often coexist, and this decrease in the inspiratory sound is variable. In patients with chronic obstructive pulmonary disease, the intensity of lung sounds varies from one area of the chest to another; in contrast, the intensity of these sounds is relatively uniform in normal persons. Clicking noises at the mouth (oral rales) are common in chronic bronchitis and other conditions in which secretions are present in the airways. They may be heard with the naked ear or by placing the stethoscope beside the mouth.

Bronchial Asthma
The hallmark of reversible airway disease is the wheeze. A large percentage of persons with bronchial asthma wheeze at some time during the course of their illness. Most patients do so during all of their attacks, and wheezing can often be heard when patients are asymptomatic. Despite these generalities, the correlation between the presence of wheezing and impairment of ventilation is poor (6, 7). Some patients with well-documented bronchial asthma are never observed to wheeze, even while complaining of symptoms. Impairment of ventilatory function can also be significant in the absence of wheezing. Conversely, wheezing can be heard over the entire chest in patients whose pulmonary function is relatively normal. The reasons for these discrepancies are not understood at this time. Most patients with uncomplicated bronchial asthma will have relatively normal lung sounds when they are asymptomatic. When slight degrees of bronchospasm are present, wheezing will be heard only over large airways or at the mouth, particularly during a forced expiratory maneuver. As the asthma becomes worse, the wheezing spreads over the entire chest. Initially, it is confined to the expiratory phase; in more severe disease, it is heard in both phases of the respiratory cycle. An ominous sign is the absence of wheezing in status asthma. It usually indicates extremely severe disease; the wheezing is presumably absent because the flow rates are so low that the wheeze is not generated or airways are so filled with mucus that large areas of the lung are receiving little ventilation.

Wheezing is so common in bronchial asthma that it is frequently forgotten that "all that wheezes is not asthma." Foreign bodies or tumors in airways can cause wheezing. It is usually dis-

---

■ **Raymond L.H. Murphy, Jr., M.D., S.D., M.P.H., is director of Pulmonary Services, Faulkner and Lemuel Shattuck Hospitals, and associate professor of medicine at Tufts University School of Medicine, Boston. Dr. Murphy received his M.D. degree at New York University in 1961. His internship and medical residency were served at St. Vincent's Hospital and Medical Center, New York City.**

Dr. Murphy has master of public health and doctor of science degrees from Harvard School of Public Health, Boston.

■ **Stephen K. Holford, S. M., is research associate in medicine at Tufts University School of Medicine in Boston and a bioengineer at Faulkner Hospital, Boston. He was an American Lung Association training fellow from 1977-1979. He is a Ph.D. candidate in Electrical Engineering and Computer Science at Massachusetts Institute of Technology.**

tinguishable by its persistence and localization to one area of the chest, but this is not always the case. Wheezing in patients with congestive failure is called cardiac asthma; this is usually of brief duration and associated with other obvious signs of cardiovascular decompensation. Wheezing is also reported in pulmonary embolization, but is relatively uncommon in the absence of underlying lung disease. The most common cause of wheezing other than bronchial asthma is chronic bronchitis; the differential diagnosis is usually made by clinical findings other than physical examination. It is also not uncommon for the two conditions to coexist.

Pulmonary Fibrosis

Fine crackles with a "close to the ear" sound are the characteristic feature of the lung sounds of interstitial fibrosis. This association has been substantiated in pathologic findings (8). Because of their quality, they have been called "cellophane" or "velcro" rales. They are most commonly heard at the lung bases. In slight degrees of the disease, they are gravity dependent, i.e., they are heard more frequently in dependent regions. They are accentuated at end-inspiration and are heard more easily on a slow, deep inspiration after breath holding at low lung volumes. As the fibrosis progresses, they are heard farther up the chest to the mid-lung regions. They are usually distinguished from the crackles of bronchitis by their end-inspiratory accentuation and higher pitch. The crackles associated with bronchitis tend to begin with the beginning of inspiration. In bronchitis, clicking noises at the mouth are common. They are not heard in interstitial fibrosis without coexisting bronchitis. The differentiation between "interstitial" rales and those of early congestive heart failure is often quite difficult.

Perspective

For purposes of clarity, this discussion has focused on lung sounds in a manner relatively isolated from the other clinical observations used in assessment of a patient. This, of course, ought never to be the case. However, the stethoscope provides information that is clearly useful but is not otherwise easily obtained. One may question the value of studying lung sounds now that advanced diagnostic techniques such as pulmonary arteriography, ventilation/perfusion scans, pulmonary computerized axial tomographic (CAT) scans, and sophisticated methods of analyzing pulmonary function are available. Even with anticipated advances, it is certainly unlikely that detection of localized mass lesions will ever be done as well by sound as by roentgenogram. Nevertheless, lung sounds can be quite useful in the daily bedside and outpatient management of patients with a variety of illnesses such as bronchial asthma and congestive heart failure. These sounds can provide crucial information in instances of upper airway obstruction, misplaced endotracheal tubes, and spontaneous pneumothorax. Because auscultation is readily performed in a variety of settings, it is important that the clinician be aware of its value as well as its limitations.

Although 160 years have gone by since Laennec's first description of the lung sounds, we still have much to learn about their nature and correlation with diseases. Recent advances in physics and engineering promise to simplify this task.

REFERENCES

1. Murphy RLH, Holford SK, Knowler WC. Lung sound characterization by time-expanded waveform analysis. N Engl J Med 1977; 296: 968–71.
2. Ploy-song-sang Y, Martin RR, Ross WRD, Loudon RG, Macklem PT. Breath sounds and regional ventilation. Am Rev Respir Dis 1977; 116:187–99.
3. Forgacs P. Crackles and wheezes. Lancet 1967; 2:203–5.
4. Forgacs P, Nathoo AR, Richardson HD. Breath sounds. Thorax 1971; 26:288–95.
5. Nath AR, Capel LH. Inspiratory crackles: early and late. Thorax 1974; 29:223–7.
6. Ishikawa S, Workum P, Holford SK, Murphy RLH. Wheezes and airflow dynamics in asthmatic patients. Presented at 4th International Conference on Lung Sounds, Chicago, Sept. 1979.
7. Marini JJ, Pierson DJ, Hudson LD, Lakshminarayan S. The significance of wheezing in chronic airflow obstruction. Am Rev Respir Dis 1979; 120:1069–72.
8. Epler GR, Carrington CB, Gaensler EA. Crackles (rales) in the interstitial pulmonary diseases. Chest 1978; 73:333–9.

BASICS OF RD

published five times a year by
AMERICAN THORACIC SOCIETY
medical section of
AMERICAN LUNG ASSOCIATION
1740 Broadway • New York, N.Y. • 10019

Vol. 8 No. 4 March, 1980

Editor/Robert G. Loudon, M.B., Ch.B.
Assistant Editor/Mary J. Thornton

Distributed by
AMERICAN LUNG ASSOCIATION
Affiliate
The "Christmas Seal" People.
We care about every breath you take.

0531

References

1. Altman, P.L. and Ditmer, D.S., Editors (1971): Respiration and Circulation, Biological Handbook Series, Federation of American Societies for Experimental Biology, Bethesda, Maryland.

2. Bethke, R.J., and Seireg, A. (1973): Analysis of vesicular lung sounds in normal and emphysematous subjects, ASME Paper 73-WA/Bio-27, Nov., 1973.

3. Bishop, F.W., Lee, Y.W. et al (1930): Studies on pulmonary acoustics IV - Notes on percussion and forced vibrations, Am Rev Tuberc 22: 347-378.

4. Cabot, R. and Dodge, H.F. (1925): Frequency characteristics of heart and lung sounds, JAMA 84: 1793-1795.

5. Dawson, J.B. (1964): Auscultation and the stethoscope, The Practitioner 193: 315-322.

6. DeGroot, M.H. (1975): Probability and Statistics, Addison-Wesley Publishing Co., Reading, Massachusetts.

7. Digital Signal Processing Committee, Editors (1979): Programs for Digital Signal Processing, I.E.E.E. Press, John Wiley and Sons, New York.

8. Duda, R.O. and Hart, P.E. (1973): Pattern Classification and Scene Analysis, John Wiley and Sons, New York.

9. Ertel, P.Y. et al (1969): How to test stethoscopes, Med Res Eng 8: 7-15.

10. Fisher, R.A. (1936): The use of multiple measurements in taxonomic problems, Annals of Eugenics 7: 179-188.

11. Forgacs, P. (1967): Crackles and wheezes, The Lancet 2: 203-205.

12. Forgacs, P. (1974): Gravitational stress in lung disease, Brit J Dis Chest 68: 2-10.

13. Forsythe, G.E., Malcolm, M.A., Moler, C.B. (1977): Computer Methods for Mathematical Computations, Prentice-Hall, Englewood Cliffs, New Jersey.

14. Fraser, R.G. and Pare, J.A.P. (1970): Diagnosis of Diseases of the Chest, W.B. Saunders Co., Philadelphia.

15. Fredberg, J.J. and Holford, S.K. (1981): On discrete lung sounds, crackles, and quadrupoles (unpublished manuscript).

16. Fung, Y.C. (1981): Biomechanics - Mechanical Properties of Living Tissues, Springer-Verlag, New York

17. Glass, G.M. and Fredberg, J.J. (1980): Mechanical impedance of the thorax at high frequencies, JASA, in press.

18. Grassi, C. et al (1966): Normal and pathological repiratory sounds analyzed by means of a new phono-pneumographic apparatus, Respiration 33: 315-324.

19. Hannon, R. and Lyman, R. (1929): Studies on pulmonary acoustics II - The transmission of tracheal sounds

through freshly exenterated sheep's lung, Am Rev Tuberc 19: 360-375.

20. Helms, H.D. (1967): Fast Fourier transform method of computing difference equations and simulating filters, IEEE Trans Audio Electroacoust, AU-15, No. 2: 85-90.

21. Hudson, L.D., Conn, R.D., Matsubara, R.S., Pribble, A.H. (1978): Rales - diagnostic uselessness of qualitative adjectives, Am Rev Resp Dis 113(4): 187.

22. Kunica, E.S. (1980): Multiple site recording of discontinuous adventitious lung sounds, M.I.T. Dept. of Mechanical Engineering, S.B. Thesis.

23. Laennec, R.T.H. (1819): De L'Auscultation Mediate, 1st Paris Edition, Brosson and Chande.

24. Lai-Fook, S.J. (1977): J. Biomechanics 10: 357-365.

25. Macklem, P.T. (1971): Airway obstruction and collateral ventilation, Physiological Rev 51(2): 368.

26. Mahalanobis, P.C. (1936): On the generalized distance in statistics, Proc Nat Inst of Sciences of India 12: 49-55.

27. McKusick, V.A. et al (1955): The acoustic basis of the chest examination, Am Rev Tuberc 72: 12-34.

28. McKusick, V.A. (1978): Cardiovascular Sound in Health and Disease, The Williams and Wilkins Co., Baltimore.

29. Metildi, P.F. and Lyman, R.S. (1929): Studies on pulmonary acoustics I - An apparatus for recording respiratory sounds, Am Rev Tuberc 19: 353-359.

30. Murphy, R.L.H. and Sorensen, K. (1973): Chest auscultation in the diagnosis of pulmonary asbestosis, J Occup Med 15: 272-276.

31. Murphy, R.L.H. (1975): Human factors in chest auscultation, Chapter 5 in Human Factors in Health Care, R.M. Pickett and T.J. Triggs, Editors, D.C. Heath and Co., Lexington, Massachusetts.

32. Murphy, R.L.H., Holford, S.K., Knowler, W.C. (1977): Lung sound characterization by time-expanded wave form analysis, NEJM 296: 968-971.

33. Nath, A.R. and Capel, L.H. (1974a): Inspiratory crackles - early and late, Thorax 29: 223-227.

34. Nath, A.R. and Capel, L.H. (1974b): Inspiratory crackles and mechanical events of breathing, Thorax 29: 695-698.

35. Oppenheim, A.V. and Schafer, R.W. (1975): Digital Signal Processing, Prentice-Hall, Englewood Cliffs, New Jersey.

36. Penkala, S.J. and Litt, M. (1970): Transducer system for recording of respiratory sounds (abstract), Proc 23rd ACEMB 207.

37. Penkala, S.J. (1971): The recording, quantification, and analysis of respiration sounds of a group of normal subjects, U. of Penn, Ph.D. Thesis.

38. Rice, D. (1980): Sound speed in the parenchyma of excised horse lungs, Presented at 5th Int Conf on Lung Sounds, London.

39. Rubin, E.H. and Rubin, M. (1962): Thoracic Diseases Emphasizing Cardio-Pulmonary Relationships, W.B. Saunders Co., Philadelphia.

40. Staub, N.C. (1963): The interdependence of pulmonary structure and function, Anesthesiology 24: 831-854.

41. Stockham, T.G. (1966): High speed convolution and correlation, Proc AFIPS Spring Joint Comp Conf 28: 229-233.

42. Toshima, M. (1954): A clinical application of the electrically represented breath sounds, Japan J Tuberc 2: 149-162.

43. Weiss, E. and Carlson, C.J. (1972): Recording of breath sounds, Am Rev Resp Dis 105: 835-839.

44. Wooten, F.T. and Waring, W.W. (1972): Spectral and intensity analysis of respiratory sounds (abstract), Proc 25th ACEMB.

45. Workum, F.W., Holford, S.K., DelBono, E.A., Murphy, R.L.H. (1981): Crackles (rales) in young adult females with normal respiratory function, unpublished manuscript.